Control of Dynamic DNA Origami Mechanisms Using Integrated Functional Components

THESIS

Presented in Partial Fulfillment of the Requirements for the Degree Master of Science in the Graduate School of The Ohio State University

By

Carl A Miller, B.S., M.B.A

Graduate Program in Mechanical Engineering

The Ohio State University

2015

Master's Examination Committee:

Dr. Carlos Castro, Adviser

Dr. Michael Poirier

Dr. Jonathan Song

Abstract

Scaffolded DNA origami has been used to construct objects with complex three-dimensional geometries via molecular self-assembly to create functional nanoscale devices in the 10-100 nm size range. The production of static DNA origami structures is well documented. Only a few designed DNA nanostructures utilize structural dynamics to achieve functionality. In contrast, there has been an emergence of work showing the functionalization of DNA nanostructures through the incorporation of functional molecules or nanoparticles. This work expands the scope of DNA origami applications by incorporating dynamic functional molecules to control dynamic components of DNA origami structures. An in depth investigation into controlling the dynamic motion of a DNA origami hinge through the integration of a transcription repressor protein is the main focus of this thesis. Investigation into the attachment of other nanoscale functional molecules to enable control over nanoscale DNA origami designs is also performed as a proof of concept. This work sets a foundation to create useful dynamic tools to explore complex nanoscale systems.

This work is dedicated to my family; without you I would not be here.

Acknowledgments

I would like to share my unending thanks to Dr. Carlos Castro for believing in me. I thank you for providing not only the opportunity to complete this work but also support, understanding, and encouragement.

I thank the Poirier lab in the Department of Physics at the Ohio State University. Dr. Michael Poirier, has helped me learn more than I thought possible during my time at Ohio State. Your passion is infectious and I hope that it remains so forever.

I would also like to thank Morgan Welsh Bernier, Gauri Nabari, and Qirui Fan, collaborators who were vital to the completion of this work.

I would like to thank the entire Nanoengineering and Biodesign Lab both past and present. I would like to thank Chris Lucas for your positivity. I thank Molly Molica for being a fantastic desk neighbor. I thank Alex Marras and Mike Hudoba for showing me the ropes in the lab. I would like to thank Randy Patton for helping me to think outside the box.

Lastly, I want to thank my family, friends, and girlfriend. Without your support, love, encouragement, distraction, and hope I would have lost my mind long ago.

Vita

June 2007 .....Newark Catholic High School

June 2012 .....B.S. Mechanical Engineering, The University of Cincinnati

June 2012 .....M.B.A. focus in Entrepreneurship, The University of Cincinnati

2012-2014……..……Graduate Research Associate, The Ohio State University

2014-2015……..……Graduate Teaching Associate, The Ohio State University

Fields of Study

Major Field: Mechanical Engineering

Table of Contents

List of Tables

List of Figures

Chapter 1: Introduction to DNA

Before an examination of DNA nanotechnology can be performed it is valuable to review the physical properties of B-form Deoxyribonucleic Acid (DNA). DNA is the molecule used by all living organisms to encode genetic information. Structurally, DNA is a polymer made up of individual nucleotide bases attached to a phosphate backbone with alternating phosphate and sugar groups which provide directionality to each strand of DNA. The direction is defined by the ends of the DNA strand with the 5' end terminating in a phosphate group and the 3' end terminating in a hydroxyl off the sugar group. When bound to an antiparallel complementary DNA via nucleotide hydrogen bonding, the polymer forms a double helix structure [1]. Duplex or double stranded DNA (dsDNA) is approximated as a cylinder of approximately 2 nanometers (nm) in diameter and pitch of 3.4nm [2]. Each nucleotide base pair is 0.34nm in length. A schematic of dsDNA is shown in Figure 1 – Schematic of Duplex DNA.

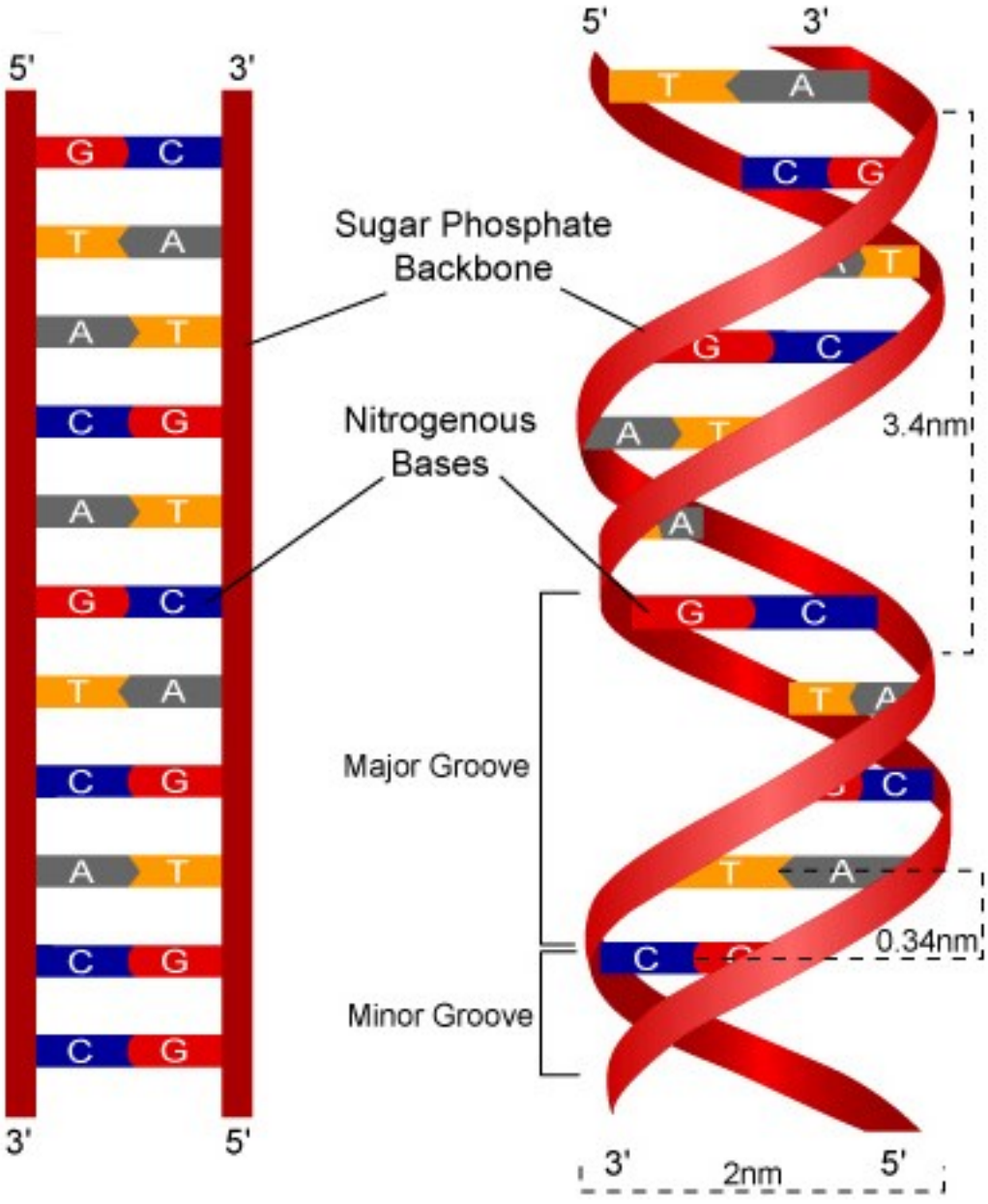

Figure 1 – Schematic of Duplex DNA [3]

Introduction to DNA based nanotechnology

DNA nanotechnology is a rapidly advancing field of research focused on the design and fabrication of DNA based nanoscale structures [4]. It was first postulated by Nadrian Seeman in 1982, that oligomeric DNA and/or RNA could be used to create variously shaped junctions and lattices via Watson-Crick base pairing [5]. Many examples of naturally occurring DNA joints and branched structures, such as the Y-shaped replication fork DNA structure that forms during DNA replication [6] and Holliday junctions [7], were well studied at this point in time. The novelty of Seeman's idea lies in the fact that he suggested manipulating the naturally occurring antiparallel symmetry of dsDNA by generating oligonucleotides of known sequence having complementarity to more than one other oligonucleotide [8]. Seeman proposed DNA junctions and possible DNA lattice networks made from those junctions as shown in Figure 2 –Potential DNA Junctions and Lattice Networks

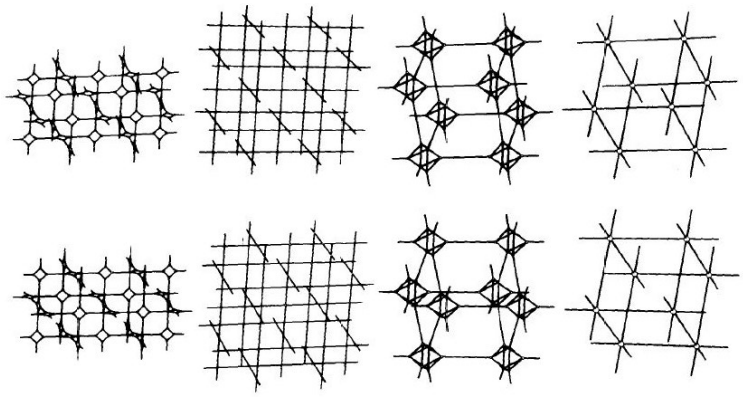

Figure 2 –Potential DNA Junctions and Lattice Networks [5]

In the 34 years that have followed Seeman's initial work, the study of DNA nanotechnology has exploded. Nadrian Seeman has remained a leader in the field creating the first closed polyhedral object in the form of a DNA box [9], developing a biped DNA walking device [10], and creating a nanomechanical device that acts as an artificial ribosome [11]. By exploiting the programmability of DNA and RNA, researchers have developed synthetic DNA based cargo carriers showing promise in in vivo applications due to the nontoxic nature of DNA and RNA, the ability of DNA to be bound to targeting molecules, and the stability of DNA base pairing [12]. Such therapeutic applications of synthetic nanoparticles are limited by many biological barriers such as size, shape, and surface properties which can affect toxicity, circulation half-life, and biocompatibility [13]. Bhatia et al. have shown that conquering these barriers is almost certainly possible. Bhatia et al. showed that an icosahedral DNA nanocapsule labeled with an anionic ligand-binding receptor could be used to carry pH sensitive imaging agents into targeted cells of Caenorhabditis elegans to map cellular and organellar pH [12].

By recognizing DNA as a polymer with well-defined structural and chemical properties, researchers have been able to use DNA to actuate nanoscale structures and molecules. One method for using DNA to actuate nanostructures is called strand displacement. Strand displacement is a process by which two strands of DNA hybridize and supplant one or more previously hybridized DNA strands [14]. This method utilizes the presence of a toehold region of single stranded DNA (ssDNA) at the end of a section of dsDNA that is complementary to some other ssDNA "fuel" strand that ultimately acts as the

actuator [15]. The fuel strand begins Watson-Crick base pairing to the toehold region and eventually displaces the strand of DNA to which it is not complementary. A schematic of strand displacement can be seen in Figure 3 – Schematic of Strand Displacement.

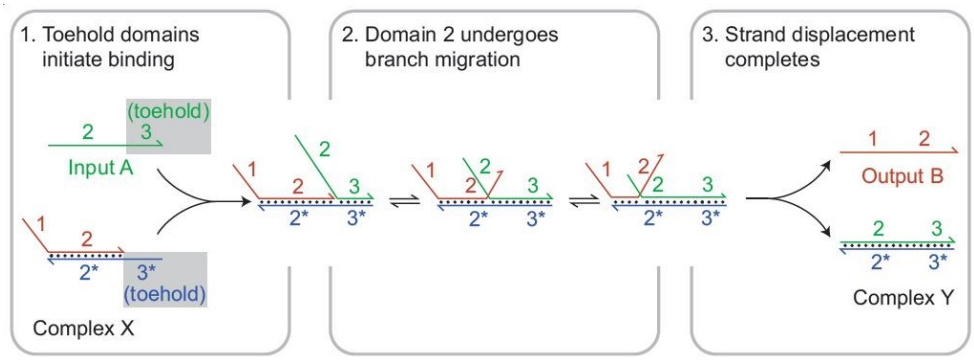

Figure 3 – Schematic of Strand Displacement [14]

This novel method of actuation occurring on the nanometer scale has given rise to functional DNA nanostructures such as 'DNA walkers' [10], [16], [17] and molecular tweezers [18]. DNA walkers have been used to transport nanoscale objects from one point to another along a prescribed track [17]. Frequently, DNA walkers use some form of strand displacement to introduce movement of a structure through the addition of a fuel strand that triggers a strand displacement reaction [16]. Reif et al. chose to use a simple linear arrangement of evenly spaced toehold regions located along a track allowing the travel of a walker strand along the length of the track [17]. Lund et al. developed a multi-limbed DNA walker that allowed programmed motion by modifying

the sequence of each of the walker's arms [16]. An evenly spaced grid of 5 differently sequenced ssDNA overhangs was created. Three ssDNA strands, each piecewise complementary to one of the grid overhangs and to a fuel ssDNA molecule, were introduced and bound to the corresponding grid strands. Through the addition of differently sequenced ssDNA fuel strands, it was possible to induce programmed multistep motion. Liu et al. developed an application for DNA walkers to perform multistep organic synthesis in a single solution [19] and can be seen in Figure 4 – Multistep organic synthesis mediated by a DNA walker.

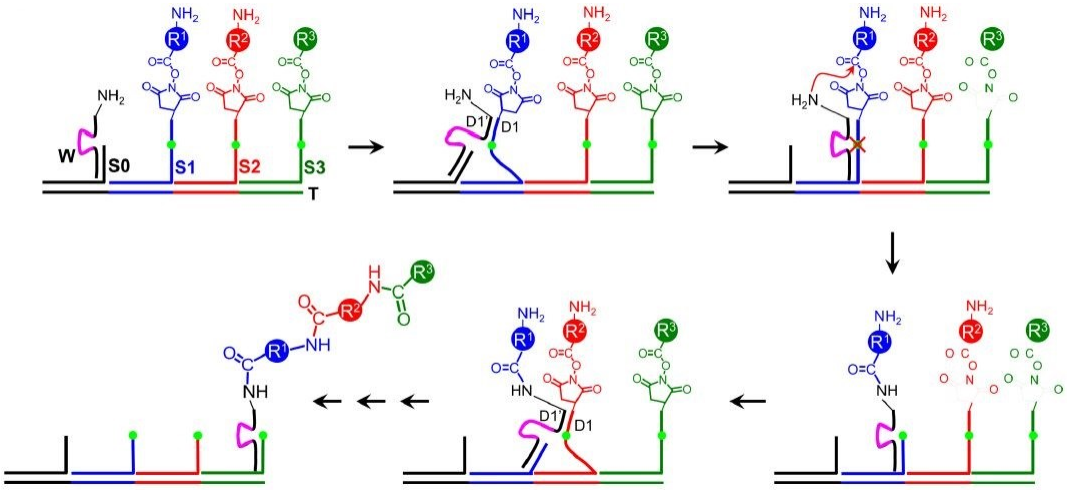

Figure 4 – Multistep organic synthesis mediated by a DNA walker [19]

In addition to facilitating transport and targeted delivery of cargo, DNA is being used to create large, megadalton scale, complex nanostructures called DNA origami [20].

Introduction to DNA origami

As was previously stated, DNA origami refers to megadalton sized nanostructures made from DNA designed to fold into a specific geometry. Specifically, scaffolded DNA origami are DNA nanostructures that are formed through the folding of a long (1000 – 8000 bases) single stranded DNA template molecule called a scaffold with many shorter scaffold-complementary oligonucleotides called staple strands [21] [22]. The scaffold strand forms one half of the double helix structure of the DNA origami structure. The scaffold is generally a long continuous DNA molecule in either linear or circular form [21]. The staples must be short (~30-50 bases) linear strands of DNA that are piecewise complementary to sections of the scaffold molecule (Figure 5 – Short staple strands bind to the long, continuous scaffold molecule).

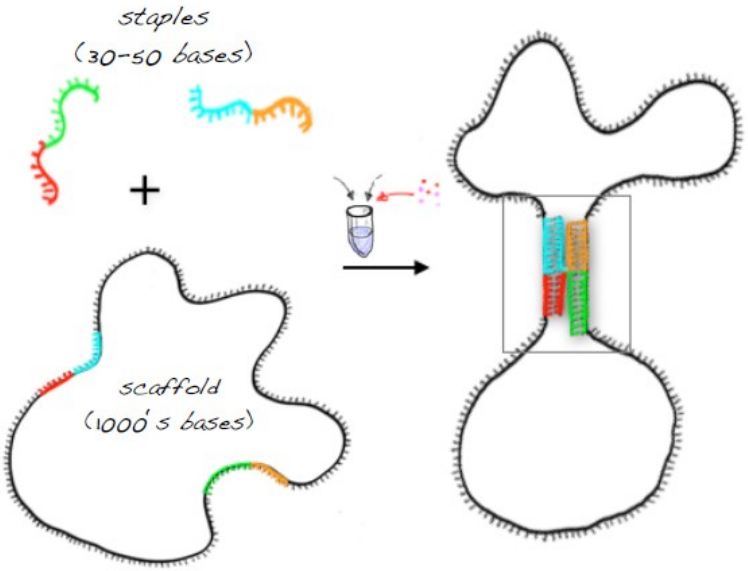

Figure 5 – Short staple strands bind to the long, continuous scaffold molecule

Through the appropriate design of many staple sequences, the scaffold can be programmed to fold into 2-D and 3-D structures of great complexity. In the last decade there have been numerous publications showing the creation of such 2-D and 3-D DNA origami structures (Figure 6) [20] [21] [22] [23].

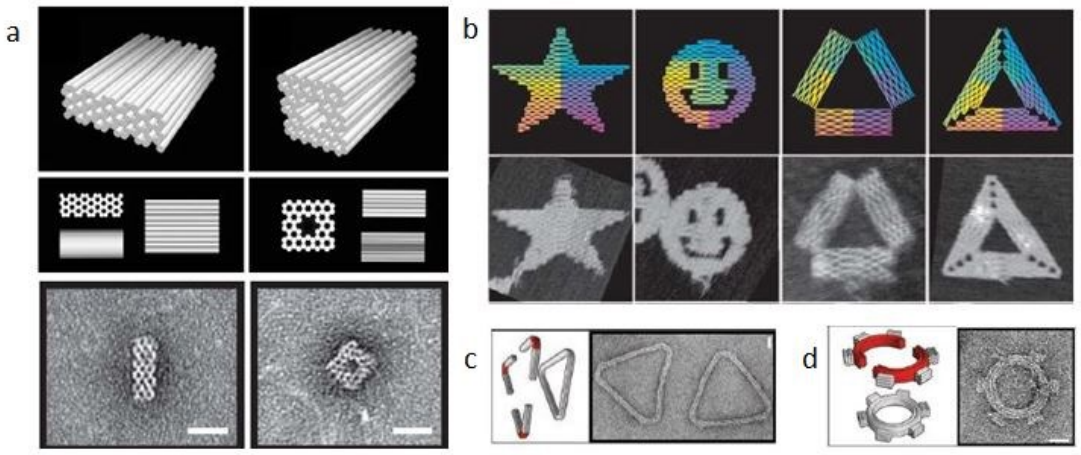

Figure 6 – 2D and 3D object built with scaffolded DNA origami. A) 3D multilayer, honeycomb lattice rectangular box and rectangular tube [18]. B) Single layer DNA origami shapes [16]. C) A DNA origami triangle assembled from three 3x6 helix bundles with a 120° angles. D) A 6 tooth nano-gear assembled from two halves.

As can be imagined, performing this design process by hand is tedious and fortunately unnecessary thanks to the development of a DNA origami CAD software called caDNAno [21] [24]. caDNAno facilitates the DNA origami design process by generating staple sequences at the click of a button, after designing a structure.

The first step in DNA origami structure design is to route the scaffold through every helix of a planned DNA origami structure in a raster style [20] [21] [24] (Figure 7a). Once a

scaffold routing has been planned it is necessary to know the sequence of the scaffold. Although shorter [20] or longer [25] scaffolds can and have been used, this work uses the single-stranded M13mp18 bacteriophage genome [20] [21] [25]. This genome is naturally 7,249 bases long, but derivations of this genome can be as long as 8,064 bases and are readily available from New England Biolabs or Tilibit Nanosystems. The scaffold sequence ultimately defines the sequence of each of the short staple strands. The staple strands are routed through the structure along the scaffold. Staples are routed to cross over from helix to helix to add stability to the finial structure (Figure 7b). Both scaffold and staples must also be routed in a manner that prevents any geometric inconsistencies in the structure. For example, geometric inconsistencies can arise if the scaffold is routed as if it were not a single loop of DNA or if cross overs are forced in the wrong locations along the dsDNA helices.

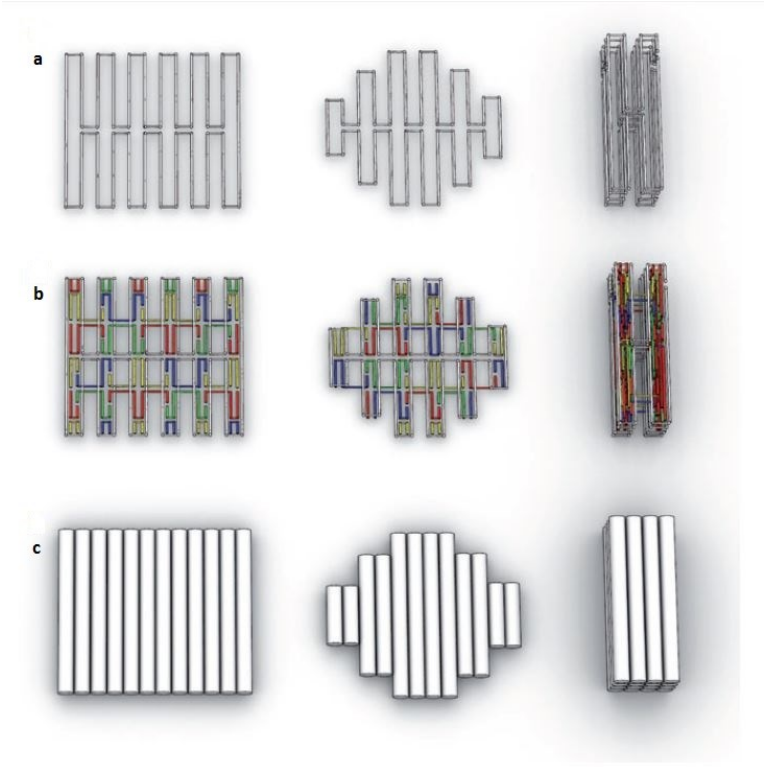

Figure 7 – DNA Origami Scaffold and Staple Design. A) Raster style scaffold routing, b) routing staples along designed scaffold route, c) Cylindrical approximation of final structure shape [17].

In DNA origami structures, helices of dsDNA are connected to other, adjacent helices of dsDNA through numerous immobilized Holliday junctions in which a staple or the scaffold 'crosses over' from one double helical domain to a neighboring antiparallel double helical domain [20] [21] [22] [24]. The presence of these antiparallel cross overs causes bowing of the dsDNA between crossovers due to effects from electrostatic repulsion and the position of the cross over with respect to the proximity of the target helix of DNA. The possible locations of these crossovers are well defined because of the structure of double helical DNA molecules occurring when the backbones of one half of

the duplex DNA within adjacent helices are as close as possible [24]. The point at which the backbones of two adjacent pieces of DNA are at their closest varies depending upon the cross sectional lattice structure; square or honeycomb [21] [22] [23]. In a honeycomb lattice each double helical domain can have up to 3 adjacent neighbors in three fold symmetry [21] [22]. In a square lattice each double helical domain can have up to four neighboring helices with four fold symmetry [21] [23]. Geometrically, in a honeycomb lattice of B-form DNA, adjacent helices can be attached via staple or scaffold cross with a three-fold symmetry [22]. This translates to a helix of dsDNA encountering a binding location to an adjacent helix of dsDNA every 7 base pairs or 2/3 turns (240^{o}) [21] [22]. Accordingly, the same two adjacent helices can be joined via cross overs every 21 base pairs (i.e. two full turns or 720^{o}). In a square lattice of B-form DNA, a staple strand is positioned for a crossover to an adjacent helix every 8 base pairs or 0.75 turns and can cross over to the same adjacent helix every 32 bases [23]. Figure 8 shows examples of potential staple cross overs for simple 3D box shaped DNA origami for both the square lattice and the honeycomb lattice.

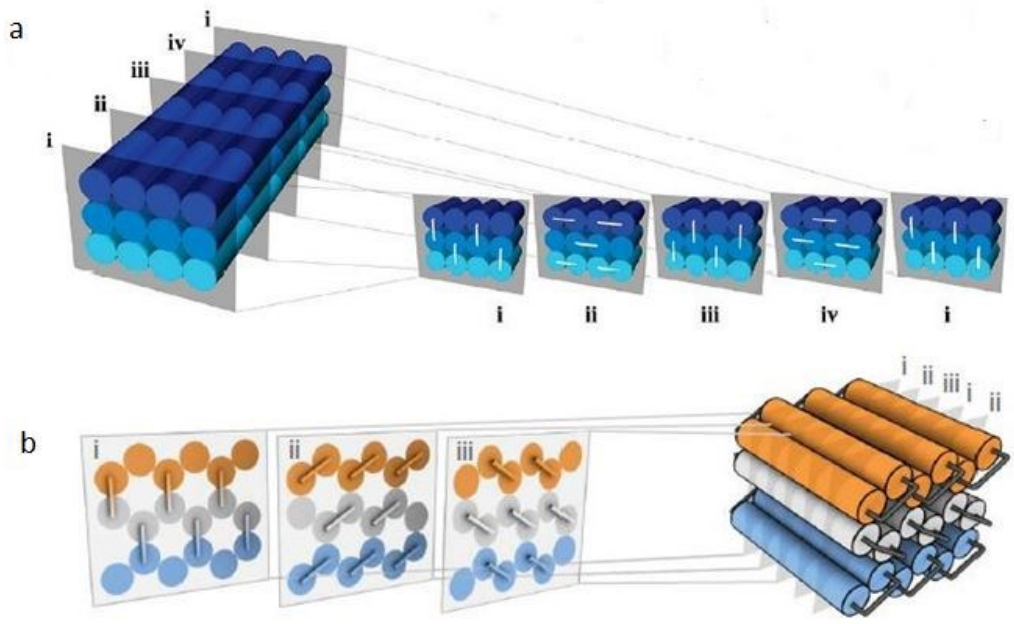

Figure 8 – Potential cross over locations in square (a) and honeycomb (b) lattice DNA origami structures. Cross sectional diagrams occurring every 8 base pairs for the square lattice and every 7 base pairs for the honeycomb lattice are numbered using roman numerals

caDNAno, the software used to define the sequence of staples allows users to create a two dimensional representation of both two and three dimensional structures by showing the locations and connections of staple cross overs [21] [24].

The production of static DNA origami structures is well documented and examples of such structures can be seen in Figure 6 – 2D and 3D object built with scaffolded DNA origami. A) 3D multilayer, honeycomb lattice rectangular box and rectangular tube [18]. B) Single layer DNA origami shapes [16]. C) A DNA origami triangle assembled from three 3x6 helix bundles with a 120° and Figure 7 – DNA Origami Scaffold and Staple Design. A) Raster style scaffold routing, b) routing staples along designed scaffold route, c) Cylindrical approximation of final structure shape [17]. Currently, most DNA

structures utilize either structural dynamics to achieve functionality [26] [27] or rely on the incorporation of secondary static molecules for functionality [19] [28] [29]. Dynamic DNA origami structures have been created by creating locally flexible regions through the strategic placement of ssDNA in the otherwise mechanically stiff, dsDNA structure, thus creating single or multiple degrees of freedom (**Error! Reference source not found.**) [30]. In addition to creating dynamic structures with design limited ranges of motion and degrees of freedom, Marras et al. achieved programmable motion of DNA origami mechanisms through a distribution of short sequence DNA-DNA interactions that acted like a zipper, forcing a DNA origami Bennett linkage into a higher energy configuration. Zhou et al. created DNA origami that had regions of planned compliant areas such that structural configuration and mechanical properties could be tuned by making very small changes to lengths of built in ssDNA scaffold loops (Figure 9) [26].

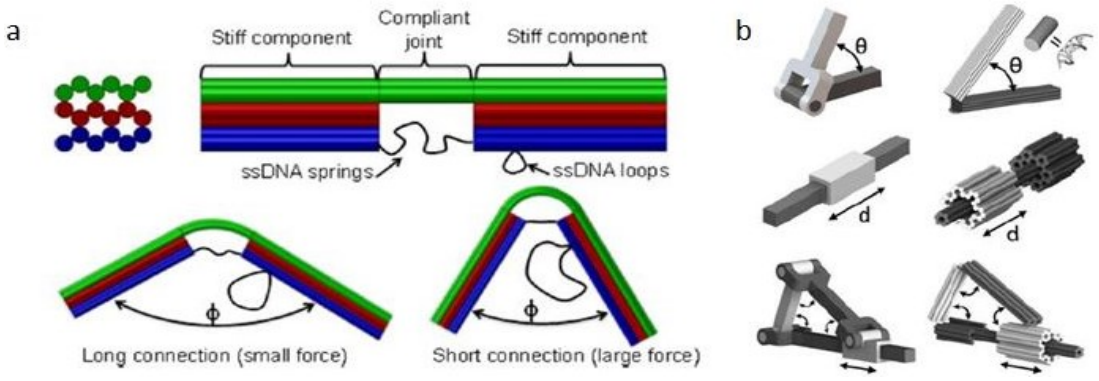

Figure 9 - Compliant and Dynamic DNA Origami Nanostructures. (a) a compliant joint bent by controlling the length of scaffold loops. (b) Three DNA origami structures designed after macroscale mechanisms with labeled motion.

There are multiple examples of storing mechanical energy in DNA nanostructures in addition to compliant deformation and distributed DNA binding actuation including pre-stressed DNA origami tensegrity structures [31] and i-Motif quadruplex compaction translated into cantilever bending motion [32]. In addition to providing functionality by storing mechanical energy when in higher energy structural configurations, techniques are widely available to integrate secondary molecules into DNA origami structures to provide functionality to structurally static nanostructures. The functionalization of DNA origami structures with secondary molecules has been demonstrated by Sacca et al. in the orthogonal patterning of the surface of DNA origami structure with functional proteins [33] and by Bui et al. in the incorporation of STV-biotin molecules to bind quantum dots into periodic arrays [34]. In these studies, chemically labeled DNA was required to interact with the secondary molecules in order for said molecules to attach. Methods for chemically labeling DNA oligomers are well defined [35] and most labeling schemes are commercially available.

Introduction to Research

It has been demonstrated in current publications that DNA origami nanostructures can be designed to achieve limited ranges of dynamic motion. It has also been shown that DNA origami nanostructures can be functionalized by integrating secondary molecules into the nanostructure. The research that is to be presented in this thesis demonstrates that in addition to using DNA-DNA interactions to achieve programmable motion of dynamic DNA origami nanostructures, it is possible to use well-defined methods to incorporate secondary molecules in order to achieve programmable and tunable control over DNA origami nanostructures. This study on controlling the dynamics of DNA origami structures involves integrating molecules of interest into three well folding structures. These structures include a dynamic DNA origami hinge (Figure 9a), a DNA origami raft called the ligand presentation platform (Figure 9b), and a flexible 10 Helix Bundle (Figure 9c). The particles to be integrated and the method of control over dynamics or motion varies with each structure and will be discussed in greater detail along with the design of each of these structures in Chapter 2 sections 2 to 5. As a note, all DNA is purchased from Sigma-Aldrich or Eurofins. All scaffold DNA is synthesized by the Nanoengineering and Biodesign Lab.

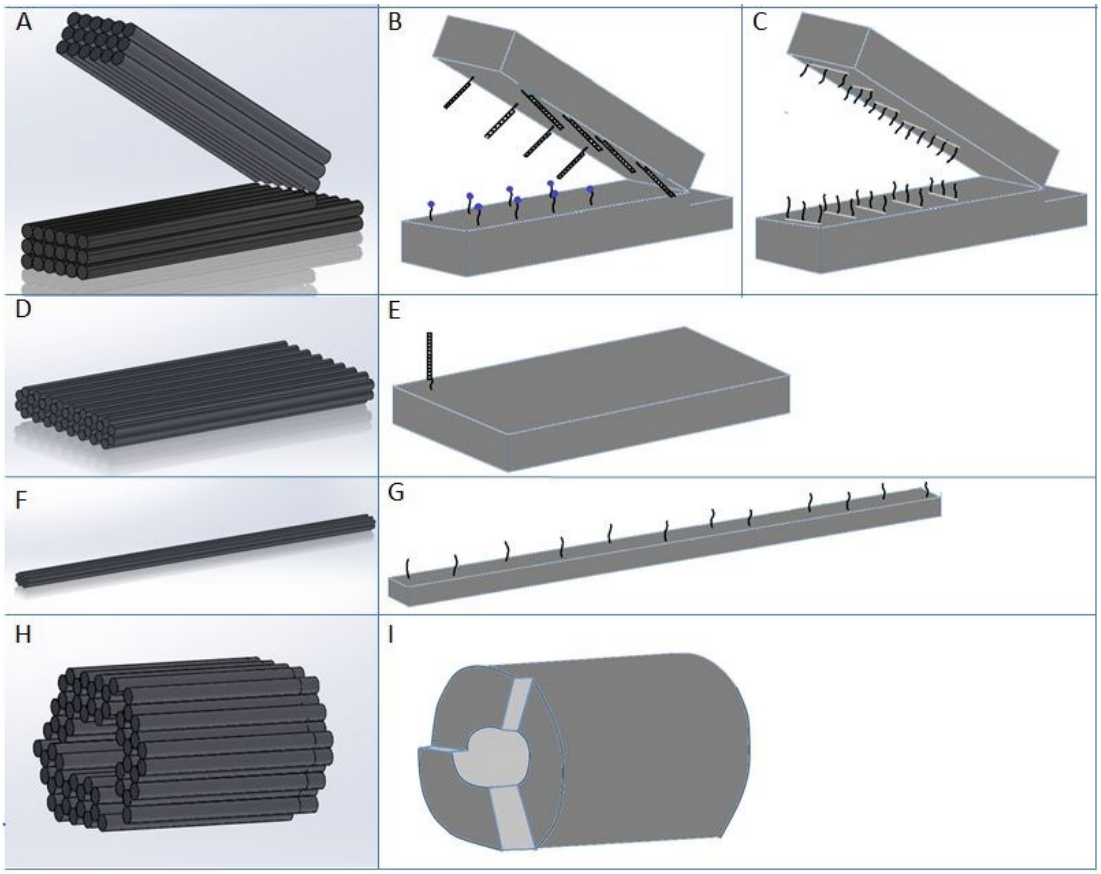

Figure 10 – Cylinder models of A) DNA Origami Hinge, B) with 8 potential protein bind sites, C) with 30 potential nanoparticle bind sites, D) DNA Origami platform E) with protein recognition sequence bind site, F) 10 Helix Bundle G) with 12 nanoparticle bind sites (high density overhangs on bottom of structure in (E) and (G) and on the ends of (I) are omitted.

Chapter 2: Fabrication of DNA origami nanostructures

A discussion of the protocols used to fabricate, purify, and image DNA origami nanostructures is presented in this chapter. Once the design process has been completed and all necessary staples and scaffold is available, one can fabricate DNA origami nanostructures via molecular self-assembly. The following is a summary of the protocols used to create, purify, and image the DNA origami structures that will be discussed in later chapters.

Folding Reactions

The reactions in which DNA origami structures undergo a self-assembly process and fold into the designed structure are thermal ramps. A mixture of scaffold and staple DNA are heated to 65°C and then cooled slowly over long time periods. The components of the folding reaction are shown in Table 1 - Folding Reaction Components

Components	**[µl]**
Scaffold @ 100 nM	**10**
Staples @ 500 nM	**20**
10x FOBXM (50mM TRIS, 10mM EDTA, 50mM NaCl)	**5**
ddH20	**10**
10x MgCl2 Mastermix	**5**
TOTAL	**50**

Table 1 - Folding Reaction Components

The staples and scaffold[1] are combined in a fixed stoichiometry into a stabilizing buffer called FOBXM, and a 10*[final concentration] $MgCl_2$ solution. A screen of magnesium concentrations is required for each newly designed structure. The magnesium in the

[1] The scaffold is suspended in 1xTE buffer which is 1mM EDTA and 5mM Tris. The staples are suspended in double distilled H20 (ddH20) from Eurofins.

folding reaction solution is a divalent ion responsible for contributing a charge shielding effect on the duplex DNA [21]. Charge shielding is necessary because of electrostatic repulsion between closely spaced, negatively charged DNA can prevent annealing of duplex DNA. Typical ranges of magnesium concentration that are screened for structure folding are 10mM to 24mM. The protocol used in the Nanoengineering and Biodesign Lab screens magnesium from 10mM to 24mM in steps of 2mM. A Biorad thermal cycler was used to heat each of the reactions to 65° and cool at the rate outlined in Figure 11 below.

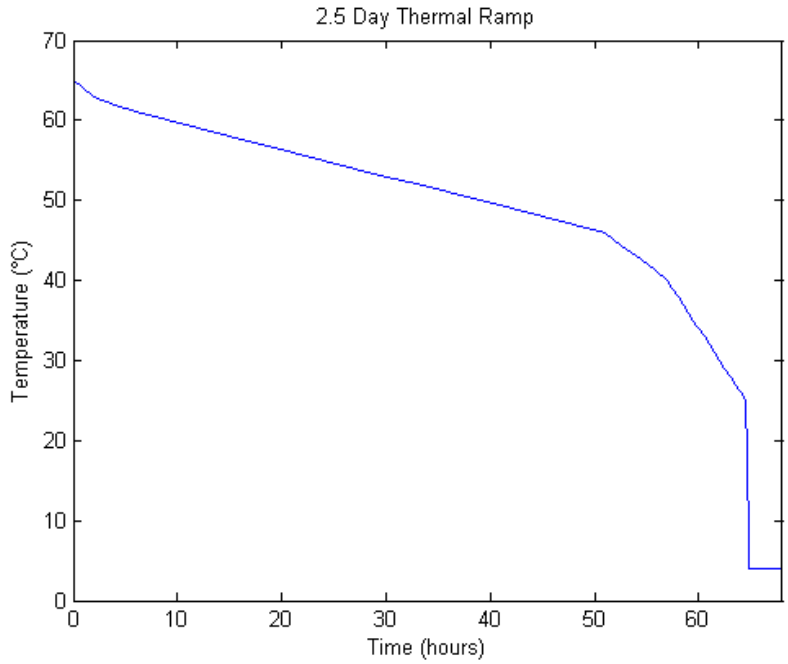

Figure 11 - Plot of Temperature vs Time for the 2.5 day thermal ramp

The ramp shown takes ~2.5 days to complete. Upon the completion of the thermal ramp there will be a mixture of well folded structures and various states of poorly folded structure. The newly folded DNA origami is stable at room temperature if the structures were well designed, but are typically stored at 4°C long term.

Purification and Yield Analysis

The structures are purified via 2% agarose gel electrophoresis containing 1xTAE (40mM Tris + 20mM Acetic Acid + 1mM EDTA), 11mM $MgCl_2$, and 1uM ethidium bromide (EtBr) to act as a nucleic acid stain. The structures are mixed with a Ficoll PM400 loading solution that increases the density of the sample liquid so that it will sink into the wells and no DNA has the opportunity to diffuse away into the gel running buffer. The gel is run at 70V for 4 hours in 0.5xTAE running buffer with 11 mM $MgCl_2$. The negatively charged DNA in the wells near the negative electrode is pulled through the gel towards the positive electrode. Running structures through the gel can separate them since smaller molecules move faster and further than larger structures due to hydrodynamic mobility through the gel. The entire gel rig is cooled by an ice water bath to prevent joule heating of the gel and running buffer. A typical gel running set up is shown in Figure 12 - Agarose Gel Electrophoresis Running Set Up.

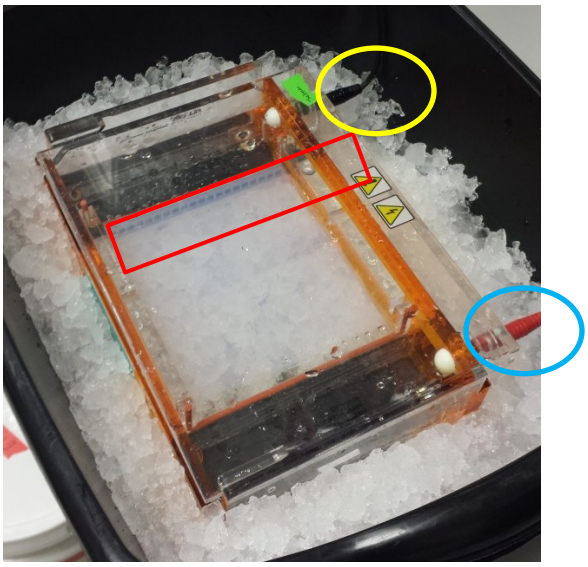

Figure 12 - Agarose Gel Electrophoresis Running Set Up. Wells are outlined in red, negative electrode is circled in yellow, positive electrode is circled in blue

Once the gel run has been completed, the gel can be imaged on a UV light table. The UV light induces fluorescence of EtBr molecules. The fluorescence of EtBr is 25 fold more intense when the molecules are bound to dsDNA than when in solution [36]. A typical fluorescent gel image is shown below in Figure 13.

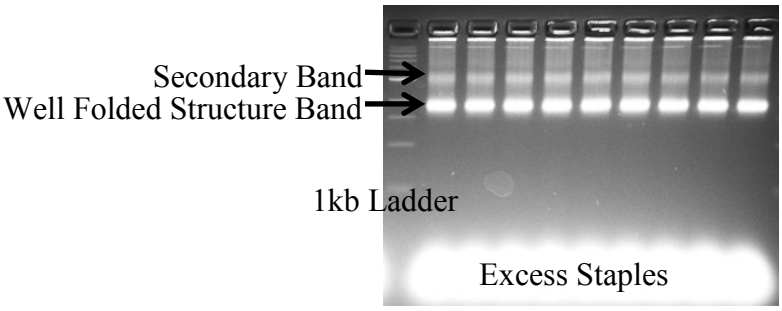

Figure 13 - Ethidium Bromide Stained DNA Origami Electrophoresed in a 2% Agarose Gel

As can be seen in this image most samples are not homogenous and contain multiple species of the desired structure. These other species appear in agarose gels as secondary bands. The well folded structures are contained within the leading band in a gel lane because well folded structures will be the most compact of all the species of structures in the sample and therefore move the fastest through the gel. The excess of staples appears in the form of a bright smear on the gel in front of the leading band. Bands of interest can be cut out of the gel for later imaging and experimentation. The structures are removed from the agarose through a centrifugal filter tube. The resulting 20uL to 50uL of 0.5xTAE + 10mM $MgCl_2$ contains the purified structures suspended in solution. Typical molar yield of a folding reaction and subsequent agarose gel electrophoresis purification can range from 1nM to 5nM of well folded structure.

In addition to electrophoresis, DNA origami nanostructures can be precipitated out of solution through the addition of a solution of 15% PEG 8000, 5mM Tris, 1mM EDTA, and 500mM NaCl [37]. The contents of a self-assembly reaction in solution are combined in a 1:1 ratio and mixed thoroughly. The sample is then centrifuged at 16000g at room temperature. The DNA origami structure aggregates in a pellet that sticks to the bottom of the sample tube. The supernatant is pipetted off and the sample is resuspended in a desired buffer. PEG purification does not separate different forms of structures (poorly folded vs well folded) but rather uses the depletion of high molecular weight molecules through excluded volume effects that arise from using PEG polymers as a crowding agent (Figure 14). It does allow for removal of excess staple strands.

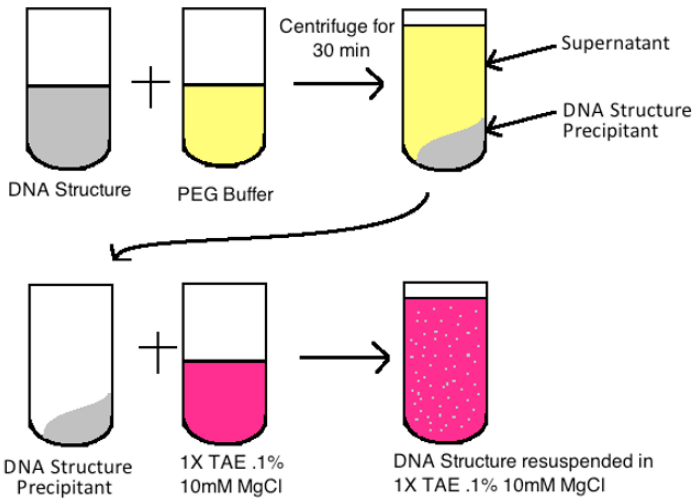

Figure 14 - PEG 8000 Precipitation of DNA Origami Structures

Imaging DNA Origami Nanostructures

Once structures have been folded and purified, they can be imaged via a transmission electron microscope (TEM) or an atomic force microscope (AFM). The Nanoengineering and Biodesign Lab typically images using a FEI Tecnai G2 Bio TWIN TEM at The Ohio State University Campus Microscopy & Imaging Facility. A Formvar carbon film on 400 mesh copper grid purchased from Electron Microscopy Sciences is glow discharged for 45 seconds. A 4uL drop of sample containing structure is deposited onto the glow discharged side of the Formvar grid. The droplet is left on the grid for 4 minutes. A 10uL and 20uL droplet of 2% Uranyl formate (UFo) solution is deposited onto a clean surface when less than 1 minute of sample incubation time remains. UFo will crystalize at a higher rate when exposed to light and so should be protected from ambient or direct light for as long as possible. UFo is used to negatively stain structures

that have been deposited onto a Formvar grid. The structure sample is wicked off of the grid by touching the edge of the grid to a small piece of filter paper. The 10uL drop of UFo is picked up by touching the face of the grid that the structure droplet was on to the droplet of UFo sitting on the clean surface. The grid is kept upside down and touched to the filter paper again to wick away the 10uL UFo droplet. The 20uL UFo droplet is picked up in the same way the previous droplet and the sample is allowed to sit upside down with the droplet of UFo on the grid for 40 seconds. It is important to leave the grid and droplet with the sample side down to prevent deposition of large UFo crystals onto the imaging surface. The droplet is wicked away by touching the edge of the grid to a piece of filter paper. The grid is allowed to dry upside down and the put into a grid case for transport to the TEM.

Rapid Folding of DNA Origami

Recently, steps have been made at shortening the time scale of folding reactions from days to hours [38]. This rapid fold process involves heating the folding reaction components listed in Table 1 - Folding Reaction Componentsto 65° C to allow for complete unfolding of any duplex DNA. The reaction is then cooled to a specific threshold temperature and then held at that temperature until folding is complete. Sobczak et al. showed that holding these reactions at the correct temperature for 2 hours generated 9 fold higher yields of well folded structures. The proper folding temperature of a designed structure is found by heating identical folding reaction components to 65°C followed by cooling them to a range of constant temperatures. Based upon literature, the

temperature range tested for the structures to be discussed is 42°C to 58°C for 4 hours. In some cases, however, the range tested was more fine because 42°C to 58°C showed inconclusive results for an exact temperature. Folding quality of each reaction is then assessed side by side on a 2% agarose gel using the homogenous scaffold as a control. Figure 15 - Rapid Fold Threshold Temperature Determination. Two structures were folded and melted at a range of constant temperatures to identify folding threshold temperature of A) 51°C and B) 49°C. shows two structures and images of an agarose gel showing samples from each constant temperature in a range. A clear jump in band speed emerges and intensity of the new leading band increases to some max at some temperature.

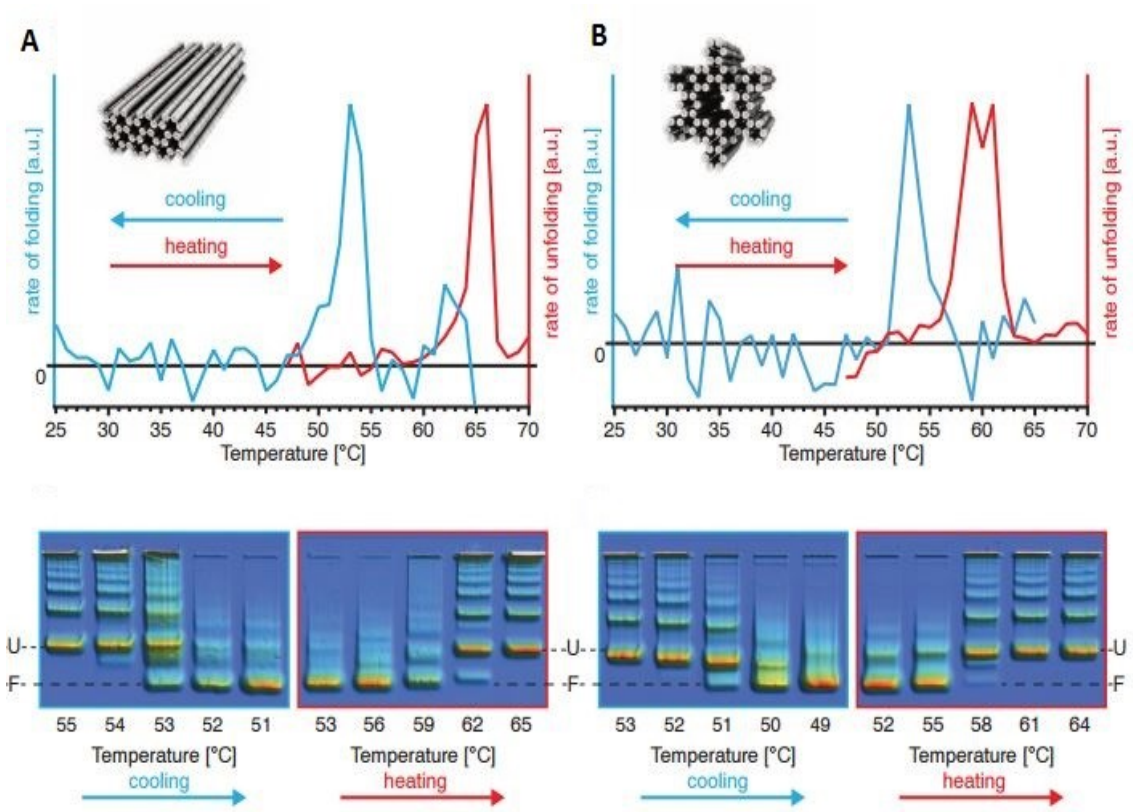

Figure 15 - Rapid Fold Threshold Temperature Determination. Two structures were folded and melted at a range of constant temperatures to identify folding threshold temperature of A) 51°C and B) 49°C.

DNA Origami Hinge

This DNA origami nanostructure is made up of two 6x3 helix square lattice bundles connected together by regions of unbound single stranded scaffold DNA (Figure 16). The length of the scaffold used in this design is 8064 bases long. One bar of the hinge is extended beyond the single stranded attachment point to the second bar of the hinge to act as a stopper and limit the angular distribution of the hinge. The structure used in this work is a modified version of a well-studied DNA origami hinge discussed at length by Marras et al [30].

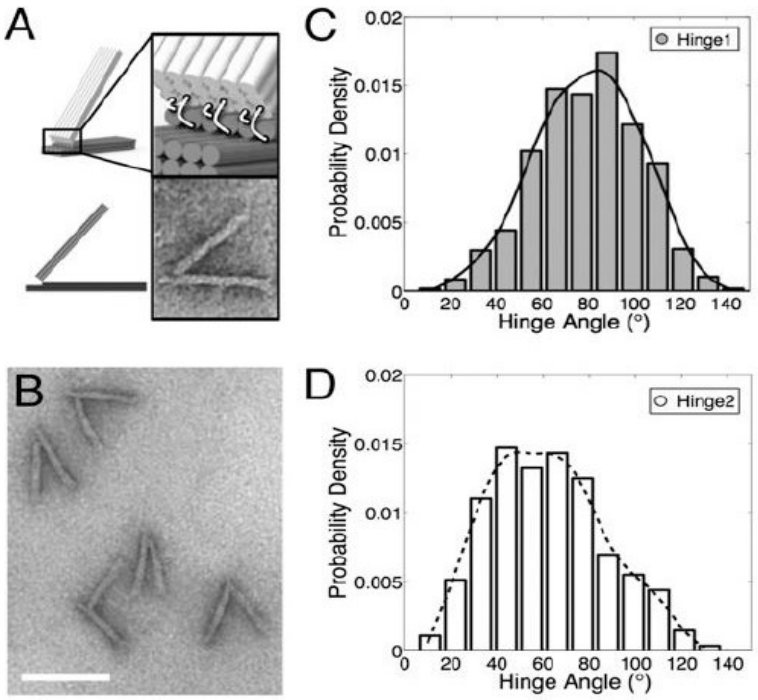

Figure 16 - DNA Origami Hinge adapted from Marras et al. A) Cylinder representation of structure showing ssDNA joint. B) TEM image of well folded hinges C) Probability distribution for hinge angle of hinge with a shorter (16nt) ssDNA joint. D) Probability distribution for hinge angle of a hinge with a longer (30nt) ssDNA joint. [30]

General Design

From previous research the hinge structure was very well defined and studied [30] which made it an excellent candidate for studies on tunable dynamics using integrated components as a latch to close the hinge. The new version of this hinge was to contain DNA overhangs that would contain specific sequences for the attachment of secondary molecules. Tuning the dynamics of this system is possible through the integration of multiple binding locations at various distances from the single stranded hinge joint. By moving the incorporated molecule away from the flexible connection between hinge arms, the local concentration of available binding locations for the secondary molecules decreases substantially indicating that the closing of hinges will occur with less frequency. The software caDNAno was used to generate a staple list to build this new structure [24] and the caDNAno staple routing and cross section can be seen in Appendix 5.1

Appendix A: caDNAno Scaffold and Staple Routing Images. Two different designs were created, both using a scaffold that is 8064 bases long. Design 1 contains 188 staples and has integrated binding locations for an *E.Coli* transcription repressor protein called LexA. Design 2 contains 189 staples and was to contain attachment locations for Azobenzene modified ssDNA labeled onto gold nanoparticles. These particles are intended to act as a 'latch' on the hinge and minimize the angle between hinge arms. An in depth discussion of each of these molecules and their structure is to come.

Both designs were determined to fold well in a 2.5 day thermal ramp as shown in Figure 11 - Plot of Temperature vs Time for the 2.5 day thermal ramp. The hinge was folded in a 2.5 day long thermal ramp, at a range of $MgCl_2$ concentrations, and was purified via agarose gel electrophoresis and then imaged via TEM which can be seen in Figure 17 and Figure 18 respectively.

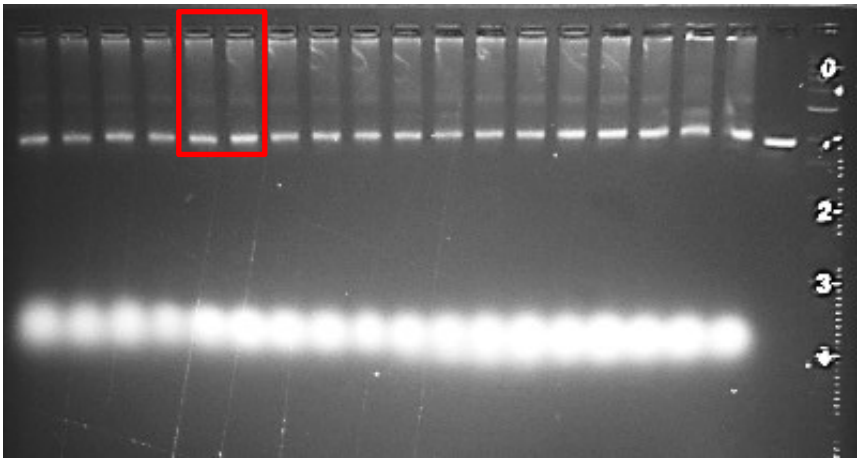

Figure 17 - Agarose Gel of folding MgCl2 Salt Screen; there are two lanes of each sample and from right to left the Mg concentrations are 6mM, 8mM, 10mM, 12mM, 14mM, 16mM, 18mM, 20mM, and 22mM.

This gel shows that the best folding of the hinge in the 2.5 day ramp occurs at 18mM $MgCl_2$ (outlined in red in Figure 15). The leading band of the 18mM $MgCl_2$ was excised and imaged via TEM. The image can be seen in Figure 18 - TEM image of DNA Origami Hinge

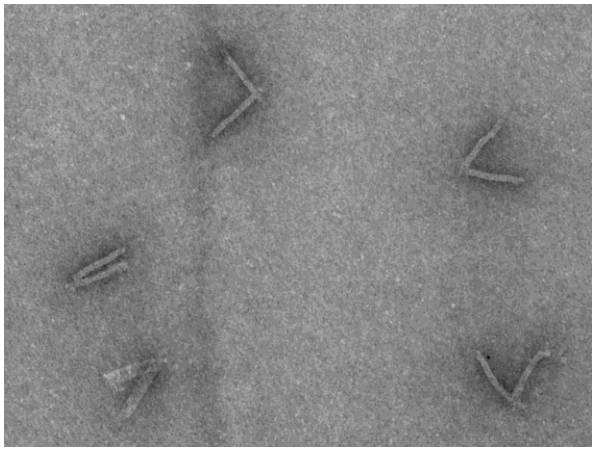

Figure 18 - TEM image of DNA Origami Hinge

Based upon the results of the 2.5 day folding ramp, 18mM $MgCl_2$ was used to determine the rapid fold threshold temperature. Eight folding reactions were subjected to different thermal ramps in which the samples are heated to 65°C for 10 minutes and then cooled to a specific temperature ranging from 45°C to 52°C for 5 hours. The agarose gel showing the contents of each thermal ramp can be seen in Figure 19.

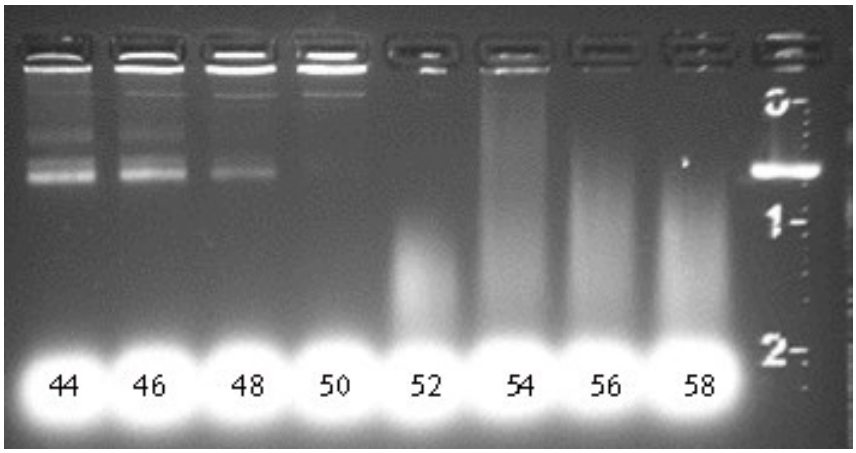

Figure 19 - Hinge Rapid Fold Threshold Temperature Optimization Gel

Based upon the images, the hinge will be folded at a threshold temperature of 50°C in 18mM $MgCl_2$.

LexA Attachment Scheme

This structure was designed to contain a binding location for an *E.Coli* transcription repressor protein called LexA. This naturally occurring protein has a well-documented involvement in mounting a cellular response to DNA damage in *E. Coli* [39]. LexA was selected for this work because it has a high affinity for its recognition sequence and because our collaborators have experience working with the protein [40]. LexA is a dimeric protein containing 202 amino acids. It is comprised of two monomeric sections linked by a flexible region. Each monomer has a COOH-terminal domain which is the area of dimerization and a NH_2-terminal domain which binds selectively to operator dsDNA sequences or recognition sequences. Dimer LexA has a molecular weight of 25kDa. The binding kinetics of LexA binding with multiple recognition sequences are

very well defined [41]. For the extent of this work, the recognition sequence that is used to bind LexA is the double stranded RecA sequence and is, from 5' to 3', TACTGTATGAGCATACAGTA. The dissociation constant of the protein to this specific sequence is 0.07 nM and a bound 'on' time of 5 minutes in 130mM NaCl [42]. These studies have indicated that the dissociation constant is highly correlated to Na+ concentration in solution.

The control over the dynamics of the structure will be achieved by using the protein LexA as a lock. By placing the double stranded recognition sequence as an overhang on the shorter bar of the hinge the LexA protein will bind specifically to the duplex recognition sequence. In order to get LexA to bind to the other bar of the hinge, the protein structure is modified via mutagenesis to LexA(S171C) by using a Quickchange site directed mutagenesis kit from Agilent Technologies. Site directed mutagenesis was also used to insert cysteines in to the dimerization domain of LexA. TCEP was used to break any disulfide bonds between the cysteine molecules and a commercially available biotin-maleamide was mixed with the modified LexA(S171C) at a 200 fold excess. Excess biotin was purified by gel filtration chromatography and labeling efficiency was found to be 40% using mass spectrometry. This LexA-biotin conjugate molecule would then attach to a streptavidin molecule attached to the DNA origami structure. This attachment scheme is shown in Figure 20.

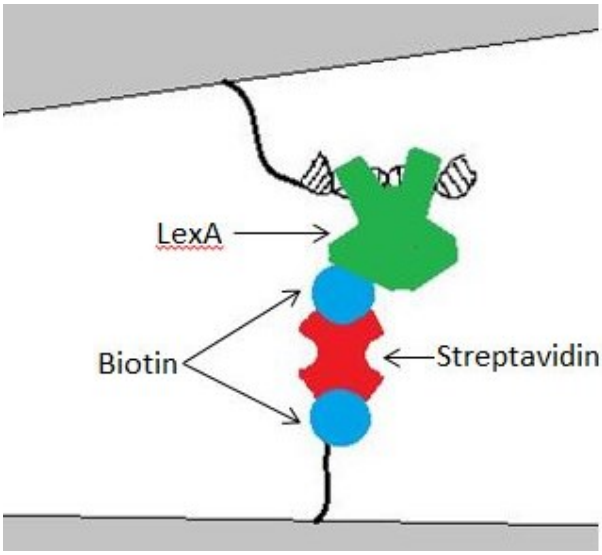

Figure 20 - LexA Binding Scheme. Grey area indicates DNA origami structure. The biotin (blue) labeled LexA (green) can be seen bound to streptavidin (red) which is bound to a biotinilated ssDNA oligomer.

Multiple attachment sites were incorporated into the design of the structure (Figure 10). Each attachment location contains the double stranded recognition sequence on the upper and shorter bar of the hinge and a biotin labeled ssDNA overhang coming out of the bottom bar of the hinge. The caDNAno staple and scaffold routing schematics as well as cross section shapes can be seen in Appendix A.

As was stated above, the recognition sequence that is being used is a modified version of the RecA sequence. The RecA sequence, itself is a reverse complementary palindrome. This sequence as ssDNA forms a very high affinity hairpin with a melting temperature of 62°C - 66°C [39]. Although this temperature is below the maximum temperature of the folding reaction thermal ramp of 65°C, because the ssDNA oligomer is complementary to itself, the local concentration of complementary DNA is very high

so hairpin formation is very likely. In order to facilitate the formation of a duplex recognition sequence, random 10 base pair long sequences were added on both the 3' and 5' end of the recognition sequence. The additional bases help to ensure that the 40 base pair long duplex sequence containing the recognition sequence has a higher melting temperature than the hairpin of the recognition sequence. The new melting temperature of this modified recognition sequence hairpin is 52.5°C and the melting temperature of the fully complementary 40 base pair long duplex sequence is 73.4°C. Pictorial representations of these hairpins can be seen in Appendix 5.3 - . This will facilitate the folding of the desired configuration before hairpin formation during the folding reaction. This will ensures that the duplex recognition sequence will be one of the first regions of the structure to form. In order to optimize the formation of this binding location the two oligomers making up the complementary strands of the correctly folded recognition sequence were run through multiple thermal ramps and then the binding was assessed by running products on a polyacrylamide gel. Multiple bands emerged from each folding ramp. The fastest band in this gel lane would correspond to the correctly folded duplex DNA. The optimization of a folding ramp that will anneal this recognition sequence was carried out. The thermal ramps tested can be seen in Figure 21 - Various Rapid Fold Ramps to Test Recognition Site Annealing.

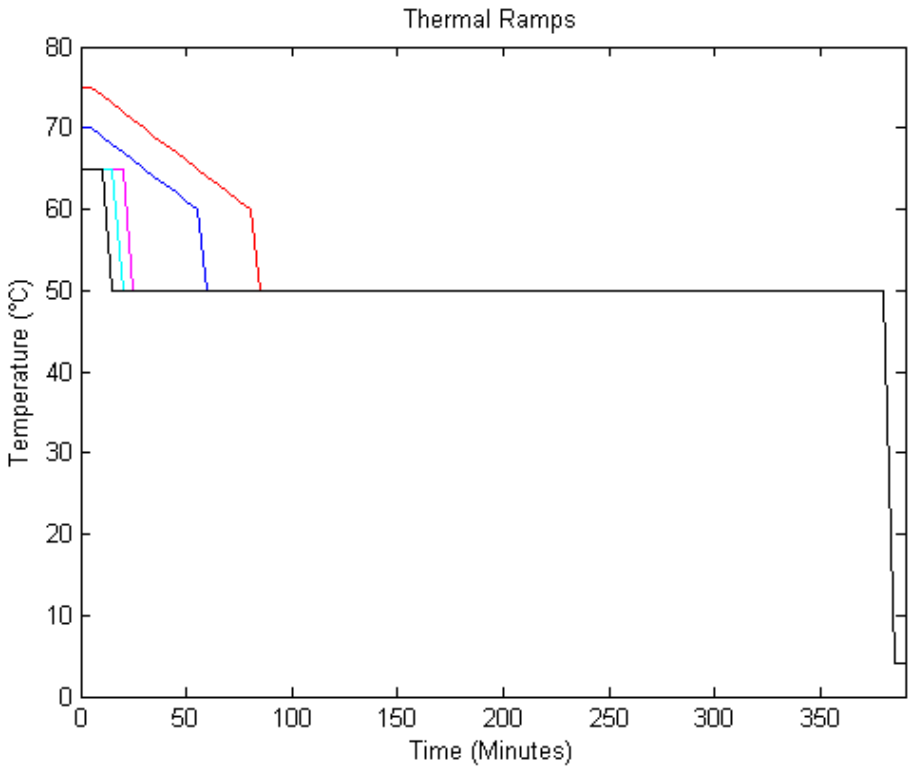

Figure 21 - Various Rapid Fold Ramps to Test Recognition Site Annealing

The figure above shows 5 thermal ramps all with slightly different high temperature ranges. The first ramp is shown in black and matches the successfully defined rapid fold thermal ramp for the hinge and keeps the hinge at 65°C for 10 minutes then cools to 50°C for 5 hours and will be called '65-ten-50'. The second ramp is shown in cyan and keeps the sample at 65° for 15 minutes then cools to 50°C for 5 hours and will be called '65-fifteen-50'. The third ramp is shown in purple and keeps the sample at 65° for 20 minutes then cools to 50°C for 5 hours and will be called '65-twenty-50'. The fourth ramp shown in blue heats the sample to 70°C then cools it at the rate of 1° every 5 minutes until it reaches 60°C then drops immediately to 50°C for 5 hours and will be

called ‘70-60-50’. The fifth ramp shown in red, heats the sample to 75°C and cools it at a rate of 1°C every 5 minutes until it reaches 60°C then drops immediately to 50°C for 5 hours and will be called ‘75-60-50’. The two oligomers comprising the recognition sequence to be incorporated into the hinge structure were annealed in each of the 5 thermal ramps shown above. Oligomer A is 83 bases long and oligomer B is 40 bases long and labeled with Cy3 fluorophore[2] to facilitate visualization of annealing. The newly annealed sample was run through a 5% polyacrylamide gel at 5nM and then imaged on a Typhoon FLA 9000 on the 570nM channel. The gel image can be seen below in Figure 20.

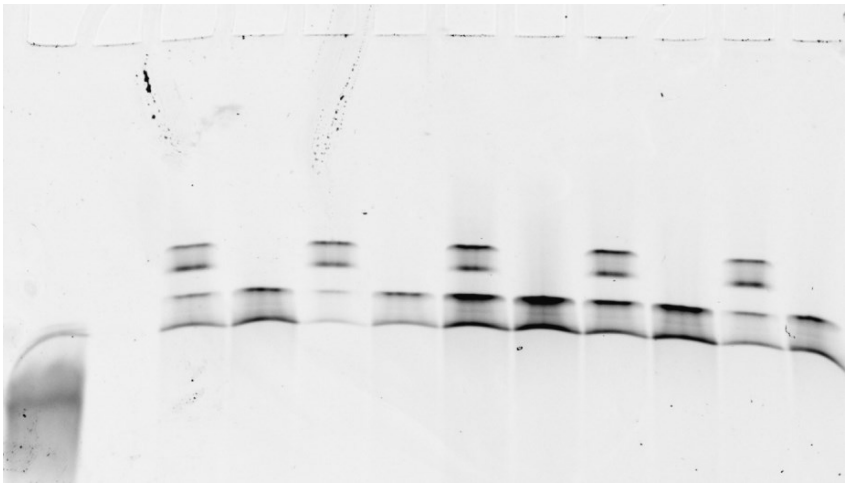

Figure 22 - PAGE Gel Image of Recognition Sequence Duplex Formation Optimization

In the image above, the samples in each lane from left (1) to right are shown in Table 2.

[2] Cy3 has an excitation peak of 550nm and an emission peak of 570nm.

Lane	Oligo A Conc	Oligo B Conc.	LexA Conc.	Ramp Description
1	5nM	5nM	0nM	Room temperature for 5 hours
2	empty			
3	5nM	5nM	10nM	75°C - 1°/5minutes - 60°C - 50°C 5 hours
4	5nM	5nM	0nM	75°C - 1°/5minutes - 60°C - 50°C 5 hours
5	5nM	5nM	10nM	70°C - 1°/5minutes - 60°C - 50°C 5 hours
6	5nM	5nM	0nM	70°C - 1°/5minutes - 60°C - 50°C 5 hours
7	5nM	5nM	10nM	65° for 10 minutes - 50°C 5 hours
8	5nM	5nM	0nM	65° for 10 minutes - 50°C 5 hours
9	5nM	5nM	10nM	65° for 15 minutes - 50°C 5 hours
10	5nM	5nM	0nM	65° for 15 minutes - 50°C 5 hours
11	5nM	5nM	10nM	65° for 20 minutes - 50°C 5 hours
12	5nM	5nM	0nM	65° for 20 minutes - 50°C 5 hours

Table 2 – PAGE Gel Contents

The fluorescent gel image shown in Figure 22 shows that all of the DNA samples without LexA contain two DNA bands. This indicates that there are 2 stable configurations of oligomer A and oligomer B. Because of the strength of base pairing reactions, calculated melting temperature of the hairpin in the recognition sequences, and the presence of equimolar concentrations of each oligomer allow the conclusion that a majority of the DNA in each sample is in double stranded configuration. The two configurations that could be adopted for double stranded DNA are 1) the 10 base pairs of DNA on either side of the recognition sequence anneal together leaving the recognition sequence in the hairpin orientation or 2) the DNA forms in the correct duplex configuration. This gel allows us to qualitatively compare the 5nM DNA sample to a sample with 5nM DNA and

10nM LexA. The most efficient LexA recognition sequence binding occurs in the sample in lanes 5 and 6. This is the ramp that we see the largest shift in intensity between leading bands of DNA and DNA-LexA samples. The next step was to test the folding of the hinge in each of the thermal ramps shown in Figure 21. The agarose gel image of each structure is shown in Figure 23 below. The samples in the gel below from left to right are: 75-60-50 ramp, 70-60-50 ramp, 65-twenty-50, 65-fifteen-50, 65-ten-50. The structures, if well folded will contain the Cy3 labeled oligomer B. The gel is imaged on the Typhoon FLA 9000 in the 570nm channel.

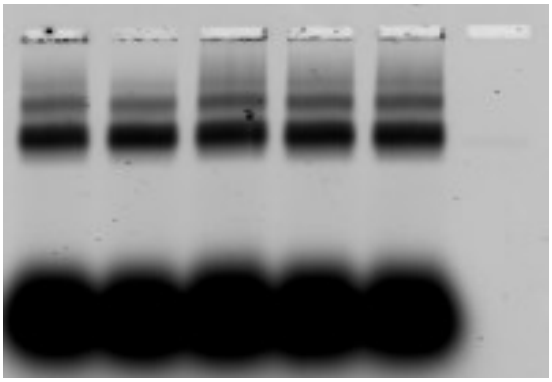

Figure 23 - Hinge Folding Confirmation in the Ramps Shown in Figure 19

As can be seen in Figure 23, the hinge will fold properly in each of the five ramps. The gel shows that the hinge that folded in the 70-60-50 (lane 2 from the left side of the gel) ramp has less material trapped in the well as well as a lower fluorescent intensity behind the slowest structure band in this lane. These results indicate that optimal folding for the hinge will occur at 18mM $MgCl_2$, at a threshold temperature of 50°C through the 70-60-

50 ramp. Transmission electron microscopy images in the Figure 24 confirm that these conditions give large yields of well folded structures.

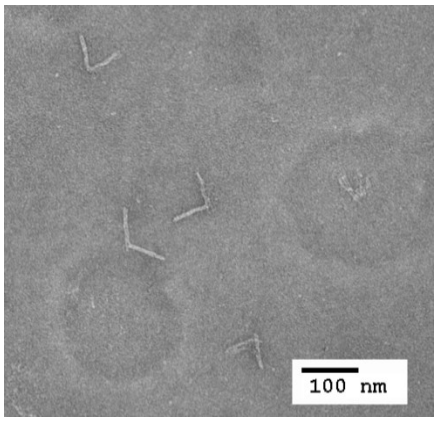

Figure 24 - Well Folded Hinges from 70-60-50 18mM MgCl2 Folding Reaction

Gold Nanoparticle Attachment Scheme

Gold nanoparticles are the second molecule of interest to be attached to the DNA origami hinge. Gold nanoparticles were chosen because of their potential to act as a localized heat source on the nanoscale [43]. Incorporating metallic nanomaterials into nanostructures to provide functionalization is well documented [34] [44]. The spatial control that DNA origami lends over metallic nanoparticles has applications in nanophotonics and nanoelectronics component construction [45].

The gold nanoparticles to be incorporated into the hinge are 5nM in diameter and purchased commercially from Nanocs. Through collaboration with Qirui Fan, a Ph.D.

candidate in Dr. Jessica Winter's lab in chemical engineering at the Ohio State University, the gold nanoparticles were covalently linked to the 5' disulfide bond on a 12 base long ssDNA oligomer. The disulfide bond is thiolated and the resulting thiol will readily bind to the gold nanoparticles in solution [46]. The ssDNA oligomer was also internally modified with 3 evenly spaced azobenzene molecules. Azobenzene is a photo-switchable molecule that will translate from the trans- conformation to the cis-conformation when exposed to UV light [47]. By attaching these molecules to the backbone of DNA, the trans-cis isomerization of azobenzene will disrupt the base pairing interaction of the nearest bases on either side of the azobenzene molecule [48]. These two orientations can be seen in Figure 25.

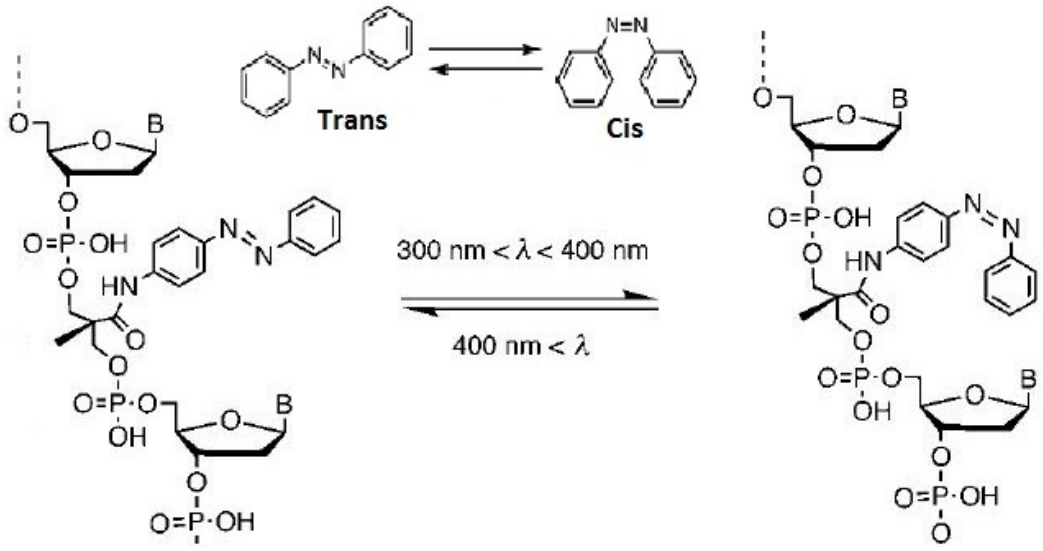

Figure 25 - Trans- to cis isomerization of azobenzene on DNA backbone [48].

The photo-switchablity of the incorporated azobenzene molecules provided control over nanoparticle binding through the application of UV light. The final product of the labeling of the gold nanoparticles is a 5nM diameter gold nanoparticle covered in a dense layer of azobenzene modified ssDNA.

In order to attach the nanoparticles to the hinge, 12 base long overhangs, that are complementary to the ssDNA attached to the nanoparticles, were placed along the interior surfaces of both arms of the hinge. The grid of potential bind sites is three overhangs across the width of the hinge arms and five down the length of the arms for a total of 15 available overhang locations on both the top and bottom arms of the hinge. Each overhang on one arms of the hinge has a corresponding overhang on the opposite arm such that a nanoparticle could bind to both overhangs and close the hinge. By selectively turning off these overhangs and changing the number of available nanoparticle bind sites in addition to the internal azobenzene modification control can be exacted over the fluctuations of the hinge.

Because the DNA origami structure for gold nanoparticle attachment (Hinge Design 2) changed very little from the DNA origami structure for LexA attachment (Hinge Design 1), the optimization of folding performed on design 1 was applied to design 2. This means that the gold nanoparticle hinge is folded in 18mM $MgCl_2$, at a threshold temp of 50°C and in the 70-60-50 thermal ramp. The structures were purified through gel electrophoresis and the imaged via TEM. Figure 26 shows the gel image and corresponding TEM image of well folded hinges containing the gold nanoparticle attachment overhangs.

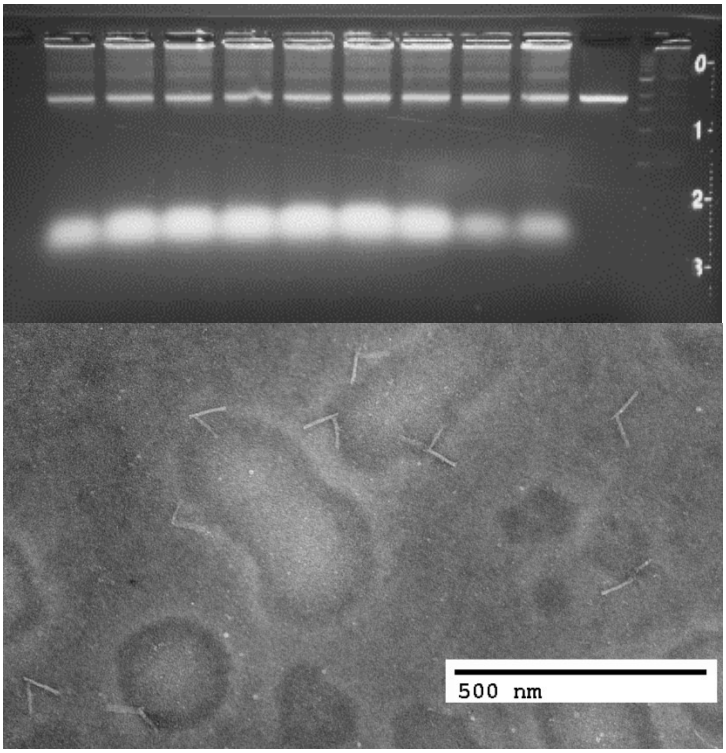

Figure 26 - TOP: 2% Agarose Gel Purification of Nanoparticle Hinge. BOT: TEM Image of Well Folded Structures

DNA Origami Platform – Ligand Presentation Platform

The ligand presentation platform (LPP) is a DNA origami platform measuring 40nm wide, 70nm long, and 7.5nm thick. The scaffold length for this structure is 7,560 bases long and contains 181 staples. The lattice structure for the LPP is the honeycomb lattice. This structure was designed to pattern and present biomolecules.

General Design

The LPP has 12 evenly spaced attachment locations number 1 to 4 along the 70nm length and A, B, and C along the 40nm length of the LPP. These potential bind sites can be seen in Figure 27.

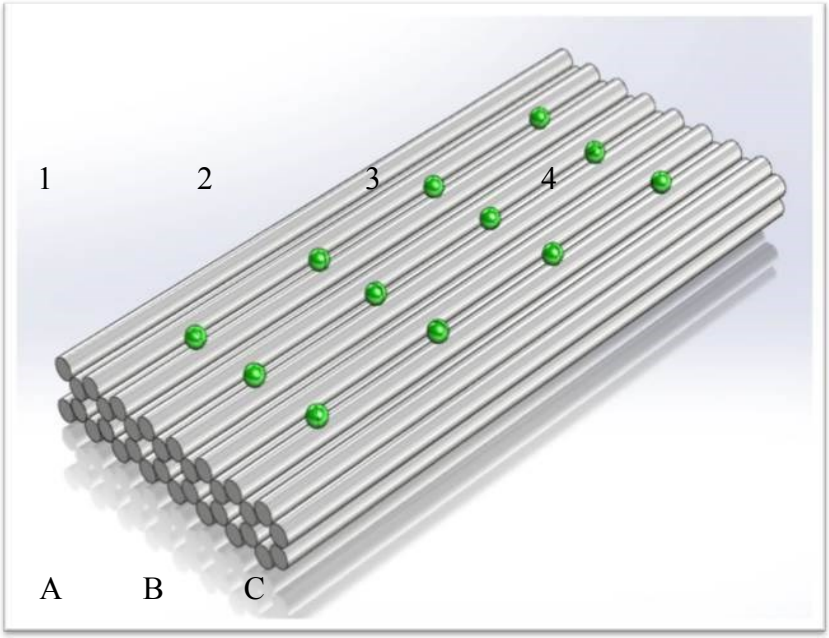

Figure 27 - Available Molecule Attachment Sites on the LPP

Figure 27 also shows the basic structure of the LPP. The scaffold is routed through the LPP such that there are single stranded loops of varying size on the ends of the structure that can allow the polymerization of multiple structures together end-to-end. The LPP presents an opportunity to integrate multiple species of biomolecules into a single DNA origami structure. Successful labeling of the LPP with antibodies at multiple locations on the structure has already been shown by the members in the Nanoengineering and Biodesign Lab. DNA binding protein attachment would add another degree of functionality to the capabilities of the ligand presentation platform. The cross section and staple routing of the structure can be seen in section 5.1.

Folding optimization was performed for the LPP in the same method as was performed to optimize folding of the hinge. Figure 28 shows the EtBr stained agarose gel showing the yield of each folding reaction in the magnesium screen for the LPP. From left to right in the image: 1000 base ladder, 7560 scaffold, 26mM $MgCl_2$, 24mM $MgCl_2$, 22mM $MgCl_2$, 20mM $MgCl_2$, 18mM $MgCl_2$, 16mM $MgCl_2$, 14mM $MgCl_2$, 12mM $MgCl_2$, and 1000 base ladder.

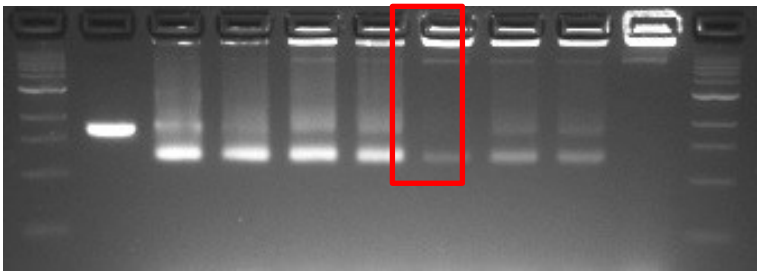

Figure 28 – Magnesium Screen for the LPP

Based upon this gel, the LPP is folded with 20mM $MgCl_2$ (outlined in red). This magnesium concentration was used to determine the rapid fold threshold temperature. Eight folding reactions were subjected to different thermal ramps in which the samples are heated to 65°C for 10 minutes and then cooled to a specific temperature ranging from 45°C to 52°C for 5 hours. The agarose gel showing the contents of each thermal ramp can be seen in Figure 29.

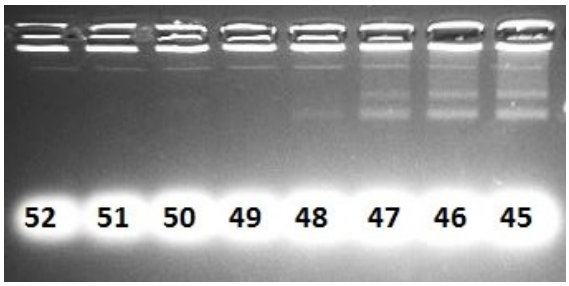

Figure 29 - LPP Rapid Fold Threshold Temperature Optimization Gel

Based upon the images, the LPP will be folded at a threshold temperature of 47°C in 18mM $MgCl_2$.

LexA Attachment Scheme

Wild type (WT) LexA was attached to the LPP via a double stranded overhang containing the RecA recognition sequence as outlined in section 2.2.2. The recognition sequence overhang was 40 base pairs long with a 5 base long single stranded length connecting the overhang to hinge. This flexible attachment to the LPP gives the double

stranded recognition sequence an increased range of motion. In order to definitively determine specific binding of LexA to the LPP, the attachment site was located in a corner of the structure at location 1A as seen in Figure 27. Folding was performed in a manner similar to the folding of the LexA hinge in order to ensure proper formation of the dsDNA recognition sequence overhang. Correct folding of the LPP containing the recognition sequence overhang was confirmed by tight band emergence on an agarose gel electrophoresis and by TEM.

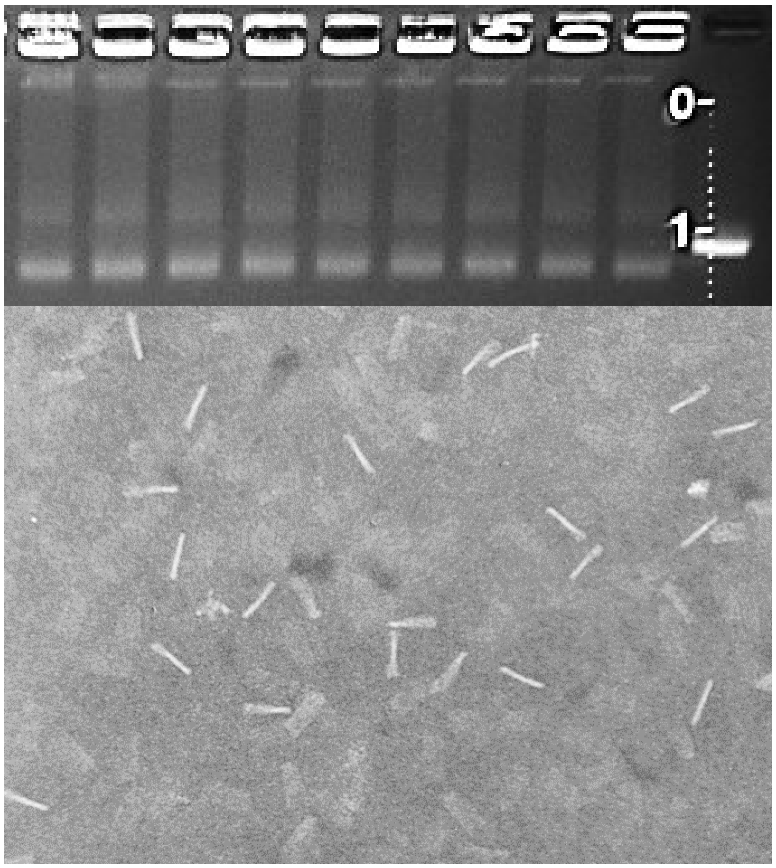

Figure 30 - TOP: 2% Agarose Gel Purification of LPP. BOT: TEM Image of Well Folded Structures

DNA Origami 10 Helix Bundle – MD Platform

The MD platform is a DNA origami 10 helix bundle. The scaffold length for this structure is 7,560 bases long and contains 164 staples. The structure is designed with a honeycomb lattice. This structure was design to test the integration of DNA labeled nanoscale micelles containing magnetic and fluorescent nanoparticles (Magdots) with the goal to use the fluorescent properties of the Magdots for structure visualization without a transmission electron microscope and the magnetic properties for control over the position of structures.

General Design

In order to attach the magdots to the MD Platform the top side of the bundle has 12 available 16 base long ssDNA attachment overhangs that are complementary to a 16 base long ssDNA oligomer conjugated to the magdots. In order to visualize the magdot labeled structures and to quantify the magnetic force applied to the structure it is necessary to be able to fix the MD platform to the surface of a glass coverslip for imaging on a Nikon TiE inverted total internal reflection fluorescence microscope. To accomplish attachment to a surface, the bottom of the structure was designed to have 70 available ssDNA overhangs sites that are complementary to a biotinilated ssDNA oligomer that is bound to the surface of the coverslip. The biotinilated oligomer is bound to a streptavidin molecule that is nonspecifically bound to the coverslip. The density of the oligomers on the surface of the coverslip that are to bind to the overhangs on the bottom of the structure is controlled through the use of Casein as a blocking protein. Casein binds to

glass at similar rates and strengths as streptavidin so by exposing the surface to both casein and streptavidin in solution, the number of surface attachment sites can be reduced or increased. The imaging sample attachment construct to bind structures to the coverslip can be seen in Figure 31.

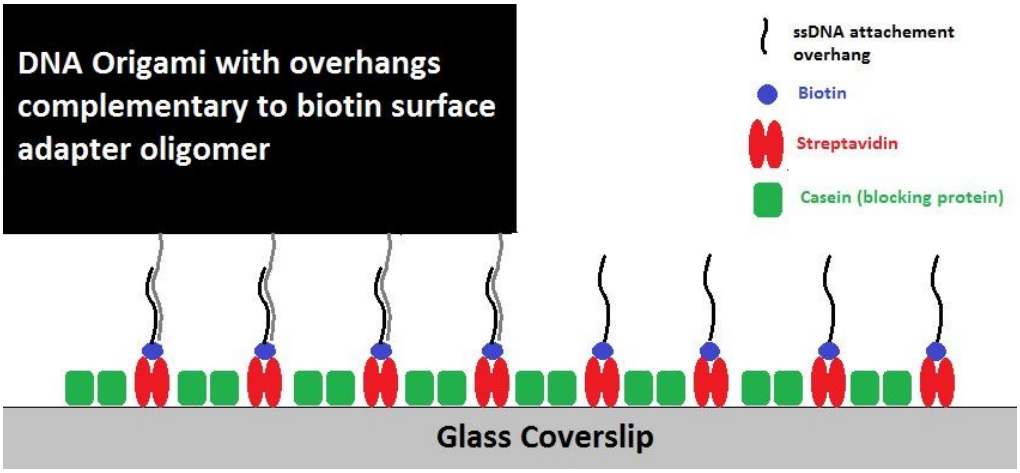

Figure 31 - Imaging Sample Surface Attachment Construct

Each site can either be 'on', meaning it contains an overhang, or 'off', meaning it does not contain an overhang. There are 2 'on' configurations for each overhang location; 5 base long overhangs or 10 base long overhangs. By varying the number and length of the bottom surface attachment overhangs the binding strength to the surface oligomers can be increased or decreased. The force required to rupture dsDNA by shear is defined as:

$$F_c = 2f_c\left[\chi^{-1}\tanh\left(\chi\frac{N}{2}\right)+1\right];\ \chi^{-1}=\sqrt{\frac{\kappa}{2R}}$$

Equation 1 – Shear Rupture Force of dsDNA. where f_c is the rupture force of a single bond, (N+1) is the number of base pairs, κ is the spring constant characteristic of stretching phosphate backbone, and R is the spring constant of the stretching hydrogen bonds between base pairs [49].

By using this shearing rupture force calculation and performing a force analysis on the structure with a known number of bound magdots under a defined magnetic field computation of the force applied by each magdot becomes possible. Approximations of Equation 1 for short and long duplex DNA are $F_c \sim f_c N$ and $F_c \sim 2f_c\chi^{-1}$ respectively. Folding optimization was performed for the MD platform in the same method as was performed to optimize folding of all previous structures. Figure 32 shows the EtBr stained agarose gel showing the yield of each folding reaction in the magnesium screen for the MD platform. There are two lanes of each folding reaction from left to right in the image: 1000 base ladder, 7560 scaffold, 2 x 12mM $MgCl_2$, 2 x 16mM $MgCl_2$, 2 x 20mM $MgCl_2$, 2 x 24mM $MgCl_2$, 2 x 28mM $MgCl_2$, and 2 x 32mM $MgCl_2$.

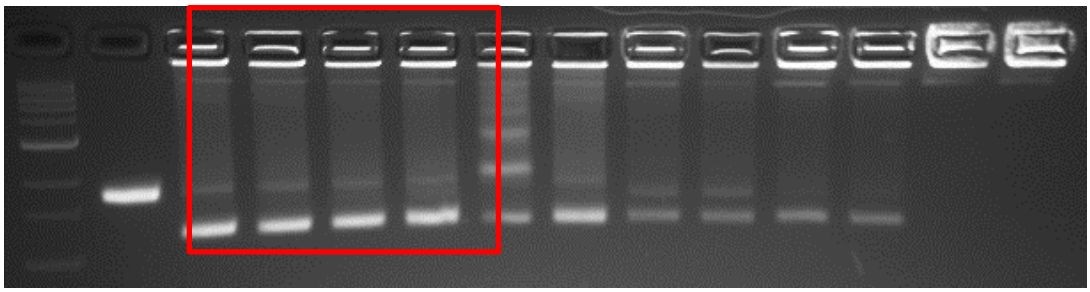

Figure 32 - Magnesium Screen for the MD Platform

Based upon this gel, the MD platform is folded at both 12mM and 16mM $MgCl_2$ (outlined in red). This magnesium concentration was used to determine the rapid fold threshold temperature. Four versions of the MD platform were tested in the rapid fold optimization ramp: A) no overhangs, B) no magdot attachment overhangs and 10, 5 base surface attachment overhangs, C) no magdot attachment overhangs and 70, 5 base surface attachment overhangs, and D) no magdot attachment overhangs and 70, 10 base surface attachment overhangs. Eight folding reactions were subjected to different thermal ramps in which the samples are heated to 65°C for 10 minutes and then cooled to a specific temperature ranging from 42°C to 49°C for 5 hours. The agarose gel showing the contents of each thermal ramp can be seen in Figure 33.

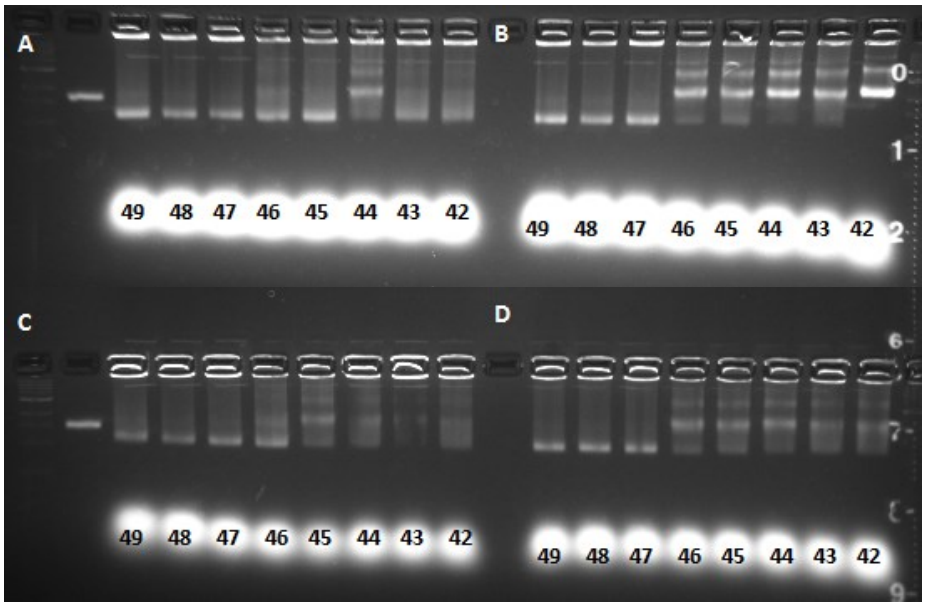

Figure 33 – MD Platform Rapid Fold Threshold Temperature Optimization Gel

Figure 31 shows that the MD platform folds differently depending upon the number of overhangs on the structure. However, 47°C has tight leading bands that run faster in the gel than the scaffold used for the structure (leftmost bands visible in image) indicating well folded structures. Based upon the images above the MD platform will be folded at a threshold temperature of 47°C in 14mM $MgCl_2$.

Magdot Attachment Scheme

The MD platform structure was designed to fold into many different configurations simply by changing the staples added to the folding reaction. Structures can be folded to contain 0 to 12 magdot attachment sites on the top of the structure and 0 to 70 surface attachment overhangs on the bottom of the structure. The magdot will bind to the MD platform through the interaction of an integrated ssDNA oligomer and the magdot attachment site overhang. The magdots used in these experiments are aggregates of amphiphilic block co-polymers in water [50]. These aggregates take the form of spheres or tubes. By assembling these micelles in the presence of hydrophobic nanoparticles said particles can be trapped in the hydrophobic interior of the micelles. The exterior, hydrophilic region of the micelle's block co-polymers is labeled with–COOH groups that are condensed via EDC chemistry thus linking the DNA oligomer to the micelle. In this case, the nanoparticles that were trapped inside the micelles were hydrophobic quantum dots with a maximum emission wavelength of 605nm and 5nm super paramagnetic iron oxide nanoparticles (SPIONs). Transmission electron microscopy was used to visualize micellular structure and size distribution (Figure 34).

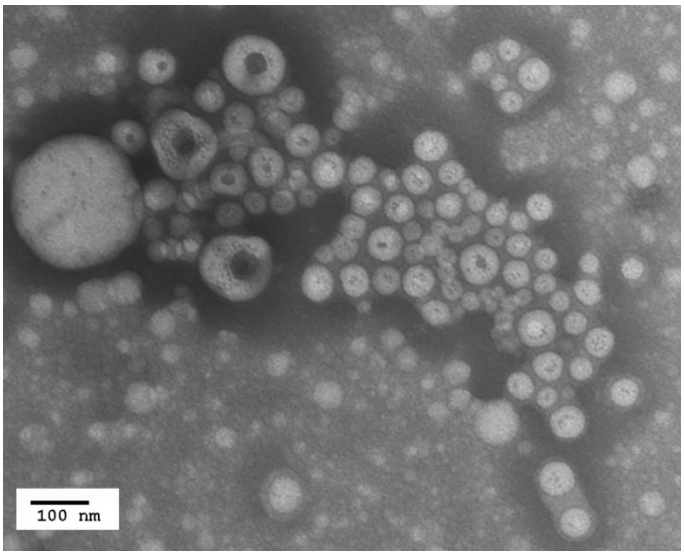

Figure 34 - TEM Image of Magdot stock

Image J was used to measure the diameter of a sample of 112 magdots. The average diameter is 35nm with the largest particle being 217nm in diameter and the smallest being 11nm. The distribution of the diameters can be seen in Figure 35.

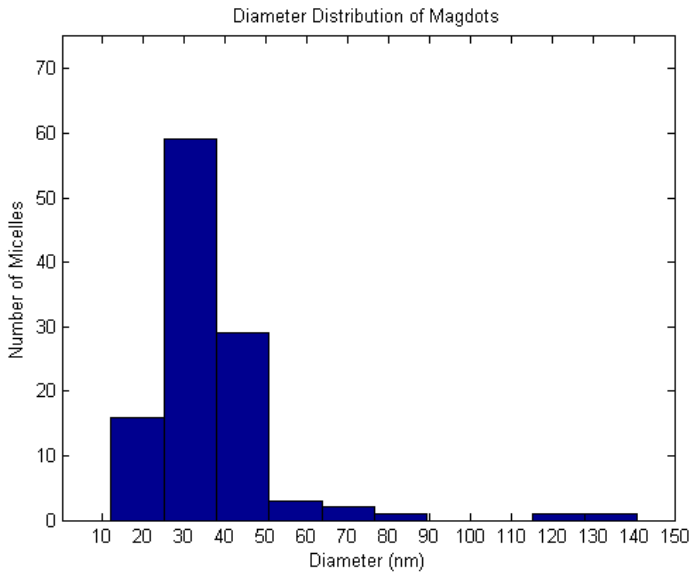

Figure 35 - Distribution of Magdot Diameters (N=112)

In order to optimize binding of magdots to the MD platform, all of the magdot attachment overhangs on the top of the structure were turned 'on' and all surface attachment bind locations were turned 'off'. Folding of the MD platform was confirmed by tight band emergence on an agarose gel electrophoresis and by TEM.

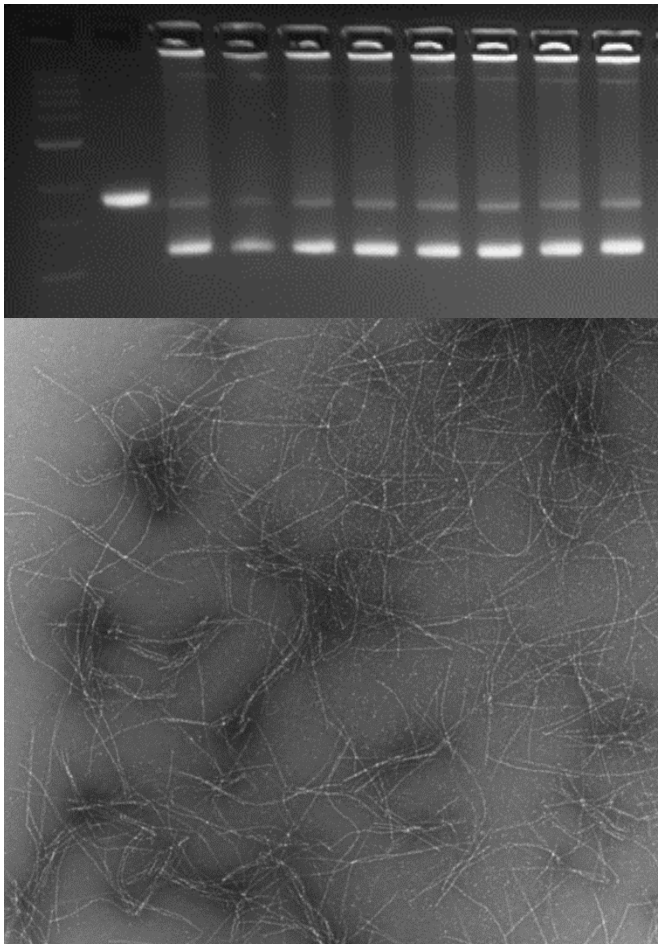

Figure 36 - TOP: 2% Agarose Gel Purification of MD platform. BOT: TEM Image of Well Folded Structures

Figure 36 illustrates that the yield of the folding reaction for this structure has a very high yield. High yields in structures with

Polymerization Optimization of 56 Helix Bundle Monomer

The 56 helix bundle monomer is approximately 40nm long and has a circular cross section with an approximate diameter of 25nm. This structure uses 7249 base long scaffold and contains 138 staples. The monomer was designed using a honeycomb lattice.

Folding optimization was performed following the same methods that have been outlined for the structures above. Agarose gel electrophoresis of a divalent salt screen in Figure 37 shows that the 56 helix bundle monomer folds at 18mM $MgCl_2$. From left to right this gel contains a 1 kilobase ladder, 7249 scaffold, 22mM $MgCl_2$, 20mM $MgCl_2$, 18mM $MgCl_2$, 16mM $MgCl_2$, 14mM $MgCl_2$, and 12mM $MgCl_2$.

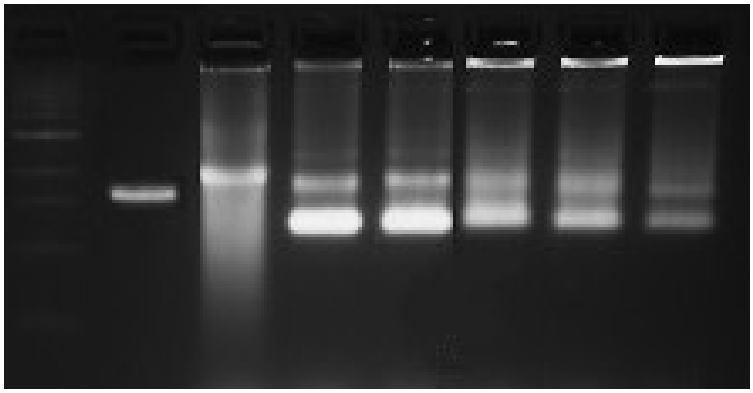

Figure 37 - Magnesium Screen for 56 Helix Bundle Monomer

This gel shows that a magnesium concentration of 20mM should be used to determine the rapid fold threshold temperature. Eight folding reactions were subjected to different thermal ramps in which the samples are heated to 65°C for 10 minutes and then cooled to a specific temperature ranging from 45°C to 52°C for 5 hours. The agarose gel showing the contents of each thermal ramp can be seen in Figure 38. The rapid folding temperature threshold is 50°C.

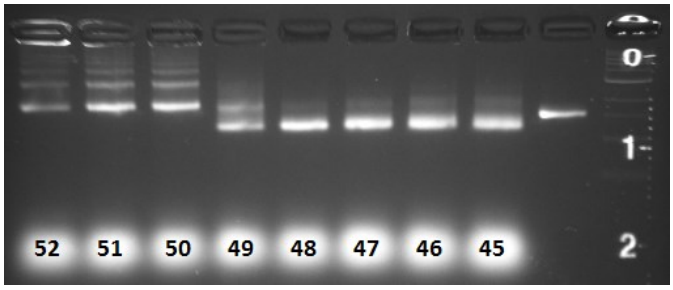

Figure 38 - 56 HB Monomer Rapid Fold Threshold Temperature Optimization Gel

Polymerization Scheme

This structure was designed to polymerize end to end to form long stiff filaments. Each end of the structure contains three different levels of helices. These levels are designed so that the end of one structure 'plugs' into the end of another. This plugging effect creates more stable filaments than other configurations. The polymerization of structures takes place after the monomers are folded. The folded monomers have 28 core overhangs on one end that are complementary to the open scaffold loops on the opposite end. The polymerization reaction is performed at 37°C over a period of up to 24 hours. Issues with aggregation of monomers and branching of polymers were resolved by polymerizing structures in the presence of a surfactant. Tergitol, purchased from Sigma Aldrich was the surfactant used in these studies. The presence of detergent, even at low levels, has been shown to reduce aggregation of biomolecules [51]. The polymerization reaction can be optimized to produce the longest filaments through the optimization of Tergitol concentration and polymerization reaction time length. Although other factors such as magnesium concentration, monomer concentration, and temperature can affect the polymerization of structures, the focus of this study was on the optimization of

surfactant concentration and total polymerization time. It was assumed that all polymerization reactions have the same concentration of DNA origami monomers and contain 16mM $MgCl_2$. Polymerization reactions were run containing 0% Tergitol, 0.1% Tergitol, and 0.2% Tergitol. Samples were drawn out of reaction vessel at 12 hours, 18 hours, and 24 hours and image on TEM. The length of the filaments in TEM images was measured using ImageJ. Histograms showing the length distribution of the 56 helix bundle filaments can be seen in section 5.2. The average length values as well as the sample size are shown in Figure 39.

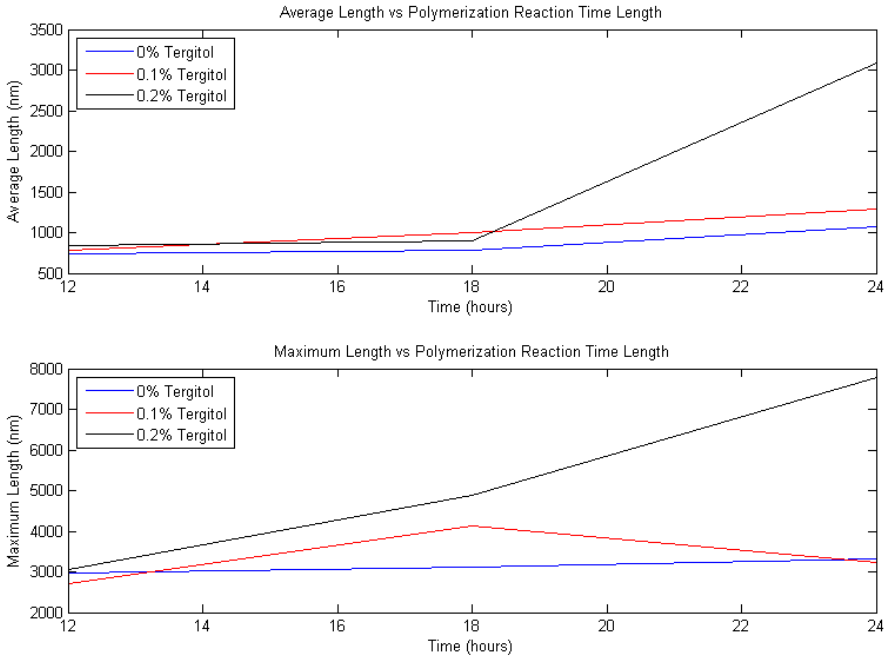

Figure 39 - Average and Maximum Filament Lengths

The data demonstrates that including Tergitol at either 0.1% or 0.2% increases the average filament length and decreases the number of branched or kinked filaments (Figure 40).

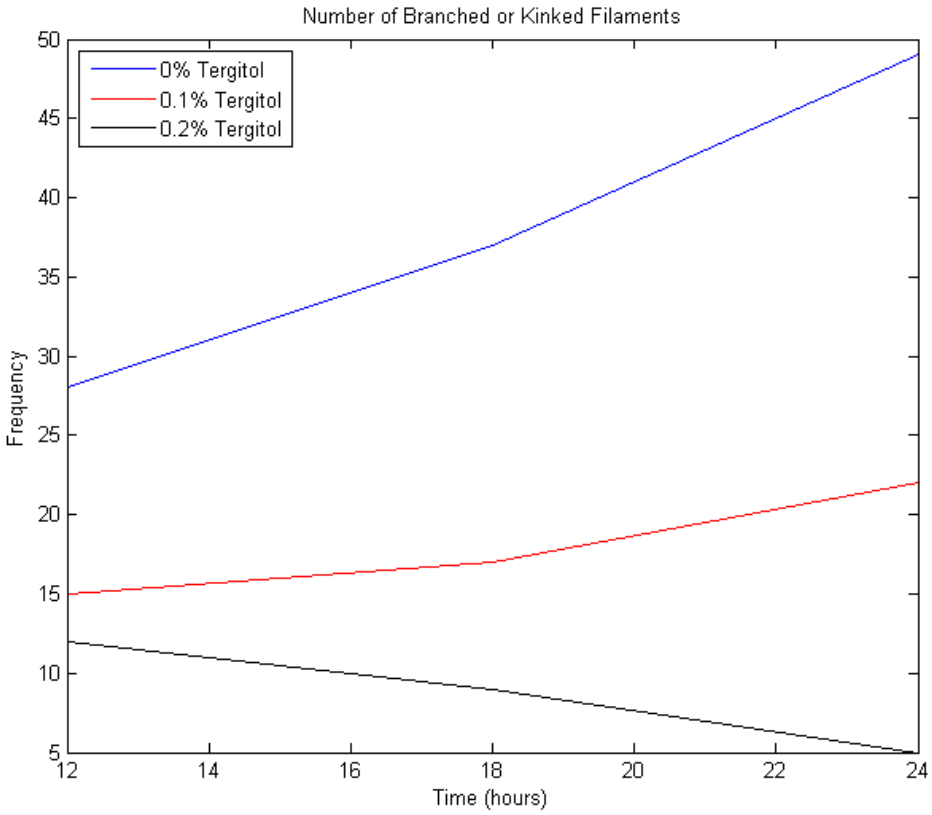

Figure 40 - Number of Branched or Kinked Filaments vs Time

The optimal conditions to polymerize the 56 helix bundle monomers into long DNA origami filaments are 0.2% Tergitol and 16mM $MgCl_2$ over a time period of 24 hours at 37°C.

Chapter 3: Results and Discussion

Determination of LexA+Biotin Dissociation Constant

Before attaching the protein to the hinge it is necessary to determine the dissociation constant (K_D) of the biotinilated LexA. It is expected that the dissociation constant of the LexA will be similar to the published value of 0.07 nM, but could vary slightly because of a difference in buffer conditions and the biotinilation of the protein [38]. It is necessary to quantify any changes in K_D of the modified protein in order to determine the lowest concentration at which specific binding of LexA to its duplex recognition sequence will occur. In order to determine the K_D of the LexA used in this work, the two oligomers forming the recognition sequence binding location on the hinge were annealed through the optimized thermal ramp described in Section 2.2.2. Oligomer A is 83 bases long and oligomer B is 40 bases long and labeled with Cy3 fluorophore to facilitate visualization of annealing through fluorescent scanning of a PAGE gel. The folded DNA was diluted to 0.2nM in 1xTE, 0.2% Tergitol, 2mM $MgCl_2$, and 500mM NaCl. LexA was mixed with the DNA at equal volumes across a range of concentrations. The mixed samples were incubated for 15 min and then run through a 5% acrylamide gel to perform an

electrophoretic mobility shift assay [48]; meaning that, the DNA duplex with the LexA bound should migrate at a different speed than the naked duplex. This gel can be seen below in Figure 41.

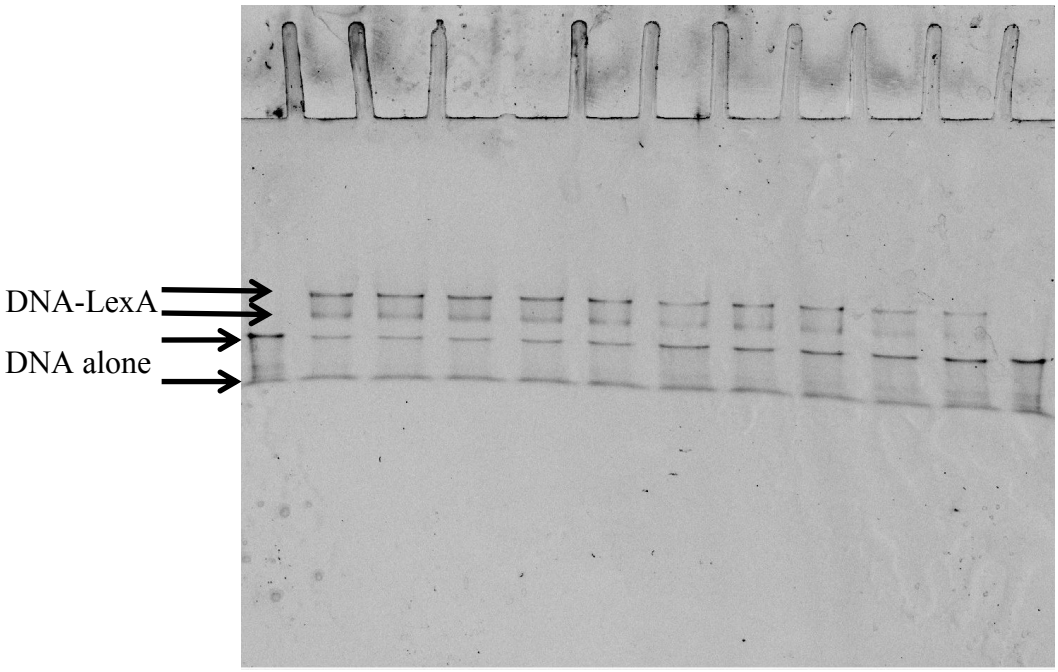

Figure 41 - PAGE Mobility Shift Assay of Biotinilated LexA

The gel was imaged on a General Electric Typhoon FLA 9500 gel scanner and analyzed in a program called ImageQuantTL V8.1. The peak fluorescent intensity values were read from each band visible in the gel. The sample contents can be seen in Table 3 - PAGE Mobility Shift Assay Lane Contents below.

Lane	1	2	3	4	5	6	7	8	9	10	11	12
LexA Conc. [nM]	0	100	40	20	10	4	2	1	0.4	0.2	0.1	0
DNA Conc. [nM]	0.1	0.1	0.1	0.1	0.1	0.1	0.1	0.1	0.1	0.1	0.1	0.1

Table 3 - PAGE Mobility Shift Assay Lane Contents

The gel shows that there are two distinct bands in the DNA only samples (lanes 1 and 12). The leading band in all samples does not vary in intensity by more than 10% and the fluctuations in intensity of this band do not correspond to LexA concentration. Therefore, we suspect these bands are a stable secondary structure of the 40 base long single stranded Cy3 labeled oligomer B that cannot bind LexA. This band was ignored for our analysis. The second band in gel corresponds to the correctly formed duplex recognition sequence and decreases in intensity as LexA concentration increases (from right to left in Figure 41 - PAGE Mobility Shift Assay of Biotinilated LexA). The 3rd and 4th bands in lanes 2 through 11 are bands in which LexA has bound to the duplex recognition sequence. We would expect to see only one band indicating specific binding of one LexA protein to the recognition sequence DNA, however, the DNA complex containing the recognition sequence has 50% of its length as ssDNA. The 4th band most likely contains LexA specifically bound to the recognition sequence and a second LexA bound non-specifically to the DNA molecule. The peak intensities of each band were used to calculate a percent bound value for each concentration of LexA. Equation shows this calculation in terms of the band numbers for each lane:

$$PB_{lane} = \frac{(3_{int} + 4_{int})}{(2_{int} + 3_{int} + 4_{int})}$$

Equation 2 - Percent Bound Calculation

Where 2_{int}, 3_{int}, and 4_{int} indicate the intensities of the respective bands. The concentration of LexA was plotted against these percent bound values on a semi-log plot. A non-linear least squares curve fit was performed in MATLAB using Equation 3. This plot can be seen in Figure 42.

$$PB = PB_{max}\left(\frac{[LexA]}{K_D + [LexA]}\right)$$

Equation 3 - Model Used to Fit Fluorescent Intensity Values

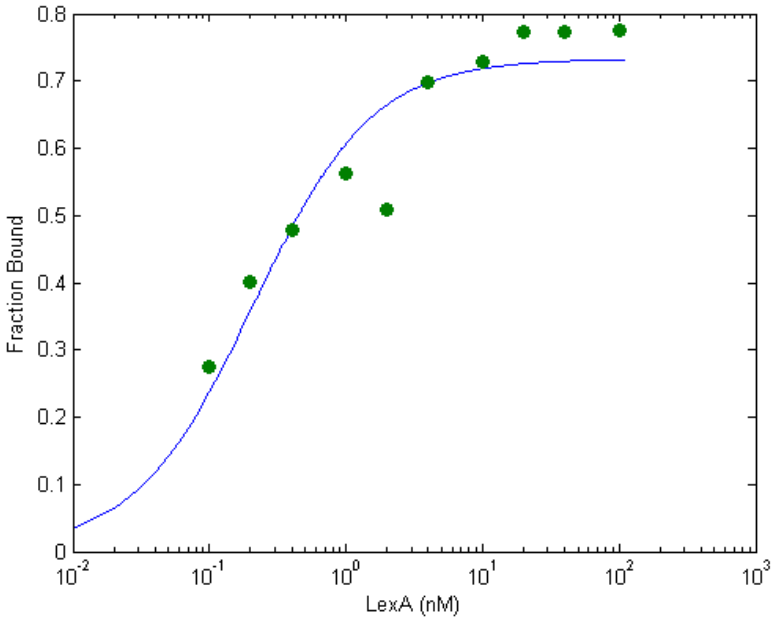

Figure 42 - Semi-log Plot of LexA Concentration Against Percent Bound

This yielded a maximum percent bound (PB_{MAX}) of 73.3% and a K_D of 0.21nM. A number of issues could cause lower than a 100% maximum percent bound including poorly formed recognition sequence overhangs, a limited 40% biotin labeling efficiency of the LexA protein, or a limited 84% binding efficiency of streptavidin. This K_D value is in reasonable agreement with the previously measured 0.07nM. The slightly higher value obtained here suggests that the biotinilated LexA may have a slightly reduced affinity for its recognition sequence compared to the wild type LexA. The 0.21 nM K_D will be the lower bound of LexA concentration used for any experiments in which specific attachment of LexA to its recognition sequence is desired.

Integration of Transcription Repressor Binding Protein, LexA into DNA Origami Structures

As was previously mentioned, LexA was labeled with biotin at 40% efficiency and was provided at a stock concentration of 22μM. The LexA attachment buffer is 1xTE containing 2mM $MgCl_2$, 0.2% Tergitol (to prevent aggregation of structures and proteins), and some concentration of NaCl that was varied to optimize binding. NaCl is necessary because LexA is much more stable for long periods of time and has a higher binding affinity in the presence of Na^+ ions.

Unlabeled LexA(S171C) Integration

In order to confirm that LexA will bind to the recognition sequence that is attached to a DNA origami structure, the LPP was used. The LPP-LexA attachment is a first step into attaching LexA to the hinge. The LPP presents the recognition sequence on a face of the structure open to solution. There is no part of the structure that could impede LexA binding unlike the hinge. The LPP was folded as defined in section 2.3 but with the addition of a high temperature ramp as described in section 2.2.2 in order to maximize the formation of well-formed recognition sequence overhangs. LexA was added to the LPP at 10 fold excess and the sample was imaged via TEM (Figure 43). Binding efficiency was 41% over a sample of 108 structures. Several examples of binding are shown in Figure 44.

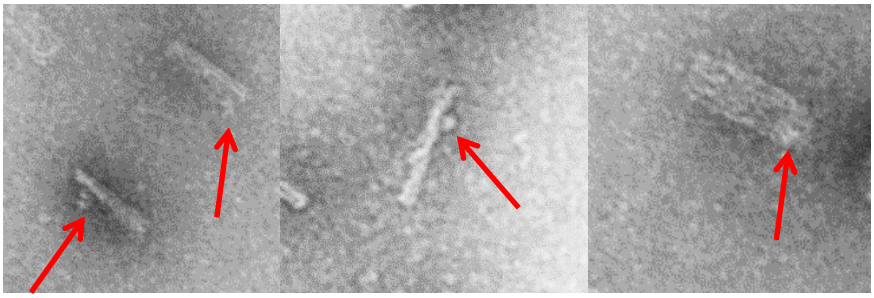

Figure 43 - LexA Bound to LPP via the recognition sequence. Arrows show location of LexA

Biotinilated LexA Integration

The hinges were folded as described in Section 2.2.2 . The short term stability of the hinges at 2mM magnesium was confirmed via TEM. However, hinges imaged after 1 week at this low magnesium concentration had begun to break apart Figure 44.

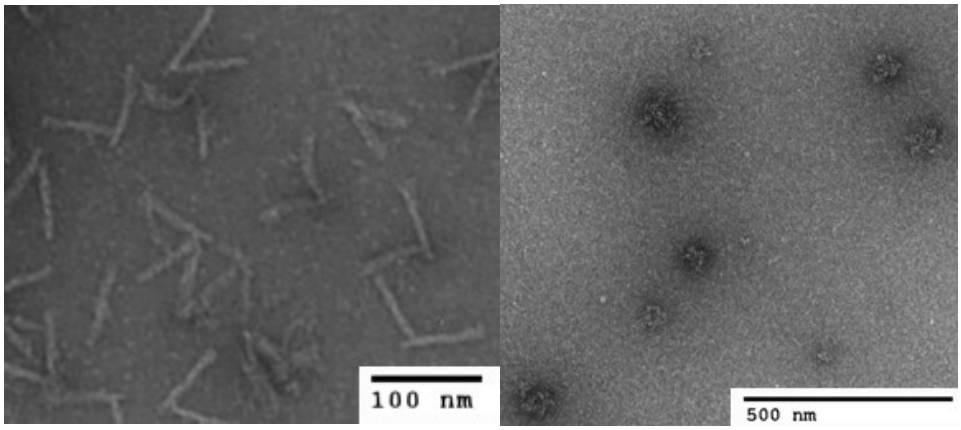

Figure 44 – Left) Hinges after 24 hours and Right) Hinges after 1 week in 1xTE, 0.2% NP40, and 2mM MgCl2

In order to optimize the attachment of LexA to the hinge, it was necessary to first show successful attachment of streptavidin to the biotinilated ssDNA overhang on the bottom arm of the hinge. Three methods of streptavidin incorporation were tested. Each method mixes streptavidin suspended in PBS with the DNA origami structures at a volume ratio of 1:4 and then removes excess streptavidin after a 30 minute incubation time at room temperature. Method 1 mixes streptavidin with agarose gel purified hinges suspended in 0.5xTAE (40mM Tris-Acetate and 1mM EDTA) at 10mM $MgCl_2$. The structures were PEG precipitated and then resuspend in the LexA attachment buffer (1xTE containing 2mM $MgCl_2$, either 200mM or 500mM NaCl, and 0.2% Tergitol to prevent aggregation of structures and proteins). Method 2 mixes streptavidin with unpurified folded structures in folding buffer conditions (Table 1). The sample was purified via agarose gel electrophoresis. This well folded structure band was excised from the gel and separated from excess agarose in a centrifugal spin column. Magnesium concentration was chelated using EDTA from the gel buffer concentration of 10mM down to 2mM. The solution was immediately brought to 0.2% Tergitol and to either 200mM or 500mM NaCl before the addition of LexA. Method 3 mixes streptavidin with agarose gel purified hinges suspended in 0.5xTAE at 10mM $MgCl_2$. The mixture was incubated at room temperature for 30 minutes and then the samples were gel purified a second time. Method 3 was eliminated as a preparation option because yield after a second gel run was very low (pM range) making visualization and the excision of bands from the gel difficult. Streptavidin is readily visible under a TEM so this was the method used to quantify attachment efficiency of streptavidin to the structure. The samples from method

1 and 2 were imaged via TEM and the percentage of structures containing streptavidin molecules was found to be ~84% (N=219) for method 1 and ~80% (N=197) for method 2. In addition to method 1 yielding higher attachment efficiency there was a much better clearance of excess streptavidin than in method 2. Streptavidin labeled hinges from method 1 can be seen in Figure 45.

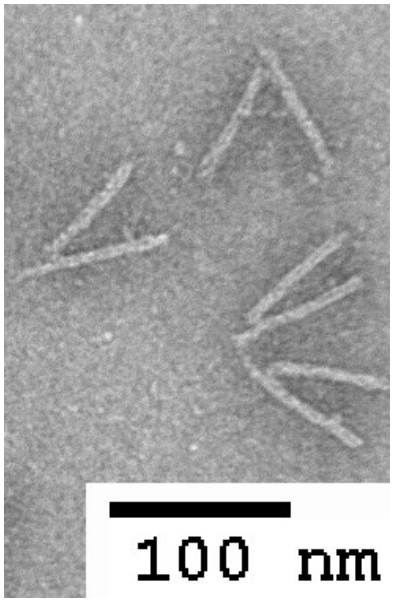

Figure 45 – Streptavidin attachment to Hinges by method 1. The streptavidin molecules are seen as small bumps on the bottom arm of the hinge.

Once the method for attaching streptavidin was defined, in order to optimize LexA attachment sodium and LexA concentrations were screened. Because the presence of sodium is vital for protein stability and affects the dissociation constant of LexA to the target recognition sequence, sodium concentrations tested will be 200mM and 500mM.

LexA was screened in terms of molar excess with respect to the hinge at 1x, 3x, 10x, 30x, and 100x. These excess values correspond to LexA concentrations of 1nM, 3nM, 10nM, 30nM, and 100nM. Each LexA concentration was imaged at both potential sodium buffer concentrations. Binding efficiency of LexA to the hinge was assessed by visual inspection on the TEM. The efficiency of LexA attaching to the hinge at either binding location is documented in Table 3.

		NaCl concentration	
		200 mM	500 mM
LexA excess	1x	<1%	<1%
	3x	6%	8%
	10x	22%	25%
	30x	37%	43%
	100x	43%	49%

Table 4 - LexA Binding Efficiency in Different Buffer Conditions. N = 115 for all conditions

Based upon these results further investigation into LexA attachment was performed at 500mM NaCl and 30x and 100x LexA and the angular distribution of these two conditions (Figure 48 and Figure 49) were compared to the angular distribution of this hinge as shown in Marras et. al. (Figure 47). TEM images of LexA attachment to the hinge can be seen below. The arrows point to the bound protein latch complex. Angular distribution data is used to verify LexA attachment because LexA and biotin proteins are difficult to visualize on the TEM.

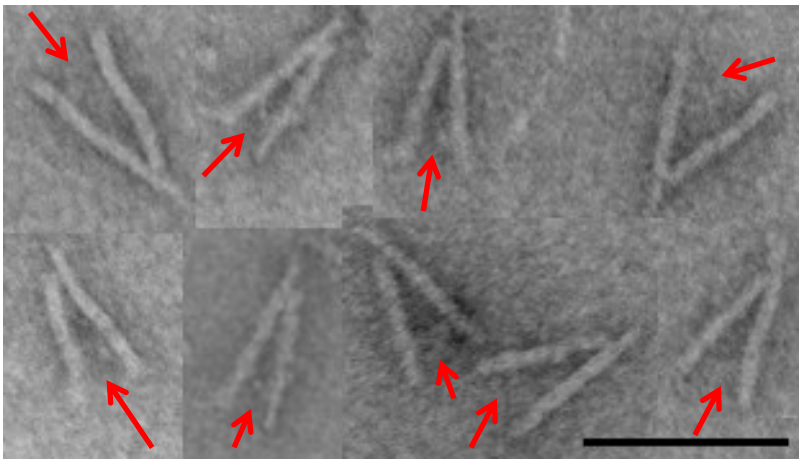

Figure 46 - LexA Attachment to the Hinge. Scale Bar is 100nm.

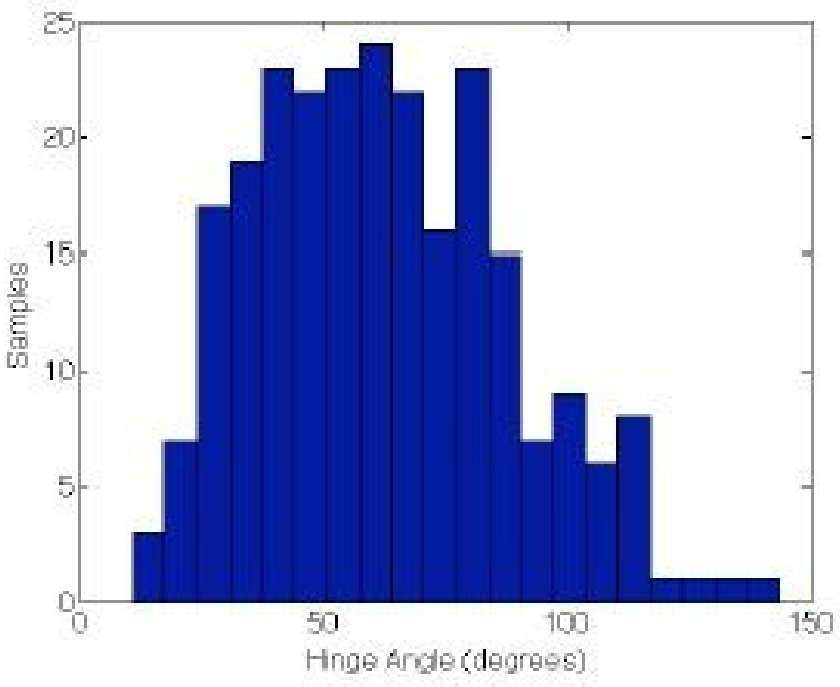

Figure 47 - Angular Distribution of DNA Origami Hinge [26]

The unmodified hinges have an angular range from ~10º to ~145º with an average angle of 62º and a standard deviation of 25.73. The corresponding values for the hinges from this work are seen below in Table 5.

	Min. Angle (º)	Max. Angle (º)	Mean Angle (º)	St. Dev.
30x LexA, 500mM NaCl	4.95	132.98	57.71	25.84
100x LexA, 500mM NaCl	9.62	134.14	52.13	27.74

Table 5- Hinge Comparison

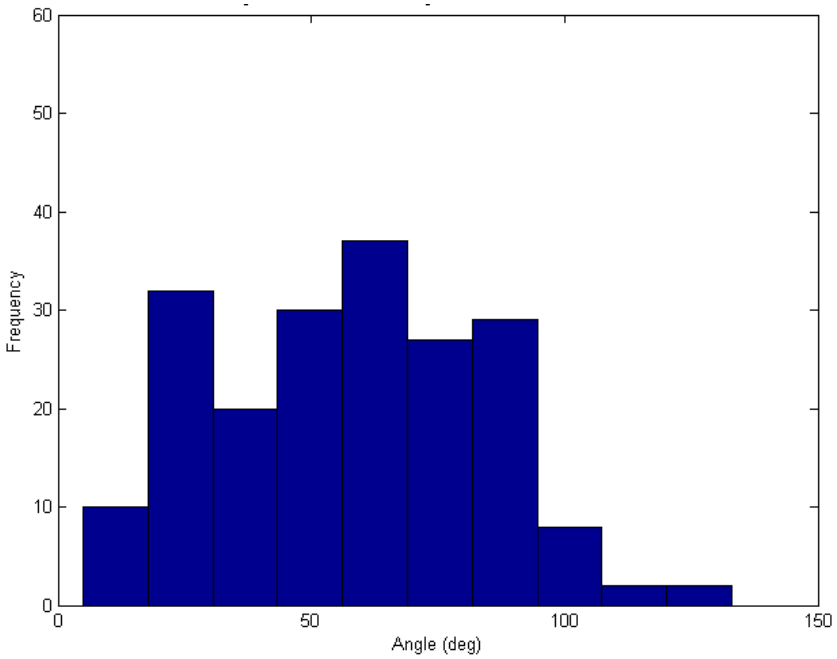

Figure 48 - Angular Distribution of Hinges with 30x LexA at 500mM NaCl

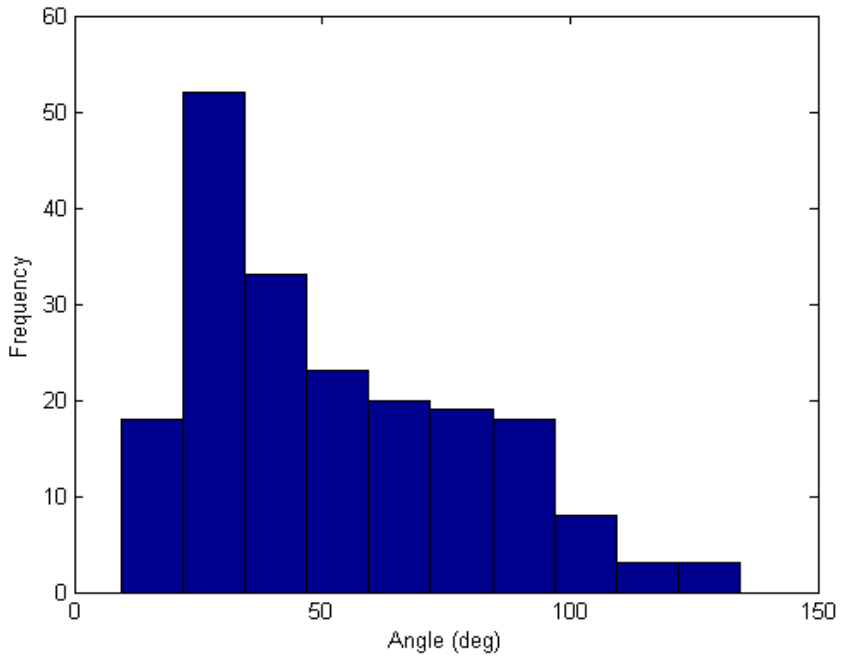

Figure 49 - Angular Distribution of Hinges with 100x LexA at 500mM NaCl

These distributions show that there is a shift of the angular distribution for both conditions tested when compared to the unmodified hinge characterized in Marras et al. The initial appearance of a peak at small angles is evident in the 30x LexA sample. The distribution shift occurring in the 100x LexA sample shows the emergence of a peak centered at 24º hinge angle. The size of each of the molecules involved (see attachment schematic in Figure 20) is approximated from the crystalline structure acquired from PDB as Biotin = 5nm, LexA = 8nm, Streptavidin = 10nm for a total complex maximum height of 28 nm. The distance from the hinge joint to the binding location is 168 base pairs or ~56nm. Therefor the maximum hinge angle in the 'closed' configuration is 30º. The center of the peak is near this expected value leading to the conclusion that the peak defines hinges in the closed configuration.

Integration of Azobenzene modified ssDNA labeled Gold Nanoparticles into DNA Origami Structures

This hinge was folded as described in section 2.2. Only 3 of the binding locations furthest from the hinge joint on the top arm of the hinge were used because confirmation of attachment was the goal of this study. Because the integration of the ssDNA labeled gold nanoparticles (AuNPs) relies solely on DNA-DNA base pairing interactions it was necessary to screen magnesium concentration and AuNP excess ratios. The magnesium conditions tested ranged from 10mM to 20mM $MgCl_2$ in 2mM steps. The AuNP excess ratios tested were 10x, 30x, and 100x.

Attachment was documented in every single condition; however, the attachment in the 30x and 100x AuNP excess samples is non-specific (Figure 50).

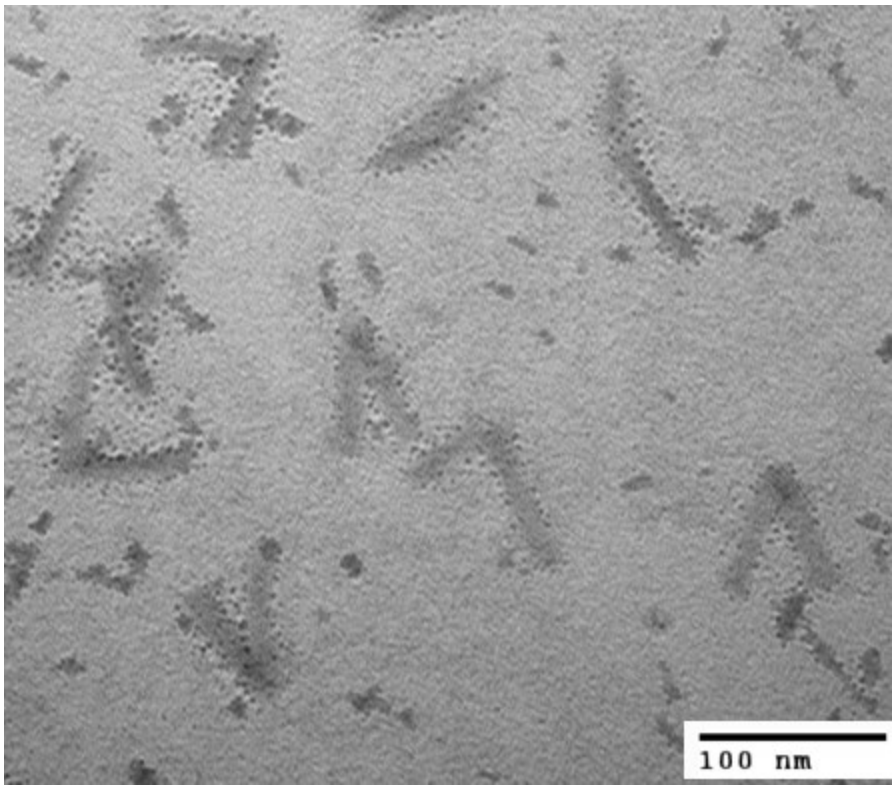

Figure 50 - Non-specific Binding of AuNP to Hinge

10x AuNP excess facilitated specific attachment of the AuNP to the hinge at the correct binding location. The binding efficiency can be seen in Table 6.

		Magnesium Concentration					
		10mM	12mM	14mM	16mM	18mM	20mM
AuNP excess	10x	50%	52%	53%	54%	47%	45%

Table 6 – AuNP Binding Efficiency of 10x excess AuNP

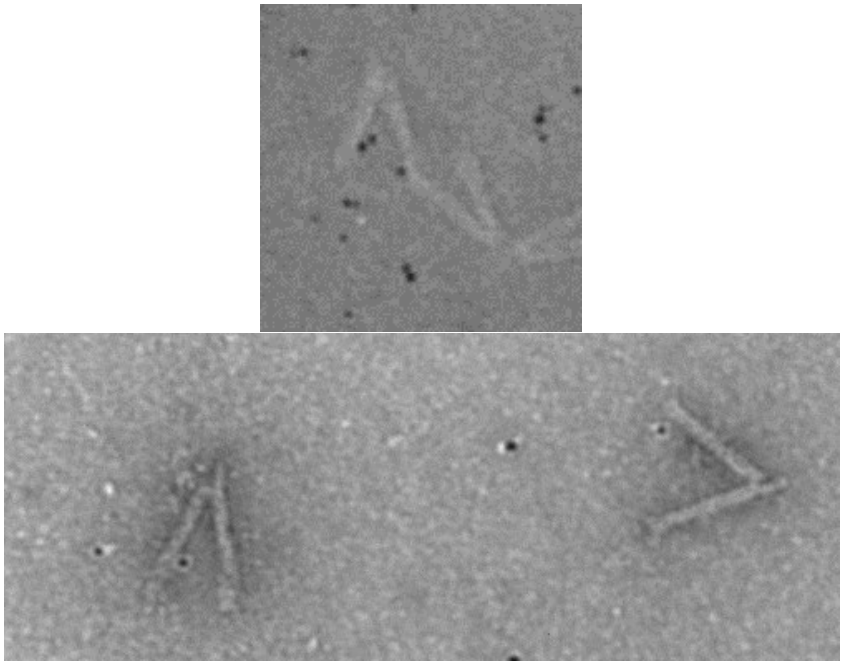

Figure 51 - Specifically bound AuNP

Figure 51 shows AuNPs bound in the correct location on the hinge. Based upon this work, the optimal conditions for incorporation of the ssDNA labeled gold nanoparticle are a 10-fold excess of AuNP to hinges at 12 mM – 16 mM $MgCL_2$.

Integration of Magnetic Quantum Dots (Magdots) into DNA Origami Structure

The MD platform was folded as described in section 2.4. For this work, all 12 magdot attachment overhangs were included and no surface attachment overhangs were included since confirmation of magdot attachment was the goal of this study. Because the integration of the ssDNA labeled magdots relies solely on DNA-DNA base pairing interactions, it was necessary to screen magnesium and magdot concentrations. Based upon the results from the AuNP binding to the hinge, the magnesium concentration used was 15mM in 1xTE. The concentration of the individual bock co-polymer molecules that make the micelle portion of the magdots is known to be 18μM. The magdot concentrations were estimated using a close packed sphere approximation and a polymer effective diameter of 5nm. Ignoring outlier data, the range of magdot diameter is approximately 20nm to 60nm. Calculating gives the range of possible magdot concentration as 10 μM at 60nm diameter up to 96 μM at 20nm diameter. This range of concentrations is not fine enough to make a reasonable estimate of magdot concentration. Therefore, TEM imaging was used to qualitatively asses the concentration of various fold dilutions from the stock concentration. Because these particles are much larger than the structures to which they are trying to attach, the ratio of particles to hinges should be low in order to prevent crowding on the imaging field. It was determined that a 10 fold dilution of the stock created a density that would allow us to identify specific binding.

Attempts to mix a 10-fold dilution of magdots with the MD platform showed sparse attachment stemming from the low concentration of magdots in the samples. It was

necessary to increase the concentration of magdots while retaining the ability to draw conclusions from TEM images which required a low concentration of magdots.

The attachment samples were prepared in two ways. The first sample, seen in Figure 52, combined a 5 fold dilution of the magdots in a 1:2 volume ratio with the MD Platform. Sample 2 combined magdots at stock concentration and the structures at a volume ratio of 1:2 and can be seen in Figure 53. Each sample was left to incubate for 1 hour before image preparation.

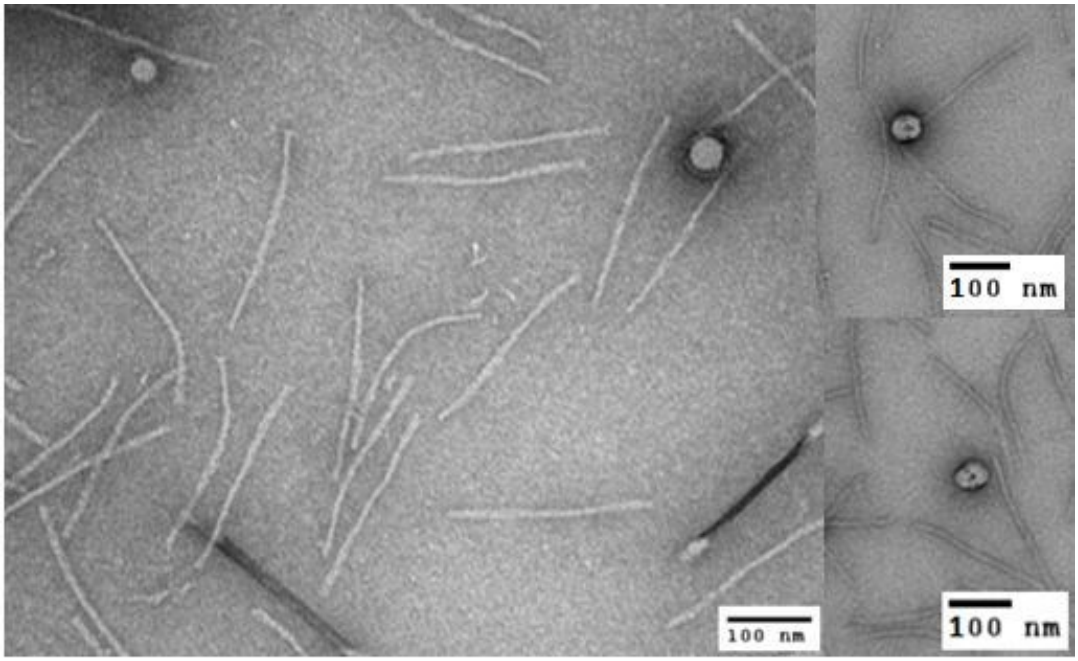

Figure 52 - Magdots attached to MD Platforms from Sample 1

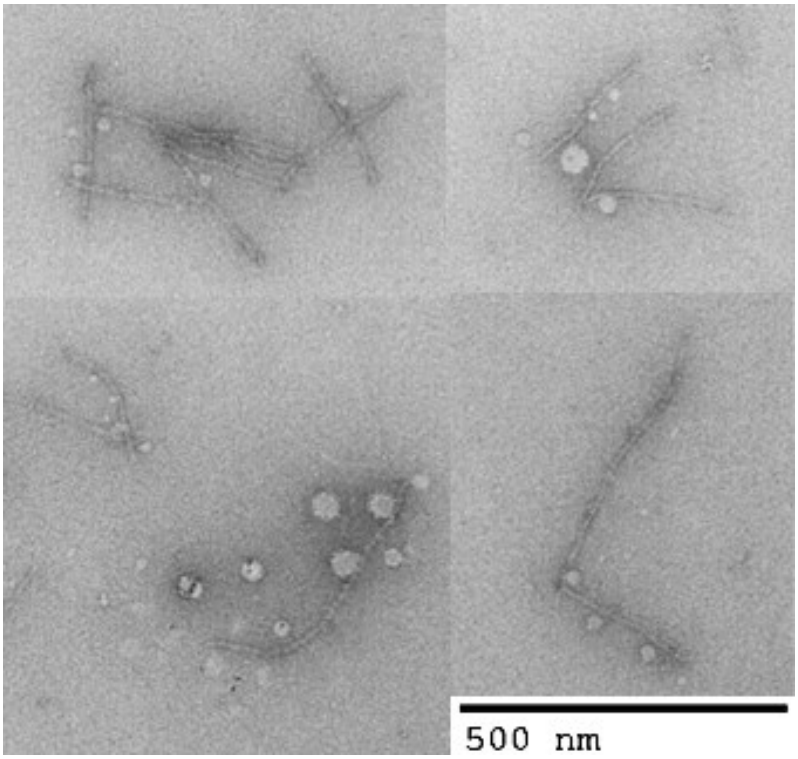

Figure 53 - Multiple Magdots Attached to MD Platforms from Sample 2

In Sample 1, the concentration of Magdots during the binding process is 5 fold less than the concentration in sample 2. This difference in concentration while the particles and structures are in solution explains why we see single magdots attached to multiple structures in sample 1 and many magdots attached to multiple structures in sample 2. This indicates that the number of attached magdots can be altered by changing the concentration of the initial magdot solution. Optimization can be performed in the future by screening dilutions from the stock concentration of magdots.

Chapter 4: Conclusions

Limitations

Measurement Errors in ImageJ

All length and angular measurements were measured in ImageJ by hand. This inevitably leads to some human error in the measurements. In order to quantify this measurement error, 15 angle measurements were taken on five different DNA origami hinges from the same TEM image. The averaged standard deviation of the measurements across all five hinges was 1.14°. This corresponded to a 3.1% error. This quantification was also performed on length measurements of DNA origami filaments. Five filaments from the same TEM image were measured 15 times each. The averaged standard deviation of the measurements across all five filaments was 38nm. This corresponds to a 3.9% error. This indicates that it is reasonable to assume that each angle contains a measurement error of ±3.1% and each length measurement contains an error of ±3.9%.

Issues with Resuspension of PEG Precipitated Structures

We experience challenges with resuspending hinges in buffer after PEG purification. The pellet can be broken apart but upon TEM imaging the structures are tightly aggregated. In order to fully break a PEG precipitation pellet apart, it was necessary to

double the concentration of Tris and EDTA in the resuspension buffer. This meant simply using a 1x solution of buffers such as TE and TAE rather than a 0.5x solution.

Conclusions

The long term goal of this project was to show that it is possible to control the dynamic motion or the physical position of DNA origami structures using integrated hybrid components including DNA binding proteins, gold nanoparticles, and magnetic nanoparticles. This work demonstrated the ability to attach LexA, ssDNA labeled gold nanoparticles, and ssDNA labeled magdots to dynamic DNA origami nanostructures. We also demonstrated that the binding efficiencies of the hybrid components can be affected by buffer conditions, the stability of each molecule, and the concentrations of both DNA structures and hybrid components.

LexA was specifically attached to the hinge with the highest efficiency of 49% at a protein concentration of 100nM (100 fold excess of protein to the 1nM hinge) in 1xTE, 0.2% Tergitol, 2mM $MgCl_2$, and 500mM NaCl. Single stranded DNA labeled gold nanoparticles were specifically attached to the hinge with efficiencies ranging from 52% to 54% in 1xTE, 0.2% Tergitol, and 12mM – 16mM $MgCl_2$. Magdots were successfully attached to the MD platform. It was shown through TEM images that varying the concentration of magdots added to a fixed concentration of MD platform could change the number of magdots attached to each structure.

In addition to verifying attachment of functional molecules to DNA origami structures it has been shown that LexA can serve as a latch component to hold the hinge in a closed configuration, which has an internal angle of 30° or less as determined through estimates of the size of the biotin-streptavidin-biotin-LexA latching complex. Measurement of angles on TEM images of hinges with LexA were plotted on a histogram (Figure 48 and

Figure 49 pp 71) which showed a left shift of the angular distribution of hinges with a second peak emerging at ~24°. When LexA was added at 100nM to 1nM hinges with LexA binding locations in 1xTE, 0.2% Tergitol, 2mM $MgCl_2$, and 500mM NaCl 56% of the hinges measured had internal angles that were less than the 30° 'closed' angle. This value can be compared to the 12% of hinges that had an internal angle of 30° or less in a sample of hinges in the same buffer that did not have integrated LexA attachment locations.

Future Work

Hinge – LexA Attachment

The hinge has 3 additional pairs of potential LexA binding locations designed into the structure. Each of these additional binding locations was in the 'OFF' state for the experiments contained here. A next step for this work will be to document angular distributions for the hinges containing the other binding locations of LexA on the hinge. This would show not only the development of a controlled 2 state switch of a DNA origami hinge using a DNA binding protein but would show that this latch can be tuned by moving the binding location of the protein latch.

Furthermore, to study the dynamics of closing and opening mediated by LexA or other DNA binding proteins, A Fluorescence Resonance Energy Transfer (FRET) pair of fluorophores can be incorporated into the arms of the hinge. FRET intensity measurements could be made both in bulk to measure equilibrium conformations of samples of the hinge or to at the single molecule level to measure conformational changes in real time in solution. The hinge should also be readied for polymerization studies to extend the upper arm of the structure. This would allow for visualization or manipulation at the micron scale, for example by attaching a magnetic particle to allow opening and closing of the hinge by magnetic force. Combining the integration of secondary components, external magnetic control over the angle of the hinge through polymerization of DNA origami monomers to the upper arm of the hinge, and the incorporation of a FRET pair to allow measurement of hinge angles in real time in bulk

solution allows the development of a nanoscale force sensor. This sensor would be able to test the forces required to break bonds holding a molecule of interest between the two arms of a DNA origami hinge. The benefit of this system over other methods such as AFM, optical tweezers, and magnetic tweezers, is that this measurement can be done in bulk on a Total Internal Reflection Fluorescence (TIRF) microscope.

Hinge –Modified ssDNA labeled Gold Nanoparticle Attachment

The angular distribution of the hinge with gold nanoparticle binding locations on both arms should be measured in the presence of 10 fold excess ssDNA labeled gold nanoparticles in the buffer conditions described in Section 3.3. The hinge has 12 additional potential gold nanoparticle binding locations designed into the structure. Each of these additional binding locations was in the 'OFF' state for the experiments contained here. The number and placement of gold nanoparticle binding locations can be varied and the angular distributions of each documented via TEM imaging.

It should be documented that the gold nanoparticle can be removed from the hinge by exposing the sample to 300 nm to 400 nm wavelength UV light and causing the trans-cis isomerization of the azobenzene molecules in the ssDNA overhangs on the gold nanoparticle. This should disrupt base pairing between the ssDNA overhang on the hinge and the ssDNA overhang on the nanoparticle, thus detaching the nanoparticle from the hinges.

This work would document a method for photo-switchable control over a DNA origami structure between 2 states. This could be used to develop photo-release DNA origami containers or cargo delivery molecules.

MD Platform – Magdot Attachment

The MD platform was designed to test the external manipulation and bulk visualization of DNA origami using incorporated magnetic and fluorescent components called magdots. The attachment of the magdots to the MD Platform was verified but must be optimized. The number of overhangs required to hold the platform to a surface should be determined. Up to 70 overhangs can be used. The controlled attachment of magdots will allow the development of a model to determine the magnetic force being used to break the duplex DNA attaching the structure to the surface. The fluorescent quantum dots contained within the magdots would allow the use of a TIRF microscope to perform bulk experiments.

When combined with the methods for the integration of secondary components discussed above, this work would develop another bulk method to probe molecular interactions of various molecules through magnetic manipulation of DNA origami structures containing integrated molecules of interest.

Appendix A: caDNAno Scaffold and Staple Routing Images

Hinge Design 1 – LexA Binding

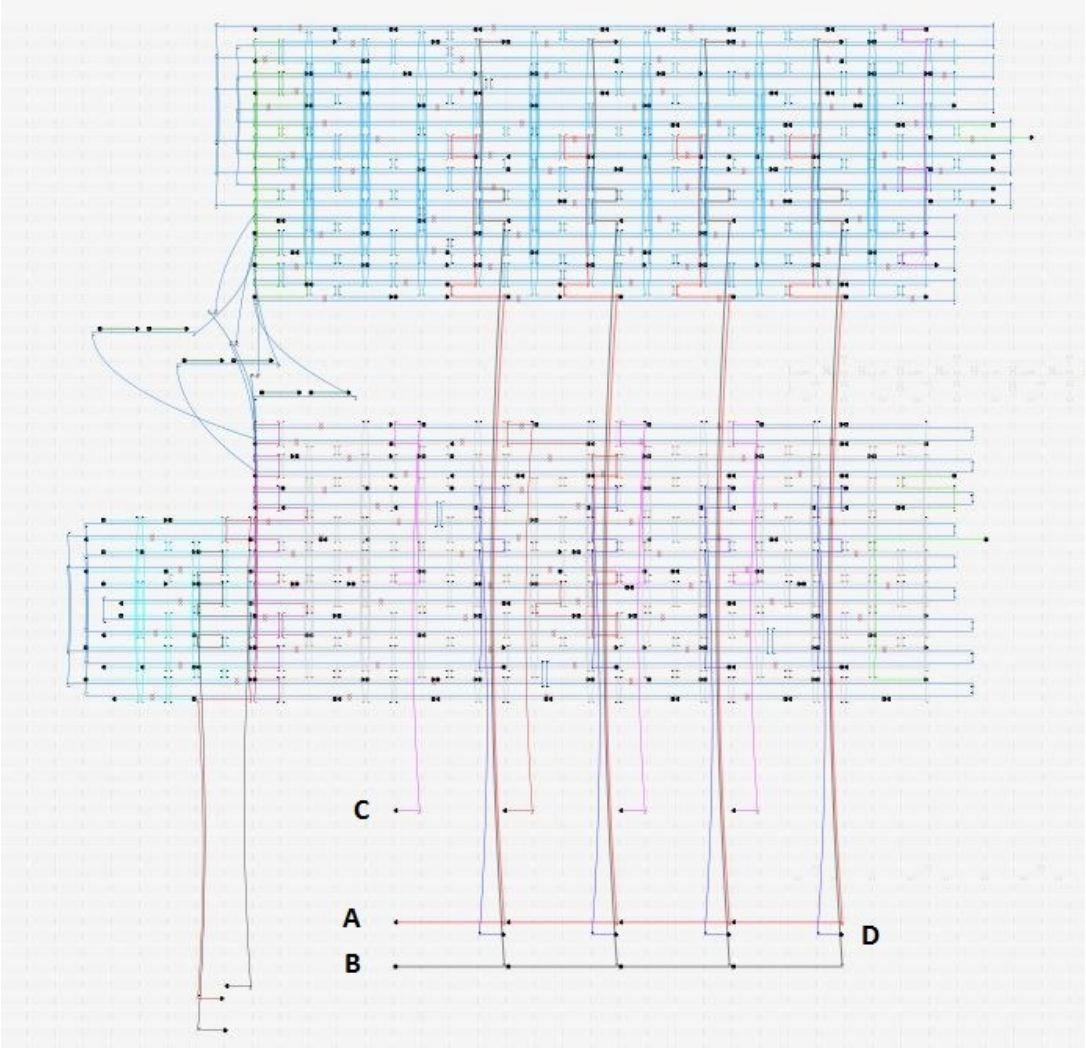

Figure 54 - caDNAno Schematic of LexA Hinge

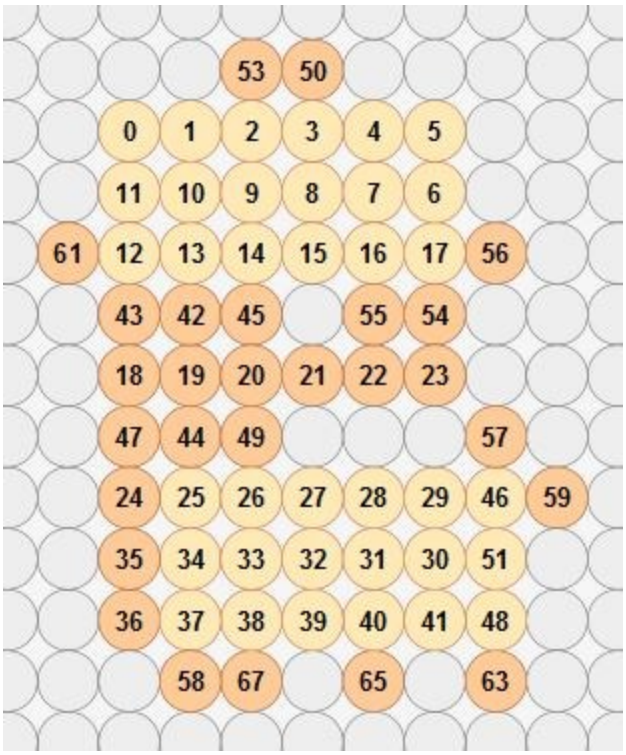

Figure 55 - Cross section of LexA Hinge

Figure 54 shows the scaffold routing (blue) and staple routing (cyan, orange, red, green, black, purple, and pink) for design 1 of the DNA origami hinge. The recognition sequence overhangs are shown in A) red (right side of structure if looking into the cross section below) and B) black (left side). Each of the 4 recognition sequence overhangs has a complementary biotin labeled overhang on the opposite bar of the hinge. These are shown in C) pink (left side) and D) navy (right side). The recognition sequence overhangs where designed such that they could adopt two orientations; parallel or perpendicular. Any overhang can be paired with the adjacent overhang location and form the binding location parallel to the helices of the hinge body. Any overhang could rather be paired with a complementary ssDNA oligomer that is not integrated into the structure

causing the binding location to form perpendicular to the helices of the structure. Figure 55 shows the cross section of the hinge. Structural helices are in beige and overhang helices (not full helices just pictorial placeholders to identify overhang locations on a cross section) are shown in orange.

Hinge Design 2 – Gold Nanoparticle Binding

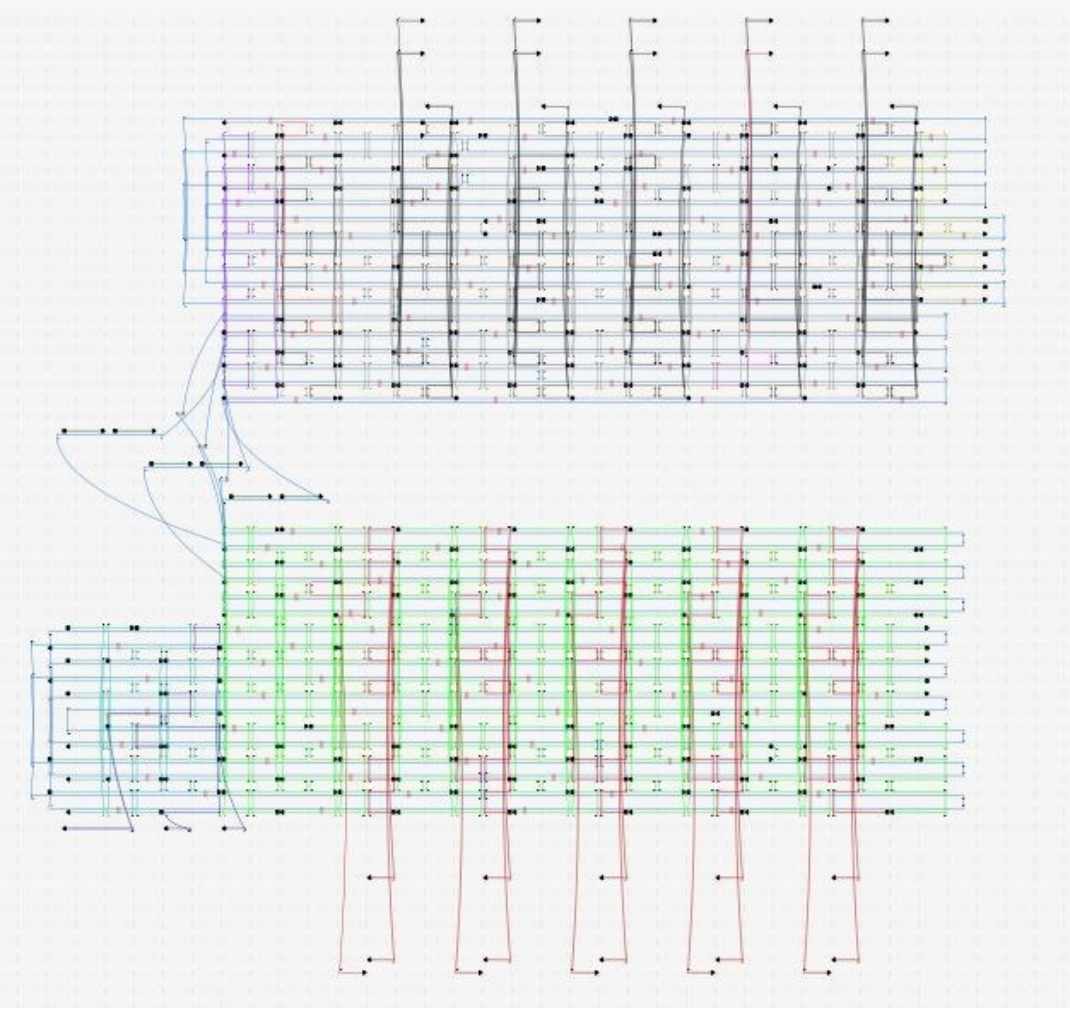

Figure 56 - caDNAno Schematic of the Gold Nanoparticle Hinge

Figure 57 - Cross section of Gold Nanoparticle Hinge.

Figure 56 shows the potential binding locations designed into the nanoparticle binding hinge. There are 15 overhangs on both the top and the bottom of the hinge. These overhangs are complementary to the azobenzene modified oligomer that is attached to the 5nm diameter gold nanoparticles. Figure 57 shows the cross section of the hinge. Structural helices are in beige and overhang helices (not full helices just pictorial placeholders to identify overhang locations on a cross section) are shown in orange.

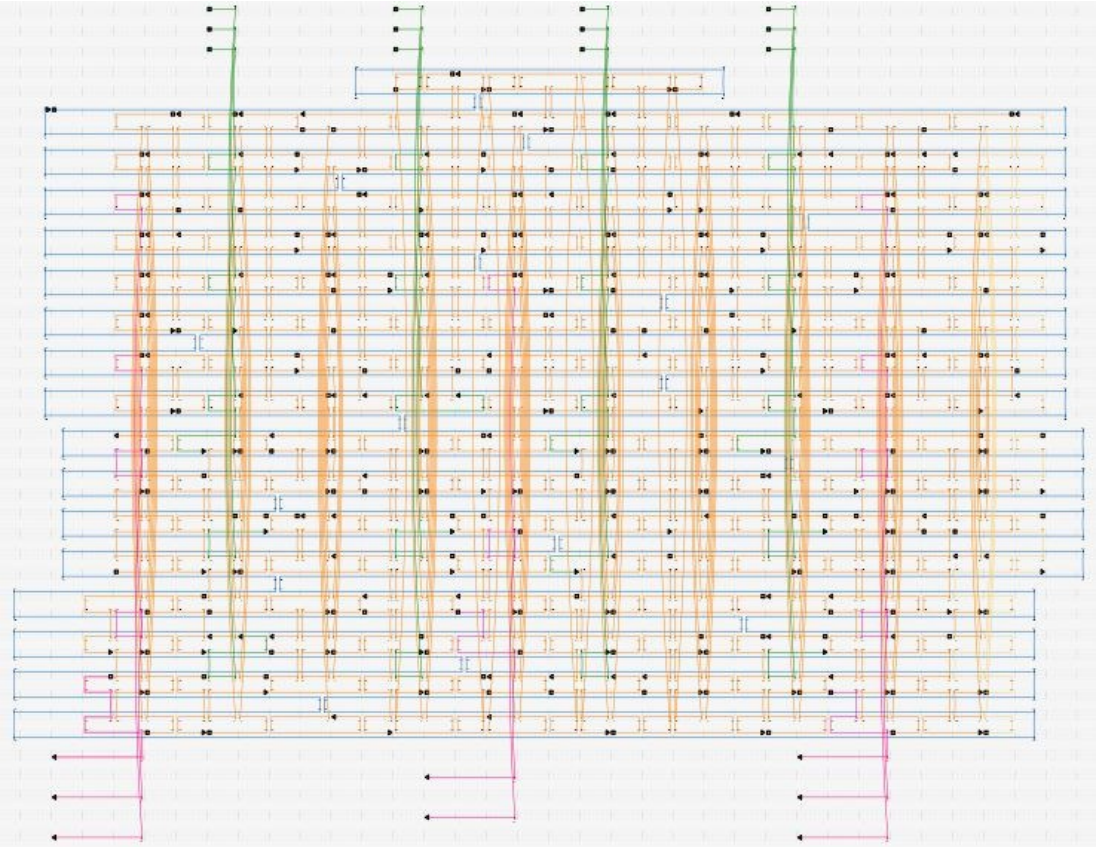

Figure 58 - caDNAno Schematic of LPP

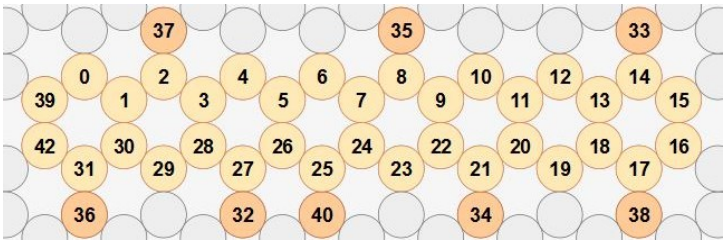

Figure 59 - Cross Section of the LPP

Figure 58 shows the ligand presentation platform. A 3D honeycomb lattice platform with 9 overhangs on one side of the structure (pink) and 12 overhangs on the other side of the structure (green). Figure 59 shows the cross section of the LPP. Structural helices are in beige and overhang helices (not full helices just pictorial placeholders to identify overhang locations on a cross section) are shown in orange.

10 Helix Bundle

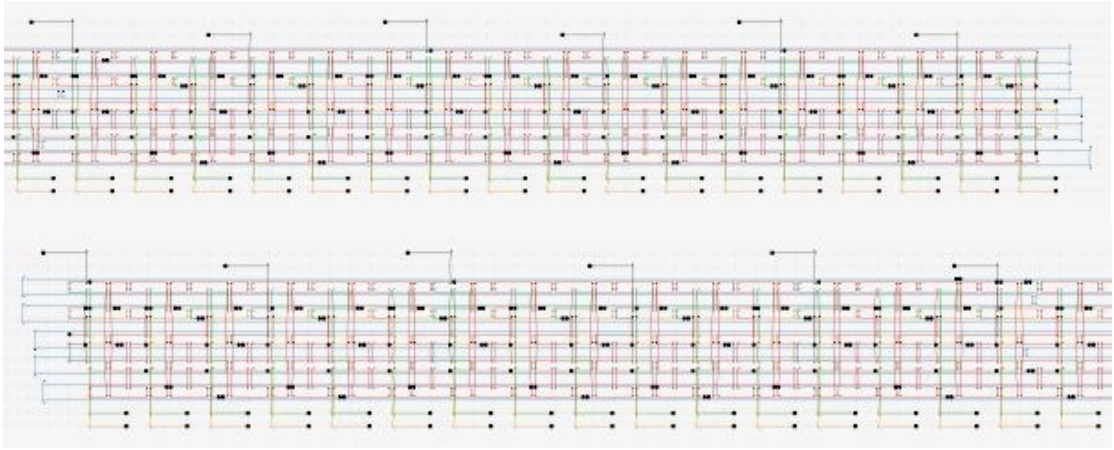

Figure 60 - caDNAno Schematic of 10 Helix Bundle from left (top) to right (bottom)

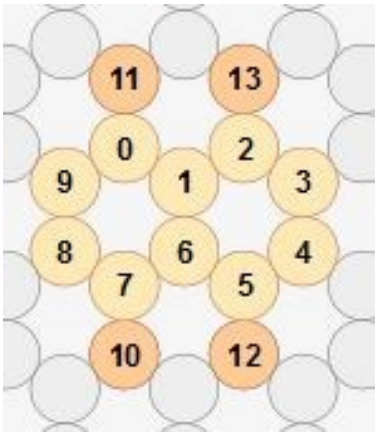

Figure 61 - Cross Section of 10 Helix Bundle

Figure 60 shows the 10 helix bundle structure and cross section. One of the wider sides of the cross section (the side on the top of the images above) has 12 binding sites for large magnetic quantum dot particles. The other side has two sets of 35 overhangs spread onto either half of the cross section. Figure 61 shows the cross section of the 10 helix bundle. Structural helices are in beige and overhang helices (not full helices just pictorial placeholders to identify overhang locations on a cross section) are shown in orange.

56 Helix Bundle – Filament Monomer Structure

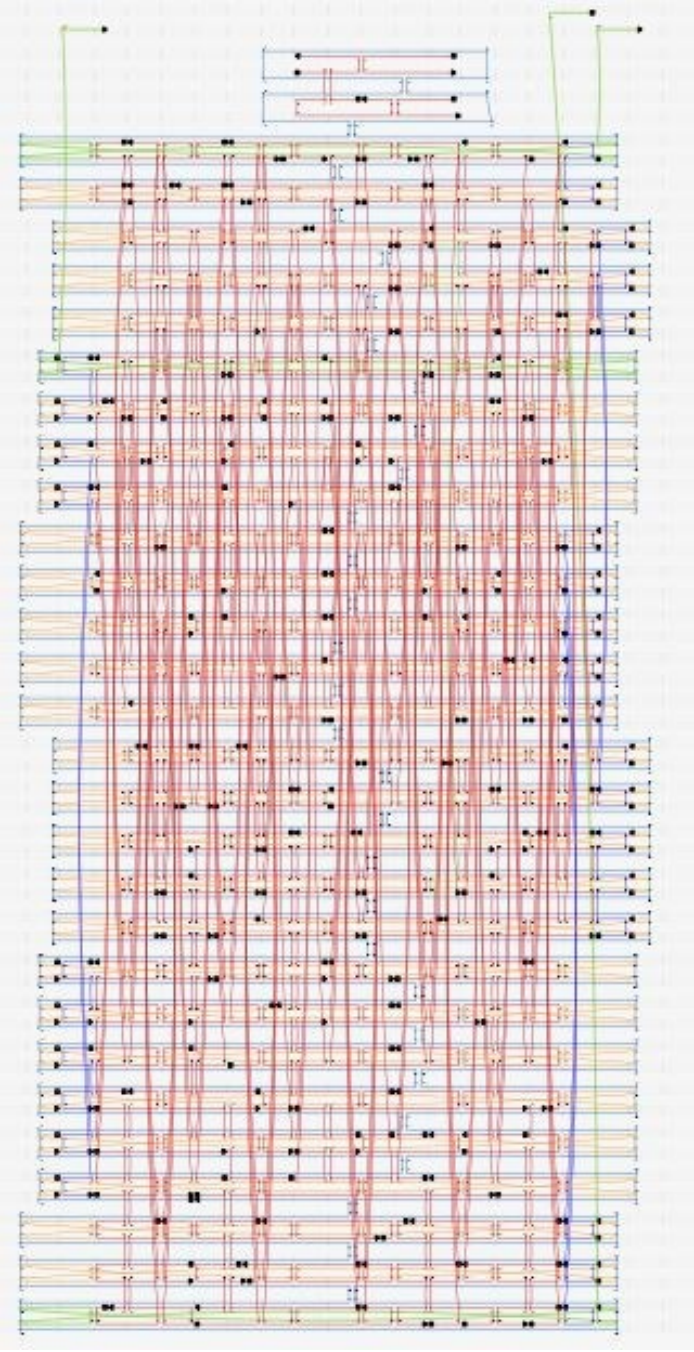

Figure 62 - caDNAno Schematic of 56 Helix Bundle Monomer

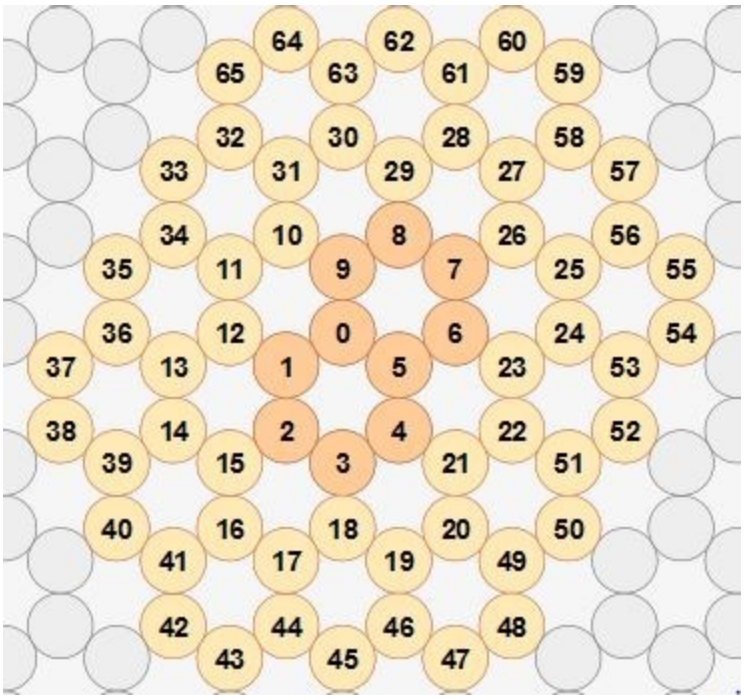

Figure 63 - Cross Section of 56 Helix Bundle Monomer

Figure 62 shows the scaffold and staple routing schematic for the 56 helix bundle monomer. Figure 63 shows the cross section of the monomer. Structural helices are in beige and empty placeholder helices are shown in orange.

Appendix B: DNA Melting Temperature Calculation

The melting temperatures of DNA oligomers used in this work were calculated using an online oligo analysis tool created by Integrated DNA Technologies at https://www.idtdna.com/calc/analyzer. The tool is called OligoAnalyzer 3.1 and uses the equation below to determine the melting temperature of duplex DNA based upon sequence, oligomer concentration, and Na^+ and Mg^{2+} concentrations.

$$\frac{1}{T_m(Mg^{2+})} = \frac{1}{T_m(1\,M\ Na^+)} + a + b\ln[Mg^{2+}] + f_{GC} \times (c + d\ln[Mg^{2+}])$$
$$+ \frac{1}{2(N_{bp} - 1)} \times \left[e + f\ln[Mg^{2+}] + g(\ln[Mg^{2+}])^2\right]$$

parameter	value (K^{-1})	standard error (K^{-1})
a	3.92×10^{-5}	0.2×10^{-5}
b	-9.11×10^{-6}	0.5×10^{-6}
c	6.26×10^{-5}	0.4×10^{-5}
d	1.42×10^{-5}	0.08×10^{-5}
e	-4.82×10^{-4}	0.7×10^{-4}
f	5.25×10^{-4}	0.2×10^{-4}
g	8.31×10^{-5}	0.2×10^{-5}

Equation 4 - Melting Temperature of DNA

Appendix C: LexA Recognition Sequence Hairpin Configurations

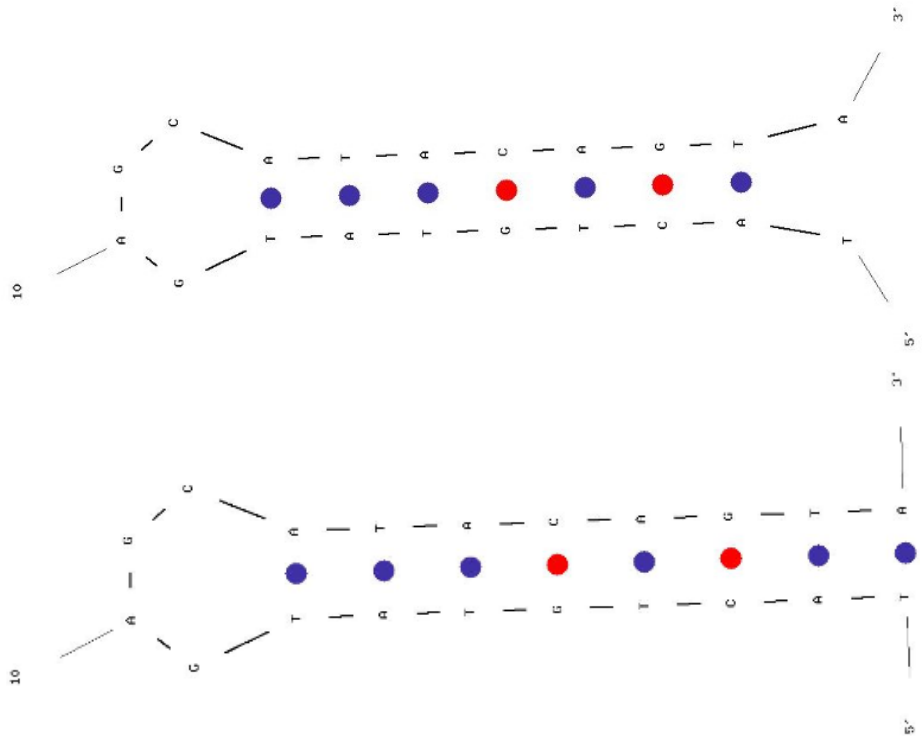

Figure 64- Unmodified LexA Recognition Sequence Hairpins. Top melting temp is 66°C and bottom melting temp is 62°

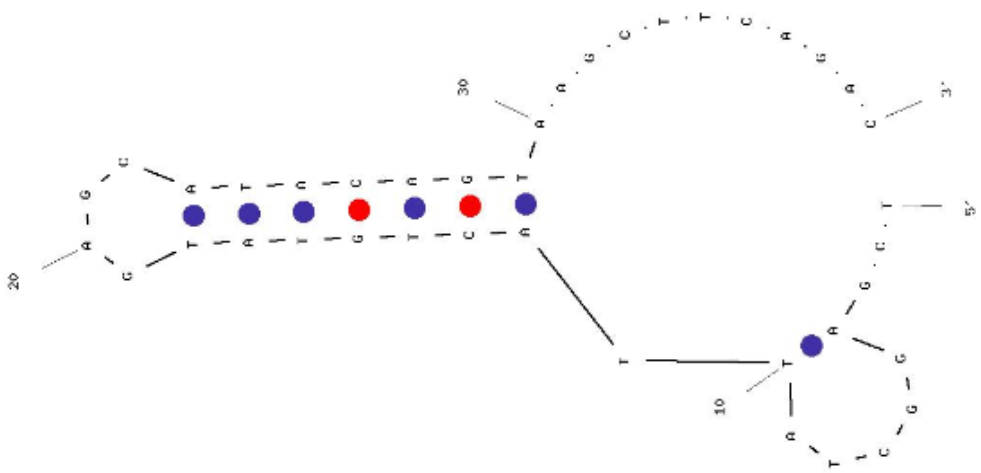

Figure 65 - Modified LexA Recognition Sequence Hairpin. Melting temp is 52°C

Appendix D: Polymerization Optimization Length Histograms

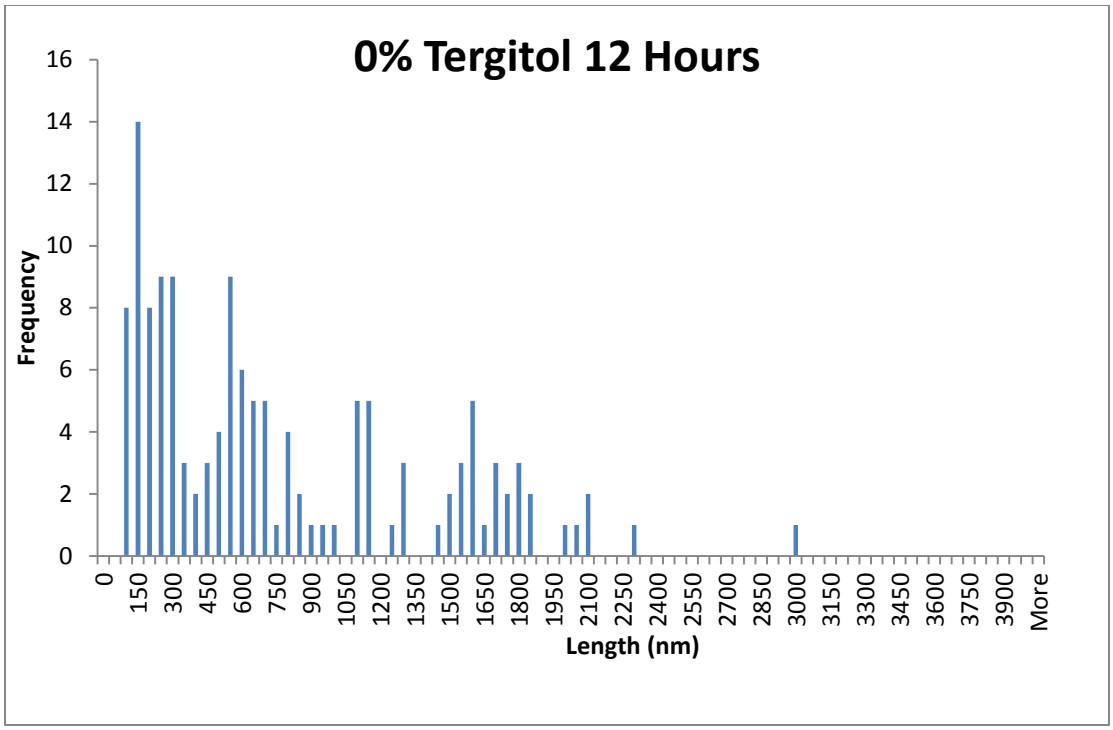

Figure 66 - 0% Tergitol 12 Hours Filament Lengths, N = 137

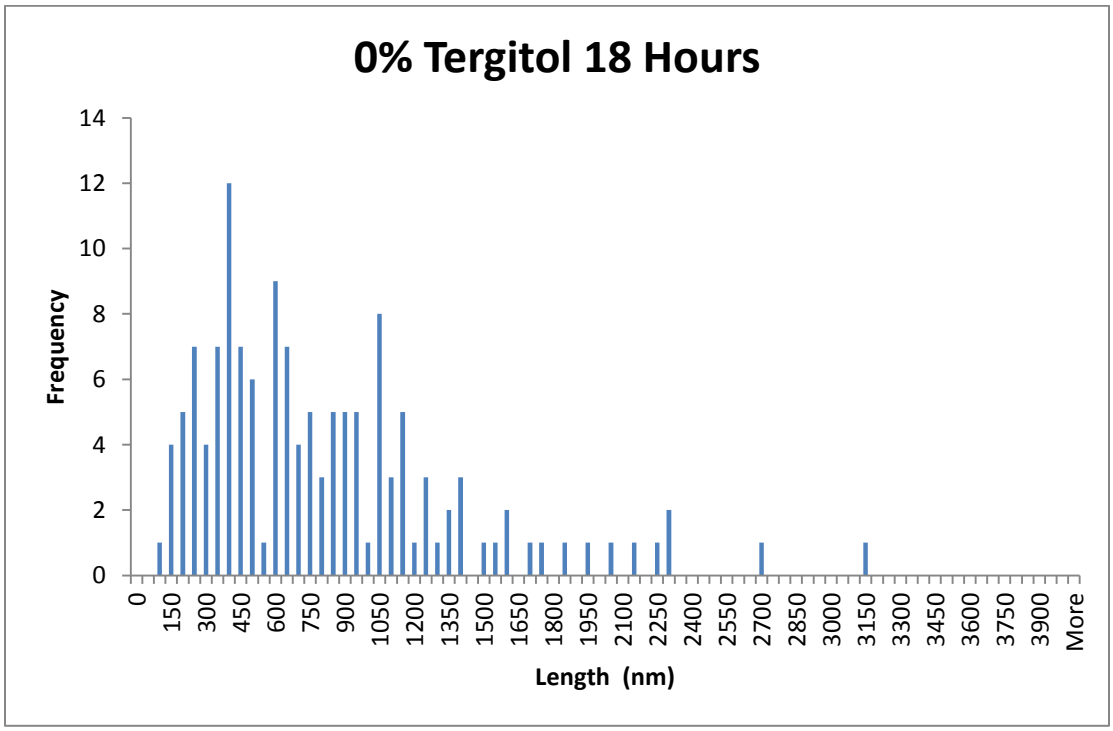

Figure 67 - 0% Tergitol 18 Hours Filament Lengths, N = 139

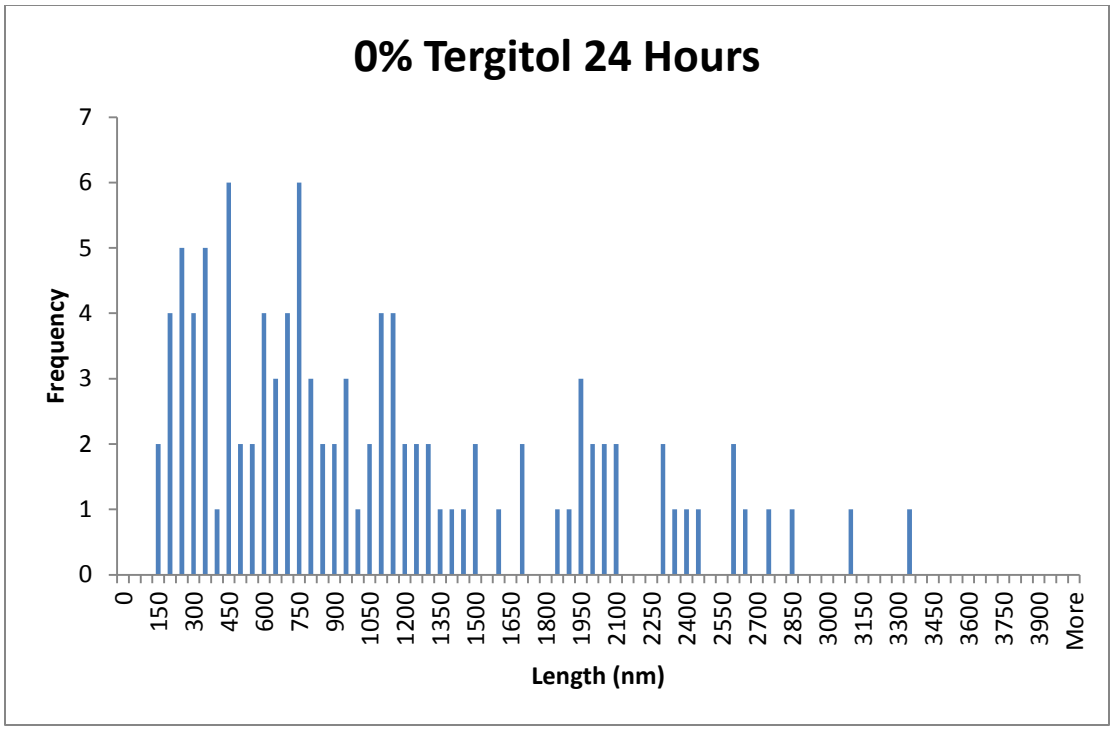

Figure 68 - 0% Tergitol 24 Hours Filament Lengths, N = 106

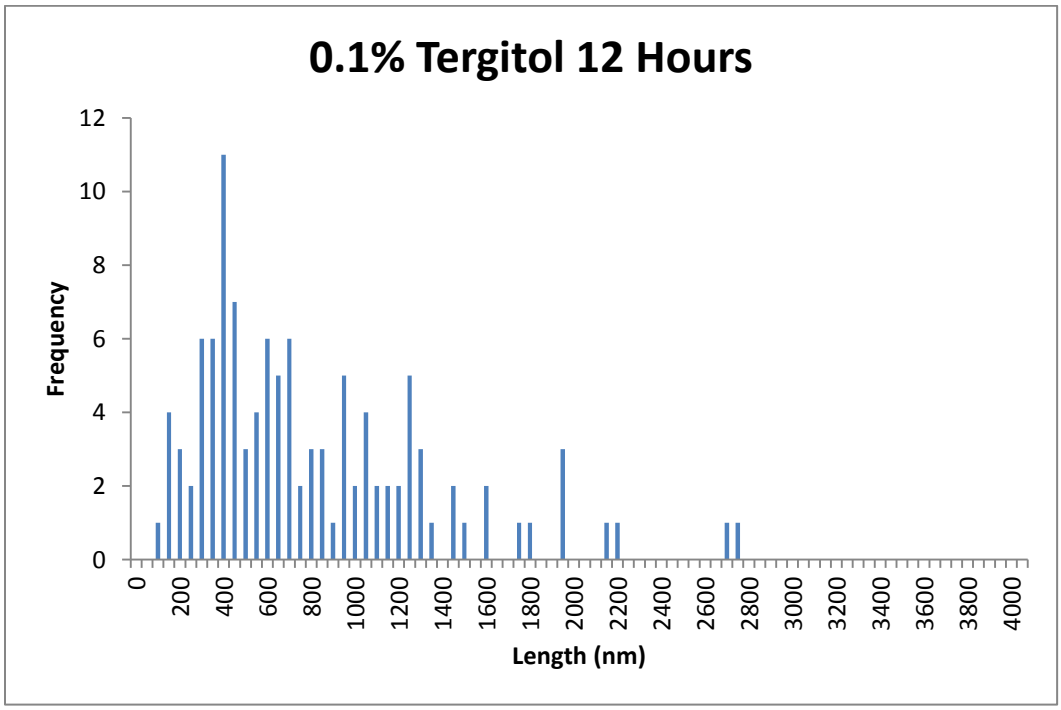

Figure 69 - 0.1% Tergitol 12 Hours Filament Length, N = 113

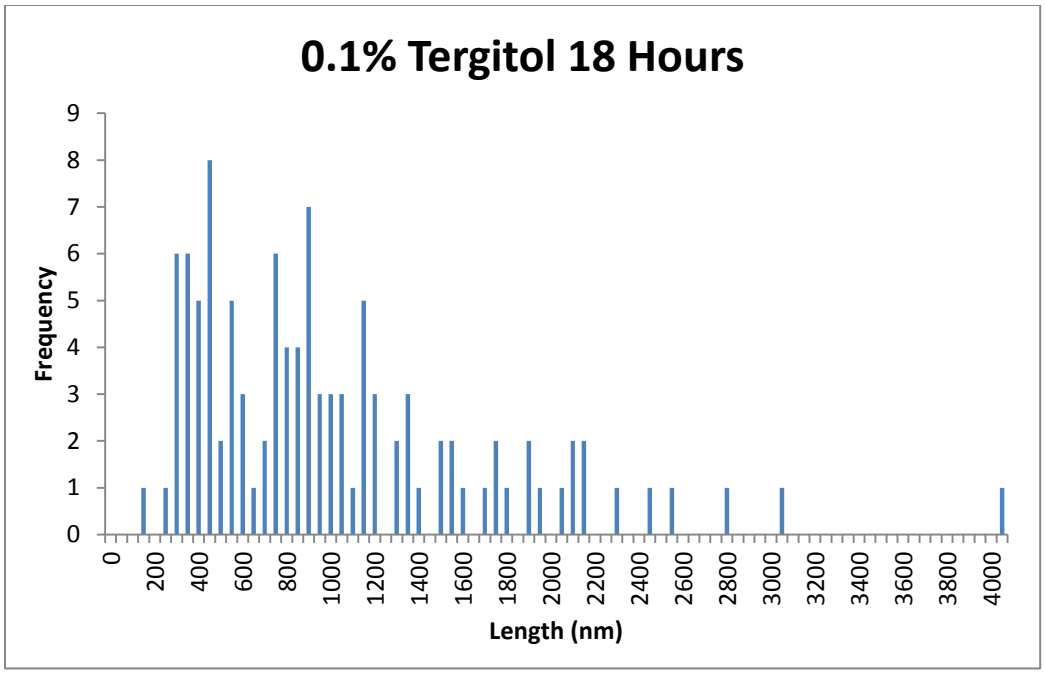

Figure 70 - 0.1% Tergitol 18 Hours Filament Length, N = 108

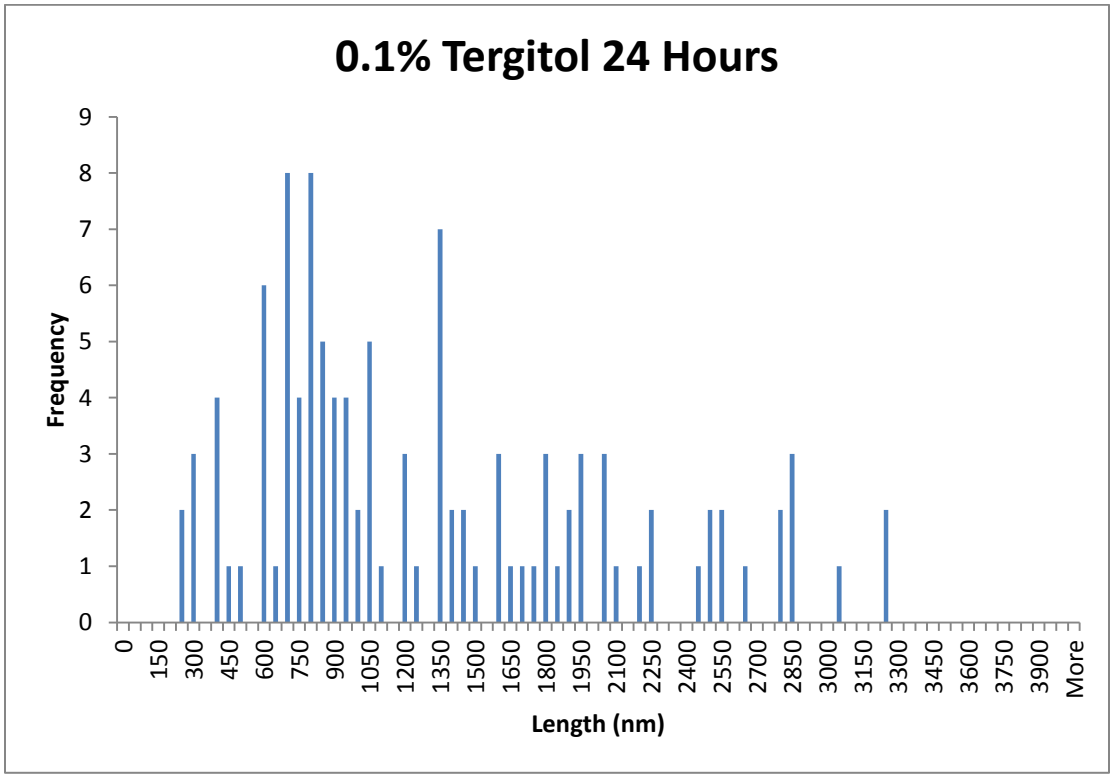

Figure 71 - 0.1% Tergitol 24 Hours Filament Length, N = 111

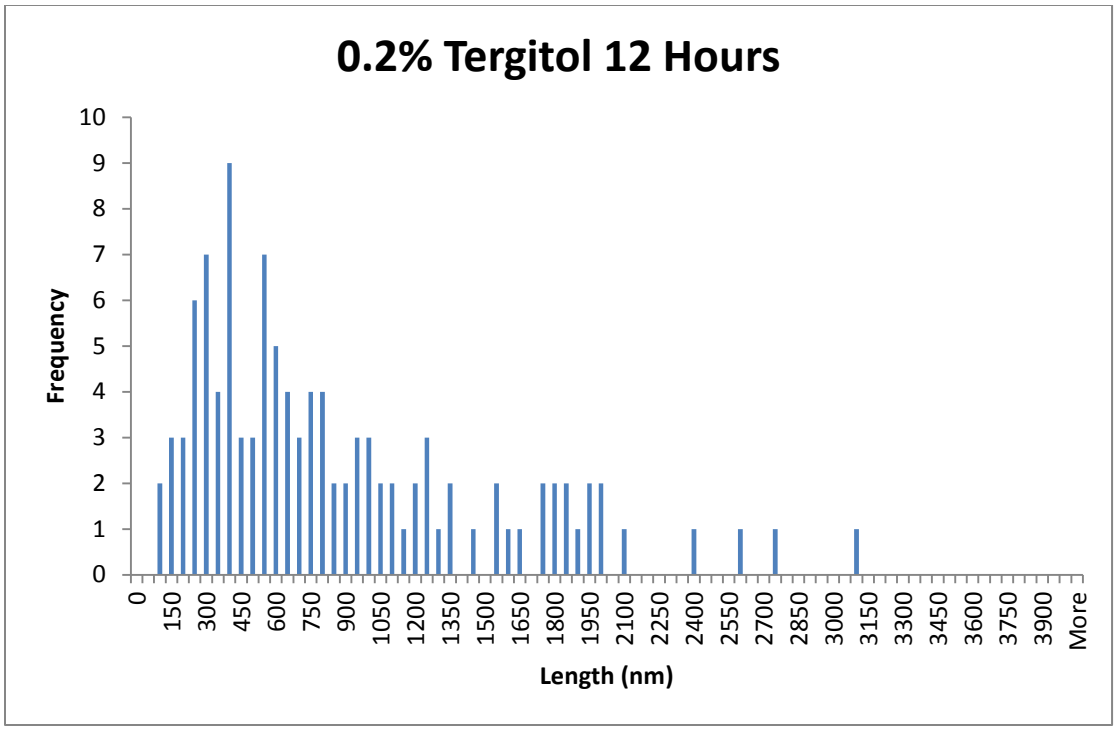

Figure 72 - 0.2% Tergitol 12 Hours Filament Length, N = 111

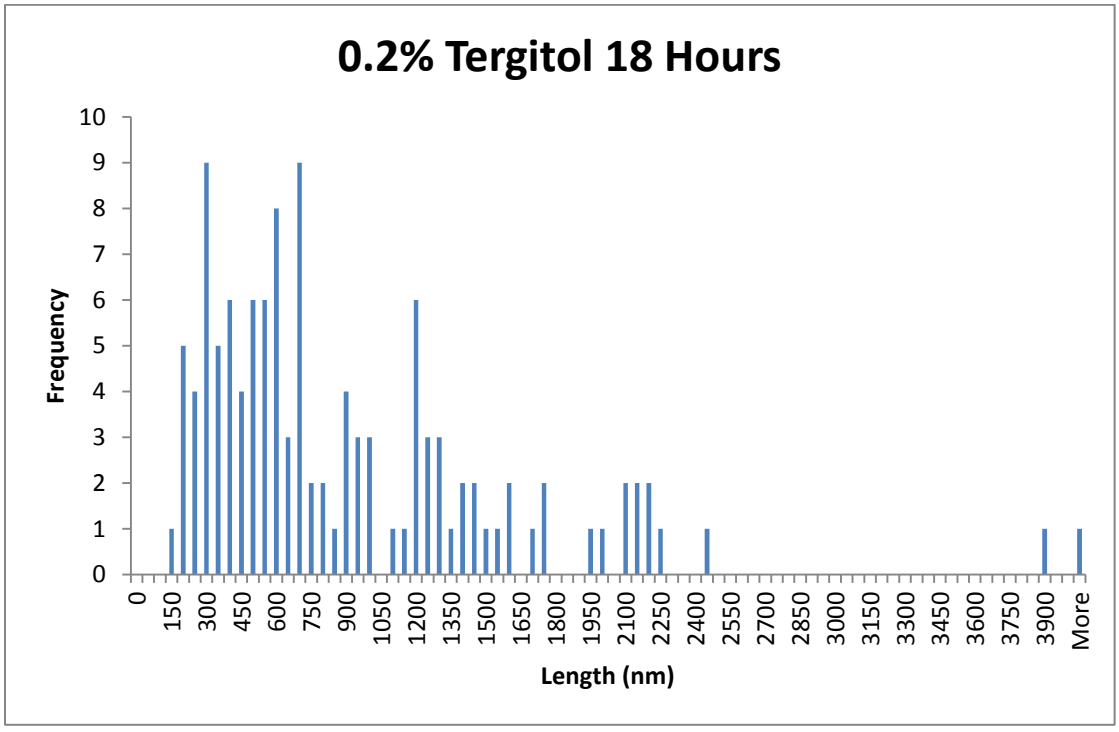

Figure 73 - 0.2% Tergitol 18 Hours Filament Length, N = 119

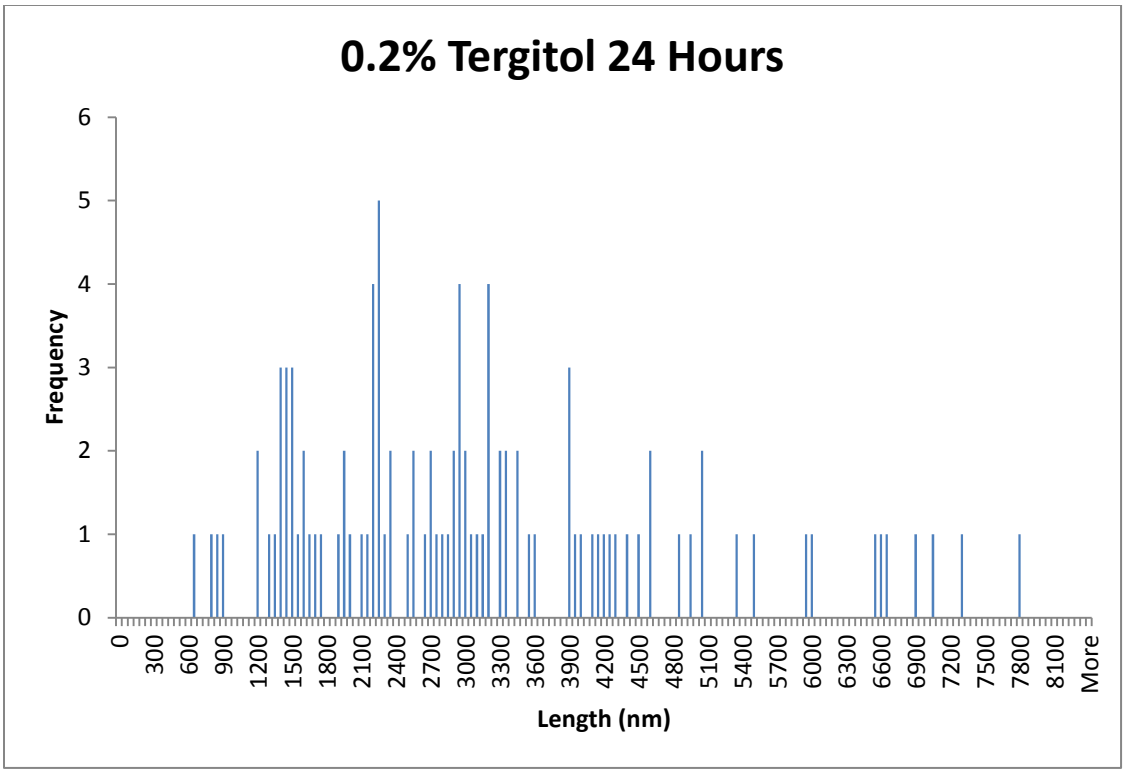

Figure 74 - 0.2% Tergitol 24 Hours Filament Length, N = 102

Appendix E: ssDNA labeled LexA

Initially, when attempting to integrate LexA into DNA origami hinges, the LexA was labeled with a DNA oligomer rather than with a biotin protein. This oligomer was complementary to an overhang located on the bottom bar of the hinge in the same locations as the currently defined biotinilated attachment overhangs. The attachment of LexA to the bottom arm was to be via DNA-DNA base paring while attachment to the top arm of the hinge occurred via recognition sequence binding. Using DNA labeled LexA was forgone because recognition sequence binding could not be achieved. The binding affinity of the DNA labeled LexA was tested through an electrophoretic mobility shift assay and the results are shown in Figure 75.

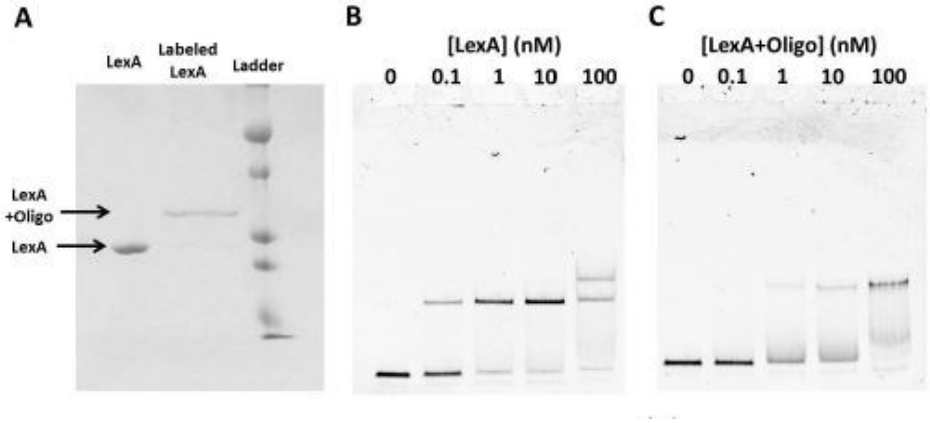

Figure 75 - LexA motility and Binding Affinity Assays [53]

Image A in Figure 75 shows a gel mobility shift of LexA after oligomer attachment. Image B shows a mobility shift of a 100 base pair long dsDNA complex containing the recognition sequence for increasing concentrations of LexA(S171C) which closely matches the results for WT LexA. Image C shows the same assay performed with the

oligomer modified LexA. These PAGE images show a substantial reduction in binding affinity of LexA to its target recognition sequence after ssDNA labeling.

Appendix F: MATLAB Code

Thermal Ramp Plot Generation

```
time = [0:5:390];
temp5hrs50 = 50*ones(1,60)
t1 = [75 75 74 73 72 71 70 69 68 67 66 65 64 63 62 61 60];
t2 = [70 70 69 68 67 66 65 64 63 62 61 60 50 50 50 50 50];
t3 = [65 65 65 65 65 50 50 50 50 50 50 50 50 50 50 50 50];
t4 = [65 65 65 65 50 50 50 50 50 50 50 50 50 50 50 50 50];
t5 = [65 65 65 50 50 50 50 50 50 50 50 50 50 50 50 50 50];
t1f = [t1 temp5hrs50 4 4];
t2f = [t2 temp5hrs50 4 4];
t3f = [t3 temp5hrs50 4 4];
t4f = [t4 temp5hrs50 4 4];
t5f = [t5 temp5hrs50 4 4];
figure(1)
plot(time, t1f,'r',time,t2f,'b',time,t3f,'m',time,t4f,'c',time,t5f,'k')
axis([0 390 0 80])
xlabel('Time (Minutes)')
ylabel('Temperature (°C)')
title('Thermal Ramps')

x = [4:1:65];
temp2half = [fliplr(x) 4 4 4 4 4];
time2half = [0 1 2 4 6:3:51 52:1:57 57.5:0.5:64.5 64.5:(1/60):64.85 65 66 67 68];
figure(2)
plot(time2half, temp2half)
axis([0 68 0 70])
xlabel('Time (hours)')
ylabel('Temperature (°C)')
title('2.5 Day Thermal Ramp')
```

LexA K_D

```
%concentration of LexA
LexAC = [0 0.1 0.2 0.4 1 2 4 10 20 40 100];
%Fluorescent Intensities
%Unbound DNA (2nd band)
UB = [294.9 213.82 151.62 139.53 120.86 144.81 77.61 76.37 69.5 59.89
63.48];
%Specific Binding to correct recognition sequence
NSB = [0 51.58 70.01 79.16 105.62 113.58 124.06 145.05 164.49 143.63
149.62];
%Nonspecific Binding
SB = [0 29.94 31.46 49.2 50.35 36.56 54.95 59.65 71.13 60.94 70.65];
% percent bound correctly
PB = (SB+NSB)./(SB+NSB+UB);
```

```
x0 = [0.5 0.01];
f = @(x,LexAC)(x(1).*LexAC./(x(2)+LexAC));

x = lsqcurvefit(f,x0,LexAC,PB)

LexACf = (0:0.01:110);
ff = (x(1).*LexACf./(x(2)+LexACf));

figure(1)
semilogx(LexACf,ff)
hold on
scatter(LexAC,PB,'filled')
hold off
xlabel('LexA (nM)')
ylabel('Fraction Bound')

figure(2)
plot(LexACf,ff)
hold on
scatter(LexAC,PB,'filled')
hold off
xlabel('LexA (nM)')
ylabel('Fraction Bound')
```

Figure 31 – Histogram of Magdot Diameters

```
A = xlsread('data.xls','Sheet1','A1:A112');
B = (xlsread('data.xls','Sheet1','B1:B17')).';
hist(A)
title('Diameter Distribution of Magdots')
xlabel('Diameter (nm)')
ylabel('Number of Micelles')
set(gca,'XTick', 10:10:150)
axis([0 150 0 75])
```

Figure 35 – Branched and Kinked Filaments vs Time

```
% plotting average length values for 56HB poly
time = [12 18 24]
%0NP4012
a1 = 739;
m1 = 2959;
bk1 = 28;
n1 = 137;

%0NP4018
a2 = 788;
```

```
m2 = 3103;
bk2 = 37;
n2 = 139;

%0NP4024
a3 = 1070;
m3 = 3328;
bk3 = 49;
n3 = 106;

%0.1 NP4012
a4 = 785;
m4 = 2712;
bk4 = 15;
n4 = 113;

%0.1 NP4018
a5 = 998;
m5 = 4129;
bk5 = 17;
n5 = 108;

%0.1 NP4024
a6 = 1286;
m6 = 3246;
bk6 = 22;
n6 = 111;

%0.2 NP4012
a7 = 845;
m7 = 3066;
bk7 = 12;
n7 = 111;

%0.2 NP4018
a8 = 894;
m8 = 4877;
bk8 = 9;
n8 = 119;

%0.2 NP4024
a9 = 3088;
m9 = 7784;
bk9 = 5;
```

```
n9 = 102;

a00 = [a1 a2 a3];
m00 = [m1 m2 m3];
bk00 = [bk1 bk2 bk3];
a11 = [a4 a5 a6];
m11 = [m4 m5 m6];
bk11 = [bk4 bk5 bk6];
a22 = [a7 a8 a9];
m22 = [m7 m8 m9];
bk22= [bk7 bk8 bk9];

subplot(2,1,1)
plot(time,a00,'b')
hold on
plot(time,a11,'r')
hold on
plot(time,a22,'k')
title('Average Length vs Polymerization Reaction Time Length')
xlabel('Time (hours)')
ylabel('Average Length (nm)')
legend('0% Tergitol','0.1% Tergitol','0.2% Tergitol','Location','Northwest')
hold off

subplot(2,1,2)
plot(time,m00,'b')
hold on
plot(time,m11,'r')
hold on
plot(time,m22,'k')
title('Maximum Length vs Polymerization Reaction Time Length')
xlabel('Time (hours)')
ylabel('Maximum Length (nm)')
legend('0% Tergitol','0.1% Tergitol','0.2% Tergitol','Location','Northwest')
hold off

figure
plot(time,bk00,'b')
hold on
plot(time,bk11,'r')
hold on
plot(time,bk22,'k')
title('Number of Branched or Kinked Filaments')
xlabel('Time (hours)')
```

```
ylabel('Frequency')
legend('0% Tergitol','0.1% Tergitol','0.2% Tergitol','Location','Northwest')
hold off
```

LexA-Hinge attachment Angular Distribution Histograms

```
A =
xlsread('ThetaB_30nm_100nM_LexA_angulardist.xls','thetaB_30nM_LexA','B2:B203');
B =
(xlsread('ThetaB_30nm_100nM_LexA_angulardist.xls','thetaB_100NM_LexA_1','B2:B1
98'));
hist(A)
title('Angular Distribution of Hinges with 30 fold excess LexA')
xlabel('Angle (deg)')
ylabel('Frequency')
set(gca,'XTick', 0:50:150)
axis([0 150 0 60])
figure
hist(B)
title('Angular Distribution of Hinges with 100 fold excess LexA')
xlabel('Angle (deg)')
ylabel('Frequency')
set(gca,'XTick', 0:50:150)
axis([0 150 0 60])
```

Bibliography

[1] D. Voet and J. Voet, "Nucleic Acid Structures," in *Biochemistry Third Edition*, John Wiley & Sons, Inc, 2004, pp. 1107-1115.

[2] M. Mandelkern, J. Elias, D. Eden and D. Crother, "The Dimensions of DNA in solution," *Journal of Molecular Biology ,* vol. 152, no. 1, pp. 153-161, 1981.

[3] D. o. Biology, "DNA Structure," Pennsylvania State University, State College, PA, 2004.

[4] "Nature.com Subject Areas," Nature.com, 2015. [Online]. Available: http://www.nature.com/subjects/dna-nanotechnology. [Accessed 12 3 2015].

[5] N. Seeman, "Nucleic Acid Junctions and Lattices," *Journal of Theoretical Biology ,* vol. 99, no. 2, pp. 237-247, 1982.

[6] S. Waga and B. Stillman, "The DNA replication Fork in Eukaryotic Cells," *Annual Review of Biochemistry,* vol. 67, pp. 721-751, 1998.

[7] R. Holliday, "The Induction of Mitotic Recombination by Mitomycin C in Ustilago and Saccharomyces," *Genetics,* vol. 50, pp. 323-335, 1964.

[8] N. Seeman, "Nanomaterials Based on DNA," *Annu. Rev. Biochem. ,* no. 79, pp. 65-87, 2010.

[9] N. Seeman, "Synthesis from DNA of a molecule with the connectivity of a cube," *Nature,* no. 350, pp. 631-633, 1991.

[10] N. Seeman, "A Precisely Controlled DNA Biped Walking Device," *Nano Letters,* vol. 4, no. 7, pp. 1203-1207, 2004.

[11] N. Seeman, "Polynucleotide nanomechanical device that acts as an artificial ribosome and translates DNA signals into polymer assembly instructions". United

States Patent WO 2006017432 A3, 29 Jul 2005.

[12] D. Bhatia, S. Surana, S. Chakraborty, S. Koushika and Y. Krishnan, "A synthetic icosahedral DNA-based host-cargo complex for functional in vivo imaging," *Nature Communications,* vol. 2, no. 339, 2011.

[13] R. Petros and J. DeSimone, "Strategies in the design of nanoparticles for therapeutic applications," *Nature Reviews Drug Discovery,* vol. 9, pp. 615-627, 2010.

[14] D. Zhang and G. Seelig, "Dynamic DNA nanotechnology using strand-displacement reactions," *Nature Chemistry,* vol. 3, pp. 103-113, 2011.

[15] R. Tsukanov, T. Tomov, Y. Berger, M. Liber and E. Nir, "Conformational Dynamics of DNA Hairpins at Millisecond Resolution Obtained from Analysis of Single-Molecule FRET Histograms," *The Journal of Physical Chemistry B,* 2013.

[16] K. Lund, A. Manzo and N. Dabby, "Molecular Robots Guided by Prescriptive landscapes," *Nature,* pp. 206-210, 2010.

[17] P. Yin, H. Yan, X. Daniell, A. Turberfield and J. Reif, "A Unidirectional DNA Walker that Moves Autonomously along a Track," *Angewandte Chemie International Edition,* vol. 43, pp. 4906-4911, 2004.

[18] M. Liu, J. Fu, C. Hejesen, Y. Yang, N. Woodbury, K. Gothelf, Y. Liu and H. Yan, "A DNA tweezer-actuated enzyme nanoreactor," *Nature Communications,* vol. 4, 2013.

[19] Y. He and D. Liu, "Autonomous Multistep Organic Synthesis in a Single Isothermal Solution Mediated by a DNA Walker," *Nature Nanotechnology,* vol. 5, no. 11, pp. 778-782, 2010.

[20] P. Rothemund, "Folding DNA to create nanoscale shapes and patterns," *Nature ,* vol. 440, pp. 297-302, 2006.

[21] C. Castro, F. Kilchherr, D. Kim, E. Shiao, T. Wauer, P. Wortmann, M. Bathe and H. Dietz, "A Primer to scaffolded DNA origami," *Nature Methods,* vol. 8, no. 3, pp. 221-229, 2011.

[22] S. Douglas, H. Dietz, T. Liedl, B. Hogberg, F. Graf and W. Shih, "Self-assembly of DNA into nanoscale three-dimensional shapes," *Nature Letters,* vol. 459, pp. 414-

418, 2009.

[23] Y. Ke, S. Douglas, M. Liu, J. Sharma, A. Cheng, A. L. Y. Leung, W. Shih and H. Yan, "Multilayer DNA Origami Packed on a Square Lattice," *Journal of the American Chemical Society,* vol. 131, pp. 15903-15908, 2009.

[24] S. Douglas, A. Marblestone, S. Teerapittayanon, A. Vazquez, G. Church and W. Shih, "Rapid prototyping of 3D DNA-origami shapes with caDNAno," *Nucleic Acids Research,* vol. 37, no. 15, pp. 5001-5006, 2009.

[25] A. Marchi, I. Saaem, B. Vogen, S. Brown and T. LaBean, "Toward Larger DNA Origami," *Nano Letters,* vol. 14, pp. 5740-5747, 2014.

[26] L. Zhou, A. Marras, H. Su and C. Castro, "DNA Origami Compliant Nanostructures with Tunable Mechanical Properties," *ACSNANO,* vol. 8, no. 1, pp. 27-34, 2014.

[27] F. Zhang, J. Nangreave, Y. Liu and H. Yan, "Structural DNA Nanotechnology: State of the Art and Future Perspective," *JACS,* pp. 11198 - 11211, 2014.

[28] J. Li, H. Pei, B. Zhu, L. Liang, M. Wei, Y. He, N. Chen, D. Li, Q. Huang and C. Fan, "Self-Assembled Multivalent DNA Nanostructures for Noninvasive Intracelluar Delivery of Immunostimulatory CpG Oligonucleotides," *ACSNANO,* vol. 5, no. 12, pp. 9696-9702, 2011.

[29] C. Sanders, "Visiting order on membrane proteins by using nanotechnology," *PNAS,* vol. 104, no. 16, pp. 6502-6503, 2007.

[30] A. Marras, L. Zhou, H. Su and C. Castro, "Programmable motion of DNA origami mechanisms," *PNAS,* vol. 112, no. 3, pp. 719-718, 2014.

[31] T. Liedl, B. Hogberg, J. Tytell, D. Ingber and W. Shih, "Self-assembly of three dimensional prestressed tensegrity structures from DNA," *Nature Nanotechnology,* vol. 5, pp. 520-524, 2010.

[32] W. Shu, D. Liu, M. Watari, C. Reiner, T. Strunz, M. Welland, S. Balasubramanian and R. McKendry, "DNA Molecular Motor Driver Micromechanical Cantilever Arrays," *Journal of the American Chemical Society,* vol. 127, pp. 17054-17060, 2005.

[33] B. Sacca, R. Meyer, M. Erkelenz, K. Kiko, A. Arndt, H. Schroeder, K. Rabe and C. Niemeyer, "Orthogonal Protein Decoration of DNA Origami," *Angewandte Chemie International Edition,* vol. 49, no. 49, pp. 9378-9383, 2010.

[34] H. Bui, C. Onodera, C. Kidwell, Y. Tan, E. Graugnard, W. Kuang, J. Lee, W. Knowlton, B. Yurke and W. Hughes, "Programmable Periodicity of Quantum Dot Arrays with DNA Origami Nanotubes," *Nano Letters,* vol. 10, no. 9, pp. 3367-3372, 2010.

[35] B. Sacca and C. Niemeyer, "Functionalization of DNA nanostructures with proteins," *The Royal Society of Chemistry,* vol. 40, pp. 5910-5921, 2011.

[36] Sigma-Aldrich, "Ethidum bromide solution," Sigma-Aldrich , 2015. [Online]. Available: https://www.sigmaaldrich.com/catalog/product/sigma/e1510?lang=en&region=US. [Accessed 02 04 2015].

[37] E. Stahl, T. Martin, F. Praetorius and H. Dietz, "Facile and Scalable Prepartaion of Pure and Dense DNA Origami Solutions," *Angewandte Chemie,* vol. 126, no. 47, pp. 12949-12954, 2014.

[38] J. Sobczak, T. Martin, T. Gerling and H. Dietz, "Rapid Folding of DNA into nanoscale Shapes at Constant Temperature," *Science,* vol. 338, pp. 1458-1461, 2012.

[39] M. Butala, D. Zgur-Bertok and S. Busby, "The bacterial LexA transciptional repressor," *Cellular and Moelcular Life Sciences,* vol. 66, pp. 82-93, 2009.

[40] F. Kuhner, L. T. S. Costa, W. Heckl and H. Gaub, "LexA-DNA Bond Strength by Single Molecule Force Spectroscopy," *Biophysical Journal ,* vol. 87, no. 4, pp. 2683-2690, 20004.

[41] S. Shaner and G. E, "Binding of Escherichia coli Lexa Repressor to the RecA operator," *Journal of Molecular Recognition,* vol. 9, no. 5/6, p. 468, 1998.

[42] Y. Luo, J. North, S. Rose and M. Poirier, "Nucleosomes accelerate transcription factor dissociation," *Nucleic Acids Research,* vol. 42, no. 5, pp. 3017-3027, 2014.

[43] M. Honda, Y. Saito, N. Smith, K. Fujita and S. Kawata, "Nanoscale heating of laser irradiated single gold nanoparticles in liquid," *Optics Express,* vol. 19, no. 13, pp.

12375-12383, 2011.

[44] B. Ding, Z. Deng, H. Yan, S. Cabrini, R. Zuckerman and J. Bokor, "Gold Nanoparticle Self-Similar Chain Structure Organizaed by DNA Origami," *Journal of the American Chemcial Society,* vol. 132, no. 10, pp. 3248-3249, 2010.

[45] J. Sharma, R. Chhabra, C. Andersen, G. K, H. Yan and Y. Liu, "Toware Reliabel Gold Nanoparticle Patterning on Self-Assembled DNA Nanoscaffold," *Jouranl of the America Chemical Society,* vol. 130, pp. 7820-7821, 2008.

[46] H. Gronbeck, A. Curioni and W. Andreoni, "Thiols and Disulfides on the Au(111) Surface: The Headgroup-Gold Interaction," *Journal of the American Chemical Society,* vol. 122, pp. 3839-3842, 1999.

[47] H. Freundlich and W. Heller, "The Adsorption of cis- and trans-Azobenzene," *Journal of the American Chemical Society,* vol. 61, no. 8, pp. 2228-2230, 1939.

[48] H. Asanuma, X. Liang, T. Yoshida and M. Komiyama, "Photocontrol of DNA Duplex Formation by Using Azobenzene-Bearing Oligonucleotides," *ChemBioChem,* pp. 39-44, 2001.

[49] S. Prakash and Y. Singh, "Shear Unzipping of Double-Stranded DNA," *Physical Review,* vol. 84, no. 3, p. 031905, 2011.

[50] Q. Fan, G. Nabar, C. Miller, C. Castro and J. Winter, "Photo-switchable Quantum Dots Based on Reversible FRET," *SPIE Proceedings,* vol. 8954, p. 89540D, 2014.

[51] E. Chi, S. Krishnan, T. Randolph and J. carpenter, "Physical Stability of Proteins in Aqueous solution: Mechanism and Driving Forces in Nonnative Protein Aggregation," *Pharmaceutical Research,* vol. 20, no. 9, pp. 1325-1336, 2003.

[52] M. Heffler, R. Walters and J. Kugel, "Using Electrophoretic Mobility shift Assays to Measure Equilibrium Dissociation Constants: GAL4-p53 Binding DNA as a Model System," *Biochemistry and Molecular Biology Education,* vol. 40, no. 6, pp. 383-387, 2012.

[53] M. W. Bernier, "The Structure of Chromatin and Its Influence on Gener Regulation," The Ohio State University, Columbus, OH, 2014.

[54] H. Lee, A. Lytton-Jean and Y. Chen, "Moleculary self-assembled nucleic acid nanoparticles for targeted in vivo siRNA delivery," *Nature Nanotechnology; Letters,* vol. 7, pp. 389-393, 2012.

[55] H. Dietz, S. Douglas and W. Shih, "Folding DNA into Twisted and Curved Nanoscale Shapes," *Science,* vol. 325, pp. 725-729, 2009.

[56] M. Marini, L. Piantandia, R. Musetti, A. Bek, M. Dong, F. Besenbacher, M. Lazzarino and G. Firrao, "A Revertible, Autonomous, Self-Assembled DNA-Origami Nanoactuator," *Nano Letters,* no. 11, pp. 5449-5454, 2011.

[57] A. Kuzuya, R. Watanabe, M. Hashizume, M. Kaino, S. Minamida, K. Kameda and Y. Ohya, "Precise structure control of three-state nanomechanical DNA origami devices," *Methods,* 2013.

[58] M. Manzanera, D. Frankel, H. Li, D. Zhou, A. Bruckbauer, P. Kreutzmann, J. Blackburn, C. Abell, T. Rayment, D. Klenerman and P. Barker, "Macroscopic 2D Networks Self-Assembled from Nanometer-Sezed Protein/DNA Complexes," *Nano Letters,* vol. 6, no. 3, pp. 365-370, 2006.

[59] Y. Yang, M. Endo, K. Hidaka and H. Sugiyama, "Photo-Controllable DNA Origami Nanostructures Assembling into Predesigned Multiorientational Patterns," *Journal of the American Chemical Society,* vol. 134, no. 51, pp. 20645-20653, 2012.

[60] B. Yurke, A. Tuberfield, A. Mills, F. Simmel and J. Neumann, "A DNA-fueled moleuclar machine made of DNA," *Nature,* vol. 406, pp. 605-608, 2000.

[61] C. Steinhauer, R. Jungmann, T. Sobey, F. Simmel and P. Tinnefeld, "DNA Origami as a Nanoscopic Ruler for Super-Resolution Microscopy," *Angewandte Chemie International Edition,* vol. 48, no. 47, pp. 8870-8873, 2009.

[62] A. Zhang, Y. Pigil and P. Rice, "Structure of the LexA-DNA complex and implication for SOS box measurement," *Nature ,* no. 466, pp. 883-886, 2010.

[63] RCSB, "LexA Protein PDB ID: 3JSP," RCSB Protein Data Bank, 21 03 2012. [Online]. Available: http://www.rcsb.org/pdb/explore/explore.do?structureId=3JSP. [Accessed 25 03 2015].

[64] Integrated DNA Technologies, "OligoAnalyzer 3.1," IDT, 2006. [Online].

Available: https://www.idtdna.com/calc/analyzer. [Accessed 19 01 2015].